Illinois U Library

The American Mineralogist

Journal of the Mineralogical Society of America

Vol. 39 JANUARY–FEBRUARY, 1954 Nos. 1 and 2

Contents

EDITOR: WALTER F. HUNT
ASSISTANT EDITOR: LEWIS S. RAMSDELL

BOARD OF ASSOCIATE EDITORS:

MICHAEL FLEISCHER
ELBURT F. OSBORN
IAN CAMPBELL
GEORGE TUNELL (1954)
ADOLF PABST (1954–55)
BRIAN MASON (1954–56)

Published bi-monthly by the Society

Mineralogical Society of America

ASSOCIATED WITH THE GEOLOGICAL SOCIETY OF AMERICA

President: Sterling B. Hendricks, U. S. Department of Agriculture, Beltsville, Maryland.

Vice-President: Harry H. Hess, Princeton University, Princeton, New Jersey.

Secretary: C. S. Hurlbut, Jr., Harvard University, Cambridge, Massachusetts.

Treasurer: Earl Ingerson, U. S. Geological Survey, Washington 25, D. C.

Editor: Walter F. Hunt, University of Michigan, Ann Arbor, Michigan.

Councillors: George T. Faust, U. S. Geological Survey, Washington 25, D. C.
Victor T. Allen, Institute of Geophysical Technology, St. Louis, Missouri.
C. Osborne Hutton, Stanford University, Palo Alto, California.
Felix Chayes, Geophysical Laboratory, Washington, D. C.
J. D. H. Donnay, The Johns Hopkins University, Baltimore, Maryland.

The enlarged issues of this journal for 1954 are made possible by a grant from the Penrose Fund of the Geological Society of America.

The American Mineralogist—Journal of the Mineralogical Society of America

A journal containing articles on mineralogy, crystallography, petrography, and allied sciences, is issued every two months. Contributions are invited from everyone. Office of Publication, Mineralogical Laboratory, Ann Arbor, Mich.

The general conduct of the journal is in the hands of the editor, **Walter F. Hunt**, Ann Arbor, Michigan, to whom all manuscripts should be submitted. To assist the editor the council of the Mineralogical Society has appointed **Lewis S. Ramsdell**, Ann Arbor, Michigan, assistant editor, and the following board of associate editors:

Michael Fleischer, U. S. Geological Survey, Washington, D. C.
Esper S. Larsen, Jr., U. S. Geological Survey, Washington, D. C.
Elburt F. Osborn, Pennsylvania State College, State College, Pa.
Adolf Pabst, University of California, Berkeley 4, California.
Austin F. Rogers, 2412 Durant Ave., Berkeley, California.
George Tunell, University of California at Los Angeles, California.

It will expedite publication if two copies of each manuscript are submitted to the editor.

Contributors of leading articles are given without charge 100 reprints (without covers) of their article. If additional reprints are desired these can be purchased at the following rates:

Pages	*1–4*	*5–8*	*9–12*	*13–16*	*17–20*	*21–24*	*25–28*	*29–32*	*Covers*
Copies									
25	$3.50	$5.00	$ 8.00	$ 9.50	$11.00	$13.00	$15.00	$16.00	$4.90
50	3.80	5.55	8.80	10.40	12.10	14.20	16.40	17.50	5.50
75	4.10	6.10	9.60	11.30	13.20	15.40	17.80	19.00	6.10
100	4.40	6.65	10.40	12.20	14.30	16.60	19.20	20.50	6.70
Addl. C's	1.20	2.20	3.20	3.60	4.40	4.80	5.60	6.00	2.40

Cover Composition $1.55.

Sent to all members and fellows of the Mineralogical Society of America. Subscription price, $4.00 per year (single copies of normal issues, $1.00 plus postage).

Entered as second class matter at the post office at Menasha, Wis., under Act of March 3, 1879. Acceptance for mailing at the special rate of postage provided for in section 1103, Act of Oct. 3, 1917, paragraph 4 section 429 P. L. & R. authorized March 13, 1922.

Notice of change of address, orders, and remittances should be sent to Dr. Earl Ingerson, U. S. Geological Survey, Washington 25, D. C.

Printed by the George Banta Publishing Company, Menasha, Wisconsin
Printed in the United States of America

THE AMERICAN MINERALOGIST

JOURNAL OF THE MINERALOGICAL SOCIETY OF AMERICA

Vol. 39 JANUARY–FEBRUARY, 1954 Nos. 1 and 2

STRUCTURAL RELATIONS AMONG DOUBLE OXIDES OF TRIVALENT ELEMENTS

M. L. KEITH AND RUSTUM ROY*

ABSTRACT

The crystal structures assumed by equimolar and 3:5 molar ratio compounds of the sesquioxides are reported, a number of them for the first time, and the effect of ionic radius ratio as the controlling variable is demonstrated. In addition, the effect of cation charge upon the cation-size-tolerance of a structure is demonstrated by comparison between $A^{3+}B^{3+}O_3$ compounds and known structures of $A^{2+}B^{4+}O_3$ compounds. Several ambiguities and discrepancies in the literature are corrected. Some properties of the compounds are recorded and consideration is given to the bearing of the results upon problems of the distribution of rare elements in natural minerals and upon the preparation of crystalline compounds with specific desired properties.

IONIC SUBSTITUTIONS

Crystal structure studies and investigations of the substitution of different elements in specific structures have developed into one of the important borderline fields between geochemistry and mineralogy on the one hand, and ceramic technology on the other hand. In the geological sciences, information on crystal structure substitutions is a guide to the distribution of elements in minerals and rocks; such investigations are becoming increasingly important as the rarer elements are being sought. This is particularly true in the case of elements which do not occur as major constituents of any known mineral but proxy for more abundant elements in common minerals. In ceramic technology, investigations of crystal structure substitutions combined with measurement of the properties of crystalline compounds and solid solutions, offer a basis for predicting the properties of crystals and crystalline aggregates and of guiding the preparation of materials with specific, desired properties, such as high melting point, low thermal expansion or high dielectric constant.

The present investigation deals primarily with the crystal structures obtained in various combinations of trivalent elements in double oxides

* College of Mineral Industries, The Pennsylvania State University, State College, Pa.

and with analogies to similar structures of double-oxide combinations of cations of other valence. Most of the double-oxide combinations encountered are 1:1 molar ratio compounds or solid solutions. A smaller number of double-oxide combinations have a 3:5 ideal molecular proportion of the component oxides and show a garnet structure. Since ionic size is by far the most important consideration, it has been possible to make several types of substitutions in a particular structure. The simplest one is the introduction of an ion similar in size and charge to one of the original ions; others include the substitution of two ions of similar size but with different charges, one greater and the other less than those of the original ions.

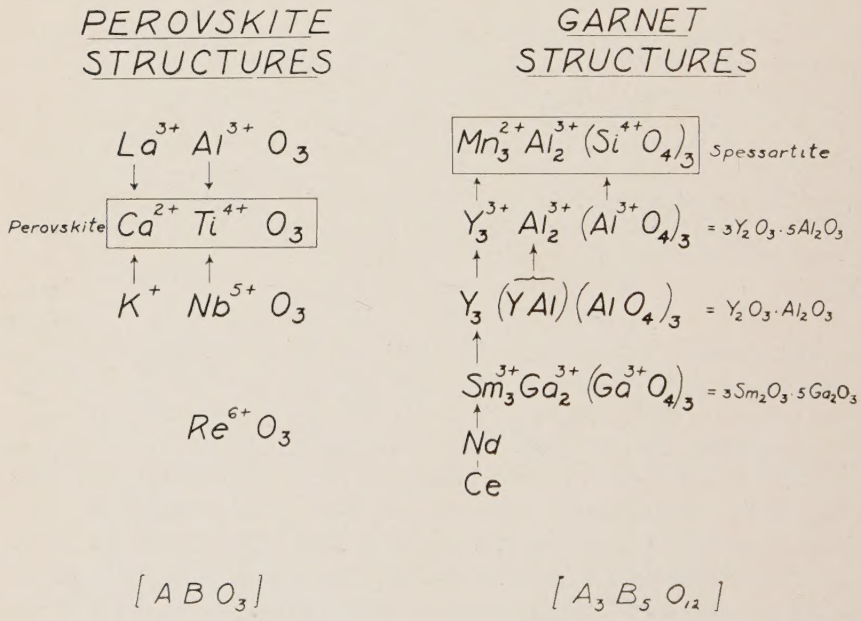

FIG. 1. Examples of Cation Substitutions in Perovskite and Garnet Structures.

Some of the demonstrated cation substitutions in perovskite structures and garnet structures are shown as examples in Fig. 1. In perovskite, a bivalent cation (Ca^{2+}) is combined with a quadrivalent cation (Ti^{4+}). Within certain limits of cation size, other combinations of a bivalent and a quadrivalent cation have the perovskite structure with varying degrees of distortion from the ideal cubic form. Further (again within certain cation-size limitations), other cation combinations with a total charge of six can proxy for the A^{2+}:B^{4+} combination. For example (Fig. 1),

both lanthanum aluminate,[a] with two trivalent cations, and potassium niobate, with a monovalent and a pentavalent cation, have the perovskite structure. As extreme examples of the substitution possibilities, rhenium oxide (ReO_3) and one form of tungsten oxide (WO_3), with cation valence of six, have distorted perovskite structures (Wyckoff, 1949, Ch. V, Text p. 15).

The garnet substitutions are somewhat more complex. Starting from the ideal formula of spessartite garnet, $Mn_3Al_2(SiO_4)_3$, it has been shown (Yoder and Keith, 1951), that yttrium can be substituted for manganese if aluminum is simultaneously substituted for silicon in order to maintain the charge balance. The result of complete substitution $Y^{3+}Al^{3+} \rightarrow Mn^{2+}Si^{4+}$ is a silica-free garnet of the formula $Y_3Al_2(AlO_4)_3$ which can be simplified to $3Y_2O_3 . 5Al_2O_3$, (yttrogarnet). The first form of the yttrogarnet formula above has the advantage of emphasizing that aluminum occurs both in six-fold and in four-fold coordination.

Previous Work

The earliest and most complete work to date is that of V. M. Goldschmidt and his students who prepared a large number of the ABO_3 compounds and determined their general structure type. Goldschmidt (1927–36) also studied the factors determining structure type and clearly demonstrated the influence of ionic radius and ionic polarizability as the controlling variables. Zachariasen (1927) made an extensive survey of the A_2O_3 structures, which may be considered as special cases of the ABO_3 structures. A large number of investigators since have prepared a few more compounds, or attempted to clarify or more closely define the relationships between ionic radius and structure type. Of the recent work especial mention may be made of the papers of Naray-Szabo (1943) and the recent classification by Wood (1951). Interest in this field has been stimulated by the exceptional dielectric properties of $BaTiO_3$ and related compounds. Much detailed information is collected in the publications of Megaw (1946), Matthias (1949), Jonker and van Santen (1949), and Roberts (1949, 1951), but with the exception of the last two studies referred to above, little attention has been given to the systematic preparation of new compounds and determination of structure types. It is worth noting that almost every oxide compound which has been found to be strongly ferroelectric was listed in Goldschmidt's original work on perovskite and related structures.

[a] This terminology is used only for convenience, and the compound is no more an aluminate than a lanthanate. We adopt the convention of placing the smaller cation in the "B" position in writing formulae.

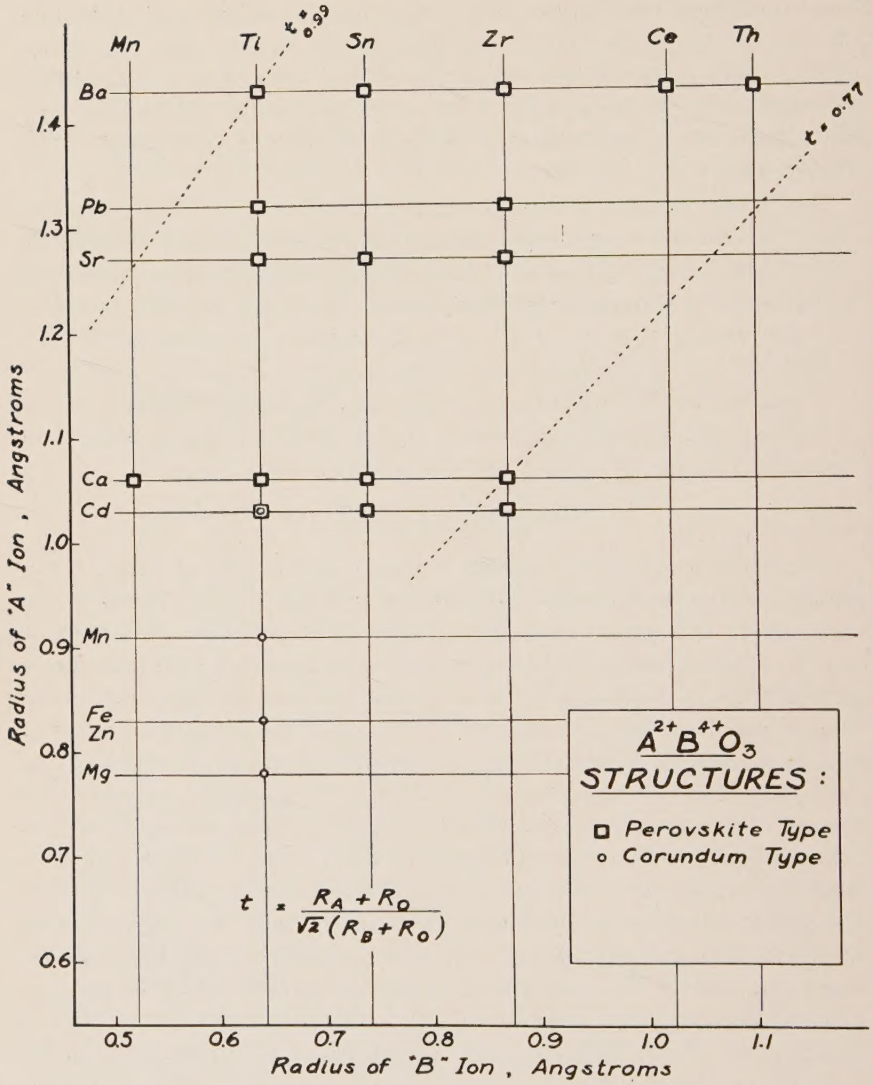

FIG. 2. Distribution of $A^{2+}B^{4+}O_3$ Structures in Relation to Cation Radii.

Figure 2 is a plot of the structures obtained in double-oxide combinations of bivalent and quadrivalent ions of different radius. The data are mostly from the literature and may be found summarized in Wyckoff (1951) or in Structure Reports (1951). Modified Goldschmidt radii are used (see Rankama and Sahama, 1950). The results are essentially

the same using any of the sets of ionic radii, the main difference being in the relative positions of In, Sc, and Y.[b]

Using the data shown in Fig. 2 . . . Goldschmidt (1927–36), developed the concept of what he called a "tolerance factor" to express, in terms of ionic radii, the limits within which a specific structure may be expected from combinations of various elements. His formula is:

$$t = \frac{R_A + R_O}{\sqrt{2}(R_B + R_O)}.$$**

** t = tolerance factor for the perovskite structure.
R_A = ionic radius of the larger cation in double oxides.
R_B = ionic radius of the smaller cation in double oxides.
R_O = ionic radius of oxygen.

Goldschmidt concluded that the perovskite structure may be expected within the limits t = 0.99 to 0.77 (see Fig. 2). The present work confirms that those limits are substantially correct for double-oxide combinations of a bivalent and a quadrivalent cation. Subsequent to the work of Goldschmidt, some perovskite structures have been reported below the tolerance limit t = 0.77, but we have not been able to confirm those reports. For example: $CdCeO_3$, $CaCeO_3$, $CaThO_3$, and $MgCeO_3$, are listed (Wyckoff, 1948) as compounds with the perovskite structure. In the present investigation, mixtures of 1:1 molecular proportion in the four binary systems involved were sintered at temperatures up to 1900° C. All show some solid solution between the component oxides but no evidence of an intermediate compound. $CaCeO_3$ and $CdCeO_3$† solid solutions have the fluorite structure, and constitute therefore an interesting example of anion-deficient solid solution. Compounds of the formula $A^{2+}B^{4+}O_3$, in which both A and B are small show the corundum —ilmenite structure.

The $A^{2+}B^{4+}O_3$ compounds which are closest to a line from $SrTiO_3$ to $BaThO_3$ on the chart (Fig. 2), approach most nearly the ideal cubic perovskite structure. In a direction toward a higher tolerance factor the structures are progressively more distorted; $BaTiO_3$ for example is tetragonal at room temperature. In the opposite direction, toward a

[b] For example, trivalent scandium and indium are assigned the same ionic radius by Pauling although the published parameters of simple isostructural compounds of indium and scandium are not the same. L. H. Ahrens (1952) presents reasons for preferring the Pauling radii, and it is probable that inconsistencies will be cleared up as more accurate crystal structure data are accumulated. For purposes of the present investigation the ratios of ionic radii appear to be more significant than close approach to absolute values of the radii.

† Conclusions regarding $CdCeO_3$ are doubtful because of loss of CdO by volatilization, especially above 1200°C.

smaller tolerance factor, the structures are distorted away from the simple cubic form, but in a different manner. Perovskite itself ($CaTiO_3$) probably should be considered as monoclinic (Naray-Szabo, 1943), while $CaZrO_3$ is reported as orthorhombic (Megaw, 1946).

The available data on compounds in which both the A and B cations are trivalent are less extensive and less well established. Some literature values are included in the results presented, but in almost every case they have been checked. It was the object of the investigation to collect more extensive data on the compounds formed from binary equimolar mixtures of the trivalent oxides, and to classify them into general structure types. The influence of certain factors on the structures can thereby be evaluated.

Preparation and Treatment of Mixtures

All of the materials used are from commercial sources and were not especially purified; the following are of C. P. grade or better; Al_2O_3, Ga_2O_3, Sc_2O_3, La_2O_3, Fe_2O_3, Cr_2O_3 and $Bi(OH)_3$. The following were quoted as being 99% pure: Y_2O_3,* Nd_2O_3,* Sm_2O_3,* and $Ce_2(C_2O_4)_3 \cdot 9H_2O$. Most of the starting materials are in an extremely fine state of subdivision.

Small batches, in most cases one gram or less, were weighed out in the required proportion and then finely ground together in a sintered alumina mortar. In some cases more reactive mixtures were prepared by dissolving the component oxides in nitric acid, diluting the solution and then simultaneously precipitating the hydroxides by adding the solution dropwise to an excess of ammonium hydroxide. The precipitated hydroxides were filtered and washed, dried below 300° C., and used especially for the low-temperature hydrothermal runs.

The general treatment procedure used was to fire the mixtures to progressively higher temperatures and to determine the phases present after different stages of treatment. For lower temperatures, charges were sintered in platinum crucibles in a globar furnace (to 1400° C.) and in a gas-air furnace (to 1650° C.). For higher temperatures (1650° to 1900° C.) a simple strip furnace was used. The strip furnace, modified slightly from the design of Roberts and Morey (1930), consists essentially of a thin sheet of 60% platinum 40% rhodium alloy, $\frac{1}{4}$ inch by $1\frac{1}{4}$ inches by .0015 inch thick, formed into a "U"-shaped element which constitutes both the resistor and the sample holder. The power source and control circuit for the strip resistor includes a constant voltage transformer, two variable transformers (Variacs), and a 25:1 stepdown transformer,

* Small amounts of some of the mixtures were also made up with 99.9% pure oxides; in no case was there any significant difference, as compared with the compounds prepared from 99% pure oxides.

which supplies up to 200 amperes at about 5 volts. The "U"-shaped resistor is supported on sheet-copper cooling fins and connected to the low-voltage side of the stepdown transformer by means of two silver blocks held in place by beryllium copper springs.

A small sample placed in the bottom of the "U" shaped strip resistor can be held at a desired temperature long enough for attainment of equilibrium and then quenched to room temperature by shutting off the current. The furnace has no refractories and the size and heat content of the strip resistor are so small in relation to the size of the silver contact blocks and copper cooling fins that the quench is very rapid, even faster than that obtained by dropping a charge from a conventional vertical tube furnace into mercury. Temperatures were read with an optical pyrometer calibrated in conjunction with the strip furnace at the melting temperatures of diopside, $CaMgSi_2O_6$ (1391.5°);[c] pseudowollastonite, $CaSiO_3$ (1546°); SiO_2 90%: CaO 10% (1708°); and rhodium (1960°).

For lower temperature hydrothermal runs, mixtures were wrapped in gold or platinum foil envelopes and heated in pressure vessels at the desired temperature and water pressure. Most of this work was done in so-called test-tube bombs (Roy, Roy and Osborn, 1950).

Examination of Products

The products in each case were examined by optical and x-ray methods; in addition, a number of them were thermally analyzed with the object of detecting possible inversion phenomena. Differential thermal analysis was performed with an automatic controller-recorder apparatus.

A set of high refractive index liquids, prepared according to the outline of Larsen and Meyrowitz (1951) proved to be satisfactory and much superior to high-index liquids previously available.[d] However, even with the extended range of index measurement (up to 2.00), the indices of refraction of most of the phases encountered are too high to be matched. A further difficulty results from the fact that a number of the more refractory mixtures do not develop any liquid at the highest temperatures attained, and the grain size of products is so small as to preclude obtaining useful information with the microscope. In many cases the fine grain size of products also has an effect on x-ray measurements. For example, it is difficult in some cases to obtain sufficiently well-crystallized material to permit distinction between an orthorhombic and a tetragonal distortion of the perovskite structure. X-ray powder diffraction data were obtained either with a 90-degree North American Philips Geiger-Counter spectrometer or with the 165 degree GE XRD-3 unit.

[c] Temperatures in degrees C., 1948 International Scale (Stimson, 1949).

[d] It was found necessary to maintain the 4 highest index liquids at a temperature of about 35°C. in order to prevent crystallization.

TABLE 1. SUMMARY OF SIGNIFICANT RUNS AND CRYSTAL STRUCTURES OBTAINED

Prepara-tion No.	Composition (Mol. Proportion of Oxides)		Initial Condition	Steam Pressure (p.s.i.)	Tempera-ture (° C.)	Time	Color of Product (Refl. Light)	Results of Microscopic and *X*-Ray Examination
			Smaller Cation Aluminum					
60	La_2O_3 Al_2O_3	1:1	f.g. oxides	—	1,640	90 min.	white	anisotropic (nearly isotropic): *$LaAlO_3$ (perovskite structure)*
			f.g. oxides	5,000	700	3 days	white	—(same)—
59	Ce_2O_3[1] Al_2O_3	1:1	f.g. oxides	—	1,640	90 min.	yel. green	mostly anisotrop., low birefringence: *$CeAlO_3$ (perovskite struct.)* and some CeO_2
58	Ce_2O_3 Al_2O_3	3:5	f.g. oxides	—	1,650	90 min.	yel. green	mostly anisotropic, low birefringence: *$CeAlO_3$ solid soln. (perovskite struct.)* and some CeO_2
61	Nd_2O_3 Al_2O_3	1:1	f.g. oxides	—	1,650	90 min.	pale viol.	anisotropic, low birefringence: *$NdAlO_3$ (perovskite structure)*
			$NdAlO_3$	5,000	600	3 days	pale viol.	—(same)—
62	Sm_2O_3 Al_2O_3	1:1	f.g. oxides	—	1,650	90 min.	yel. white	anisotropic, moderate birefringence: *$SmAlO_3$ (perovskite structure)*
			ppt. hydrox.	5,000	700	3 days	yel. white	—(same)—
67	Y_2O_3 Al_2O_3	1:1	f.g. oxides	—	1,800	2 hrs.	white	anisotropic: *$YAlO_3$ ($YCrO_3$ structure)*
			garnet and minor $YAlO_3$	—	1,700	1 hr.	white	mostly isotropic: *garnet solid solution* and small amt. of unknown phase
			$YAlO_3$	—	1,600	1 hr.	white	*garnet solid soln.* and minor $YAlO_3$
70	Y_2O_3 Al_2O_3	3:5	f.g. oxides	—	1,760	5 min.	white	isotropic: $Y_3Al_2(AlO_4)_3$ (*garnet struct.*). Inverts to high form at 1,970 ± 50° C. (Yoder and Keith, 1951)
71	In_2O_3 Al_2O_3	1:1	$InAlO_3$ (type "C")	—	1,700(L)	2 min.	pinkish white	anisotropic: unknown high form*[2]
			f.g. oxides	—	1,600	2 hrs.	pinkish white	isotropic, *$InAlO_3$ (Tl_2O_3 structure)*
			Smaller Cation Gallium					
103	La_2O_3 Ga_2O_3	1:1	f.g. $La(OH)_3$ and Ga_2O_3	—	1,000 1,475	24 hrs. 12 hrs.	colorless	*$LaGaO_3$* (perovskite structure)
79	Ce_2O_3 Ga_2O_3	1:1	f.g. oxides	—	1,700(L)	2 min.	pale brown	2 phases—1 isotropic, 1 anisotropic: CeO_2 and *$CeGaO_3$ (perovskite structure)*
			f.g. oxides	—	1,430	20 hrs.	pale brown	isotropic: *garnet* and CeO_2
			ppt. hydrox.	5,000	595	12 days	pale yellow	isotropic: *garnet* and CeO_2 (Liquidus temp. higher than No. 99)
99	Ce_2O_3 Ga_2O_3	3:5	ppt. hydrox.	10,000	600	18 days	pale orange	isotropic: *garnet* and CeO_2. Note—minor amt. of green glass in charge quenched from 1,430° C.

[1] ceria was added as the oxalate, $Ce_2(C_2O_4)_3 \cdot 9H_2O$.
(L) = completely or mostly liquid at indicated temperature.
[2] $InAlO_3$ high form has *x*-ray reflections at $2\theta = 10.1, 20.6, 31.0, 33.0, 37.7, 53.1, 55.6$ deg. (for Cu K_α).

TABLE 1—(*continued*)

Preparation No.	Composition (Mol. Proportion of Oxides)		Initial Condition	Steam Pressure (p.s.i.)	Temperature (° C.)	Time	Color of Product (Refl. Light)	Results of Microscopic and *X*-Ray Examination
77	Nd_2O_3	1:1	f.g. oxides	—	1,740(L)	2 min.	pale violet	
			$NdGaO_3$ (fused)	—	1200	3 hrs.	pale violet	anisotropic: *$NdGaO_3$ (perovskite structure)*
	Ga_2O_3		f.g. oxides	5,000	595	12 days		mostly isotropic: *garnet* and minor amt. of unknown phase
98	Nd_2O_3 Ga_2O_3	3:5	ppt. hydrox.	10,000	600	18 days	very pale violet	mostly isotropic: garnet and small amount of unknown phase
75	Sm_2O_3 Ga_2O_3	1:1	f.g. oxides	—	1,760(L)	2 min.	very pale yellow	acicular crystals, parallel extinction, uniaxial (+) moderate birefringence: (unknown structure)
			f.g. oxides	—	1,240	22 hrs.	very pale yellow	mostly isotropic: garnet and Sm_2O_3
76	Sm_2O_3 Ga_2O_3	3:5	f.g. oxides	—	1,715(L)	2 min.	very pale yellow	glass and rare acicular crystals: anisotropic high form (unknown structure); apparently inverts to garnet on grinding
			f.g. oxides	—	1,460	8 hrs.	very pale yellow	isotropic: *garnet* } (Liquidus temp. probably slightly higher than No. 75)
			f.g. oxides	5,000	650	9 days	very pale yellow	isotropic: *garnet* }
74	Y_2O_3 Ga_2O_3	1:1	f.g. oxides	—	1,810(L)	2 min.	—	glass, $N = 1.98 \pm 0.01$ (Liquidus temp. higher than No. 97)
			f.g. oxides	—	1,800(L)	2 min.	white	anisotropic acicular cryst. formed on quench, parallel extinction: (unknown structure)
			f.g. oxides	—	1,240	22 hrs.	white	isotropic, *garnet* solid solution
97	Y_2O_3 Ga_2O_3	3:5	f.g. oxides	10,000	600	9 days	white	mostly isotrop., rare larger cryst. anisotropic: *garnet* and smaller amt. yttrium hydrate
			Smaller Cation Chromium					
94	La_2O_3 Cr_2O_3	1:1	f.g. oxides sintered 20 hrs. at 1,300 deg.	—	1,860	2 min.	green	anisotropic, low birefringence: $LaCrO_3$ (*perovskite structure*)
63	Ce_2O_3 Cr_2O_3	1:1	f.g. oxides	—	1,700	1 hr.	black	translucent on thin edges, anisotropic, very low birefringence: *$CeCrO_3$ (perovskite struct.)* and small amt. CeO_2
			f.g. oxides	5,000	600	3 days	black	—(similar)—
84	Nd_2O_3 Cr_2O_3	1:1	f.g. oxides sintered 12 hrs. at 1,300 deg.	—	1,860	1 min.	greenish brown	anisotropic, very low birefringence: *$NdCrO_3$ (perovskite struct.)* and rare Cr_2O_3
65	Sm_2O_3 Cr_2O_3	1:1	f.g. oxides sintered 1 hr. at 1,600 deg.	—	1,670	75 min.	green	anisotropic, very low birefringence: *$SmCrO_3$* ($YCrO_3$ struct.) and and rare Cr_2O_3
			f.g. oxides	10,000	596	6 days	green	anisotropic: very low birefringence: *$SmCrO_3$* ($YCrO_3$ structure)
64	Y_2O_3 Cr_2O_3	1:1	f.g. oxides	—	1,860	5 min.	green	anisotropic, moderate birefringence: *$YCrO_3$ (type structure)*
			f.g. oxides	—	1,670	2 hrs.	green	—(same)—
			f.g. oxides	10,000	590	6 days	green	—(same and rare Cr_2O_3)—
100	Y_2O_3 Cr_2O_3	3:5	ppt. hydrox.	10,000	600	9 days	bright green	anisotropic, very low birefringence: *$YCrO_3$ solid solution*; *x*-ray pattern essentially identical to that of charge No. 64 (above)

TABLE 1—(*continued*)

Preparation No.	Composition (Mol. Proportion of Oxides)		Initial Condition	Steam Pressure (p.s.i.)	Temperature (° C.)	Time	Color of Product (Refl. Light)	Results of Microscopic and *X* Ray Examination
				Smaller Cation Iron				
85	La_2O_3 Fe_2O_3	1:1	f.g. oxides sintered 1,300 deg.	—	1,650(L)	1 min.	dark brown	anisotropic, very low birefringence: *$LaFeO_3$ (perovskite structure)*
66	Ce_2O_3 Fe_2O_3	1:1	f.g. oxides sintered 15 hrs. at 1,300 deg.	—	1,860(L)	3 min.	dark brown	translucent only on thin edges, anisotropic, weakly birefringent: *$CeFeO_3$ (perovskite struct.)* and small amt. of CeO_2
86	Nd_2O_3	1:1	f.g. oxides sintered 12 hrs. at 1,300 deg.	—	1,830(L)	1 min.	red brown	anisotropic, low birefringence: *$NdFeO_3$ ($YCrO_3$ structure)*
	Fe_2O_3		f.g. oxides	—	1,300	12 hrs.	red brown	—(same)—
69	Sm_2O_3 Fe_2O_3	1:1	$SmFeO_3$ fused at 1,810 deg.	—	1,680	2 min.	red brown	anisotropic moder. birefringence, magnetic: *$SmFeO_3$ ($YCrO_3$ structure)* (Liquidus temp. higher than No. 101 and No. 102)
101	Sm_2O_3 Fe_2O_3	3:5	f.g oxides	—	1,760(L)	2 min.	dark brown	
			$SmFeO_3$ solid soln. fused at 1,760 deg.	—	1,550	2 min.	dark brown	anisotropic: *$SmFeO_3$ solid soln. ($YCrO_3$ structure)* (Liquidus temp. approx. 170 deg. lower than No. 69)
102	Sm_2O_3 Fe_2O_3	5:3	$SmFeO_3$ solid soln. fused at 1,810 deg.	--	1,630	2 min.	brown	anisotropic: *$SmFeO_3$ solid soln. ($YCrO_3$ structure)* (Liquidus temp. approx. 100 degrees lower than No. 69)
68	Y_2O_3 Fe_2O_3	1:1	f.g. oxides	—	1,860(L)	3 min.	dark brown	translucent only on thin edges, anisotrop., moder. birefr.: *$YFeO_3$ ($YCrO_3$ struct.)*
73	In_2O_3 Fe_2O_3	1:1	f.g. oxides	—	1,600 (some liquid formed)	2 hrs.	yellow brown	isotrop: *$InFeO_3$ (Tl_2O_3 struct.)* and small amount of magnetite
				Smaller Cation Indium or Scandium				
80	La_2O_3 Sc_2O_3	1:1	f.g. oxides sintered 12 hrs. at 1,475 deg.	—	1,860	1 min.	pale violet pink	anisotropic: *$LaScO_3$ ($YCrO_3$ struct.)* and some unreacted La_2O_3
87	Ce_2O_3 Sc_2O_3	1:1	f.g. oxides sintered 12 hrs. at 1,300 deg.	—	1,860	1 min.	pale brown	anisotropic: *$CeScO_3$ ($YCrO_3$ struct.)*—incomplete reaction
			f.g. oxides	8,000	600	7 days	pale brown	—(same and some CeO_2)—
88	Nd_2O_3 Sc_2O_3	1:1	f.g. oxides	--	1,800	2 min.	white	anisotropic, moderate birefringence: *$NdScO_3$ ($YCrO_3$ structure)*
			f.g. oxides	8,000	600	5 days	white	—(same)—
81	Y_2O_3 Sc_2O_3	1:1	f.g. oxides	—	1,880	4 min.	very pale violet	Y_2O_3—Sc_2O_3 *solid soln. (Tl_2O_3 structure)* Some unreacted Y_2O_3 and Sc_2O_3 present
78	La_2O_3 In_2O_3	1:1	f.g. oxides	—	1,880(L)	2 min.	white	anisotropic: *$LaInO_3$ ($YCrO_3$ struct.)*
			f.g. oxides	5,000	650	9 days	white	—(same and unreacted La_2O_3)—

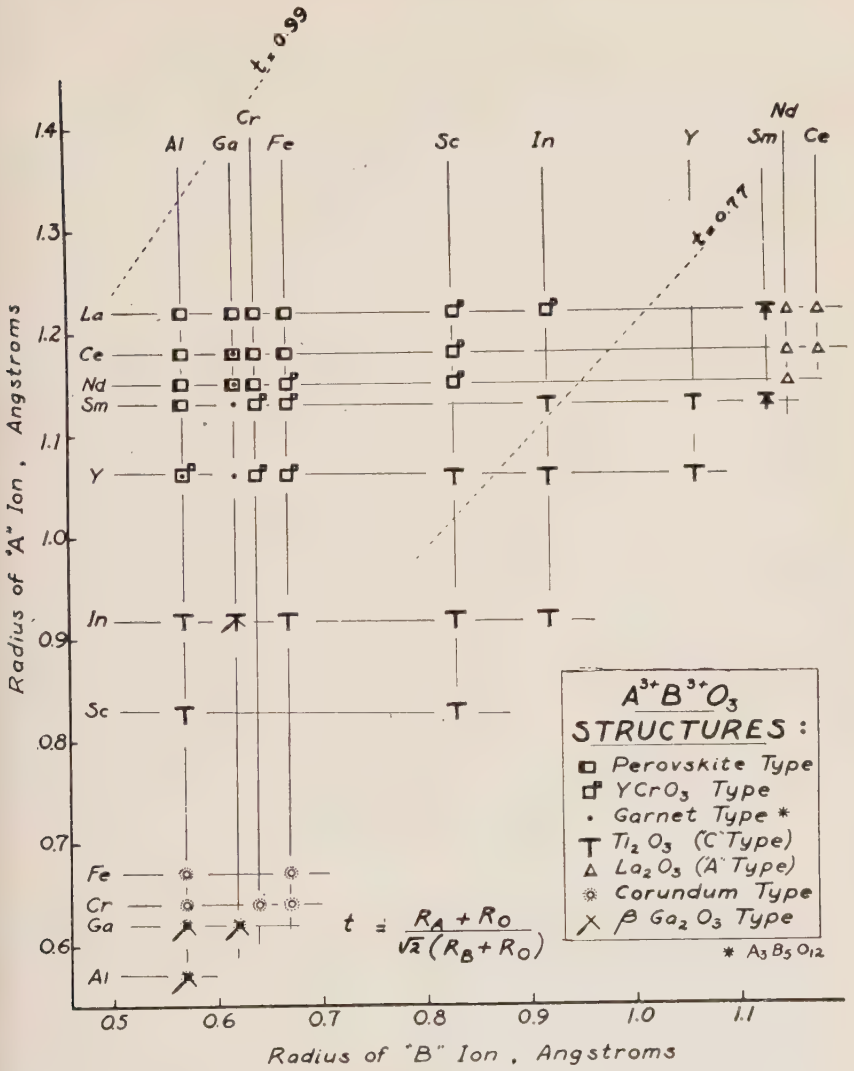

FIG. 3. Distribution of $A^{3+}B^{3+}O_3$ Structures in Relation to Cation Radii.

With both instruments filtered copper radiation was used. The spacings recorded were calibrated by running a partial pattern for NaCl on each chart; all spacings are in Angstrom units.

RESULTS

Results of the investigation are summarized in Table 1 and are shown in a schematic diagram (Fig. 3), a plot of the radius of the A^{3+} cation

versus the radius of the B^{3+} cation. Several of the compounds included in Fig. 3 have previously been reported; each was checked in the present study.

At least seven different structure types are formed by various double-oxide combinations of the trivalent elements considered. Those which either can be obtained as a "stranded" phase at room temperature or are stable at low temperatures include: perovskite, garnet, La_2O_3,* Tl_2O_3,* corundum, $YCrO_3$, and β-gallia type structures. Each structure is formed within specific limits of radius ratio. Near the limits of occurrence of each structure-type on the ionic radius chart (Fig. 3), some of the compounds and solid solutions show one structure at a higher temperature and another structure at a lower temperature. The general relationship between the principal high and low forms is as follows:†

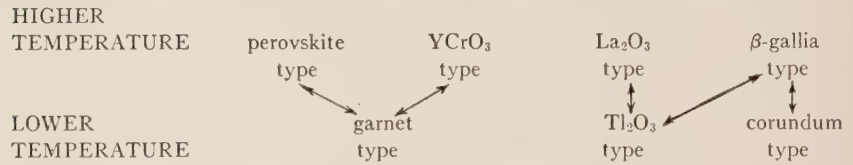

It should be emphasized that the investigation here reported is in the nature of a preliminary survey; the many binary systems represented have not been studied in detail. In some of the systems there may exist intermediate compounds other than those of 1:1 or 3:5 molecular proportion, and there may of course be other polymorphs than those recognized. Some of the polymorphs encountered have not yet been identified as to structure type, e.g. high temperature polymorphs in charges of compositions $InAlO_3$, $SmGaO_3$, $YGaO_3$ (Table 1).

It would be desirable to make complete studies of phase equilibria in some of the binary systems involved; it is proposed to attempt investigation of one or two of them as examples. Many of the systems present considerable experimental difficulty due to high liquidus temperatures. Those which show formation of some liquid in 1:1 preparations at temperatures below 1800° are: In_2O_3—Al_2O_3 and the systems in which gallium oxide and iron oxide are components. In a few cases the liquids formed could be quenched to a glass by the use of small charges on the strip furnace. In the system In_2O_3—Al_2O_3 a small amount of colorless, high index glass was encountered in a 1:1 preparation quenched from 1810°. Preparations of 1:1 and 3:5 molecular proportions in the system Sm_2O_3—Ga_2O_3 showed some glass in charges quenched from temperatures in the range 1675–1715°, while a 3:5 preparation in the system Ce_2O_3—Ga_2O_3 contained some yellowish green glass in charges quenched from tempera-

* Often called the A and C type rare earth oxide structures after Zachariasen (1927).

† The B-type rare-earth oxide structure is not considered.

TABLE 2. POWDER DIFFRACTION DATA FOR COMPOUNDS CLASSED AS HAVING THE PEROVSKITE STRUCTURE

$LaAlO_3$	$LaGaO_3$	$LaCrO_3$	$LaFeO_3$
Well-formed crystals $a_0 = 3.778 \pm .001$ Very nearly cubic Good pattern	Good pattern, a_0 (equiv.) $= 3.875 \pm .003$ V. slight distortion**	Fair pattern, a_0 (equiv.) $= 3.880 \pm .005$ V. slight distortion probably monoclinic (not tetragonal or rhombic)	Fair pattern, a_0 (equiv.) $= 3.915 \pm .005$ V. slight distortion possibly monoclinic
$CeAlO_3$	$CeGaO_3$	$CeCrO_3$	$CeFeO_3$
Fair pattern; little CeO_2 present, a_0 (equiv.) $= 3.77 \pm .02$ Tetragonal distortion reported*	Very poor pattern Abundant CeO_2, a_0 (equiv.) $= 3.87$	Fair pattern V. little CeO_2, a_0 (equiv.) $= 3.851 \pm .007$ Nearly cubic	Poor pattern CeO_2 present, a_0 (equiv.) $= 3.89 \pm .03$ Largest distortion probably monoclinic (not tetragonal)
$NdAlO_3$	$NdGaO_3$	$NdCrO_3$	
Good pattern, a_0 (equiv.) $= 3.73 \pm .01$ Rhombohedral distortion	Fair pattern, a_0 (equiv.) $= 3.86 \pm .015$ Rhombohedral or monoclinic distortion	Fair pattern, a_0 (equiv.) $= 3.84 \pm .02$ Rhombohedral or monoclinic distortion	
$SmAlO_3$			
Good pattern plus unknown phase, a_0 (equiv.) $= 3.71 \pm .01$ Probably rhombohedral distortion			

* Zachariasen (*Acta Cryst.*, **2**, 388, 1949) reported a tetragonal cell for $CeAlO_3$. Our results do not confirm this since the 111 reflection is a symmetrical doublet.

** Only a study of the first few reflections (at low angles) was made to classify the type of distortion (see Megaw, 1946). The a_0 (equivalent) reported for each of the perovskites is a somewhat arbitrary value arrived at by using a weighted average for each line which was split.

tures as low as 1430°. Only one preparation was obtained entirely as a glass: a charge of 1:1 molecular proportion in the system Y_2O_3—Ga_2O_3, quenched from 1880°, yielded a colorless glass with index of refraction $= 1.98 \pm .01$.

Liquids in the iron-oxide bearing systems crystallize very rapidly and could not be quenched to glass. Small charges in some cases undercool appreciably and then crystallize rapidly with an accompanying visible exothermic effect.

It should be noted that iron-oxide bearing systems in air cannot be considered as binary because of the presence of FeO in increasing proportion at higher temperatures. In several of the mixtures made up with Fe_2O_3 as a component, reduction in some runs was sufficient to yield a spinel phase. For the same reason, many of the earlier reports on ferrates are open to question, since no mention is made of the difficulty of maintaining iron in one valence state. The same qualification, based upon the

possibility of different valence states of cations as a function of temperature, applies to some other components of systems referred to, for example to cerium oxide.

By comparison of Figs. 2 and 3 it will be seen that $LaAlO_3$ occupies a chart position similar to that of $SrTiO_3$ (i.e. has similar ionic radius ratio); $LaAlO_3$ is the most nearly cubic‡ of the perovskite-structure combinations of double oxides of trivalent elements. If progressively smaller cations are substituted in the place of lanthanum, the structures are distorted more and more away from the simple cubic form. $LaAlO_3$ is isotropic or very nearly so, while the aluminates of cerium, neodymium and samarium exhibit low to moderate birefringence, greatest for $SmAlO_3$.

TABLE 3. POWDER *X*-RAY DIFFRACTION DATA FOR COMPOUNDS CLASSED AS GARNET STRUCTURES

hkl	$3Y_2O_3:5Al_2O_3$		$Y_2O_3:Al_2O_3$*		$3Sm_2O_3:5Ga_2O_3$**	
	"*d*"	I/I_0	"*d*"	I/I_0	"*d*"	I/I_0
211	4.89	35	4.90	35	5.04	7
220	4.24	10	4.25	10		
321	3.21	20	3.202	25		
400	3.00	30	2.995	28	3.089	35
420	2.69	100	2.681	100	2.763	100
422	2.45	25	2.447	30	2.525	40
431	2.36	5	2.350	12	2.428	5
521	2.19	30	2.187	40	2.259	10
440	2.13	5	2.125	10	2.201	12
611	1.952	30	1.945	55	2.01	15
631	1.772	2	1.768	5		
444	1.734	25	1.7307	45	1.786	20
640	1.666	40	1.662	70	1.715	30
633	1.635	10	1.6313	25	1.68	2
642	1.608	35	1.602	65	1.6584	40
651	1.528	5	1.5234	10		
800	1.503	15	1.499	30	1.544	15

Unit cell edges for these compounds obtained from the above data and analogous data for other patterns are as follows: (given in Angstroms) $3Y_2O_3 \cdot 5Al_2O_3$ $a_0 = 12.01 \pm .02$; $Y_2O_3 \cdot Al_2O_3 = 11.989 \pm .005$; $Y_2O_3 \cdot Ga_2O_3 = 12.30 \pm .05$; $Sm_2O_3 \cdot Ga_2O_3$ $a_0 = 12.465 \pm .025$; $3Sm_2O_3 \cdot 5Ga_2O_3 a_0 = 12.355 \pm .015$; $Nd_2O_3 \cdot Ga_2O_3$ $a_0 = 12.54 \pm .02$.

* The anomalous decrease in cell size from $3Y_2O_3 \cdot 5Al_2O_3$ to $YAlO_3$ is noteworthy.

** The data are given for the 3:5 composition since the solid solution does not quite extend as far as $SmGaO_3$, and the latter pattern has some other lines in it.

‡ It would appear that $LaAlO_3$ is not perfectly cubic, since several lines in the back reflection region show an asymmetric broadening of the α_1 and α_2 reflections. The maximum splitting is such that the separation is less than half the separation between α_1 and α_2.

They still show the fundamental perovskite structure with some simple splitting of *x*-ray reflections, indicating a lower symmetry, but with no apparent doubling of the cell. All such compounds, though not isotropic, have been classified as perovskite structures. *X*-ray data are given in Table 2.

When yttrium is substituted in the place of samarium, we no longer obtain a perovskite structure at moderately high temperatures, but rather a garnet, of ideal formula $Y_3Al_2(AlO_4)_3$ or $3Y_2O_3 \cdot 5Al_2O_3$ (yttrogarnet), the structure of which has been worked out earlier (Yoder and Keith, 1951). A mixture of equal molecular proportions of Y_2O_3 and Al_2O_3 can be reacted by sintering to give a phase with the same structure; the garnet structure apparently is tolerant not only to Al^{3+} in both six-fold and four-fold coordination, but also to replacement of about half of the six-coordinated aluminum by yttrium, as represented by the formula $Y_3YAl(AlO_4)_3$. Yttrium, samarium, neodymium, and cerium oxides in combination with Ga_2O_3 similarly form intermediate compounds which have the garnet structure.

Above a temperature of about 1970° C. yttrogarnet inverts to a high form called yttroalumite, which is probably tetragonal. The indexing of the yttroalumite *x*-ray pattern arrived at by Dr. G. Donnay in a preliminary study (Yoder and Keith, 1951, p. 531) was found to be unsatisfactory; using Bunn type charts a more satisfactory cell was derived which is related to the earlier-determined cell by a simple doubling of the "*a*"-axis. In the present investigation nine other new compounds have been prepared which have essentially the same structure as yttroalumite but which form at lower temperatures; this group of isostructural compounds is referred to one of them, $YCrO_3$ as the type structure. We have not found any analogue to the $YCrO_3$ structure among double oxides of cations other than those of the trivalent group. The *x*-ray pattern bears a remote similarity to those of distorted perovskite structures, but the distortion is well beyond that which gives a simple splitting of the *x*-ray reflections of perovskite and there appears to be justification for classifying the $YCrO_3$ type structures separately. Powder diffraction data are listed in Table 4.

Extensive solid solution in both the $YCrO_3$ type structures and the garnet structures makes it difficult to decide whether the $YCrO_3$ type should be considered to have an ideal 1:1 molecular proportion rather than, say, a 3:5 molecular proportion. A final answer must await completion of phase equilibrium studies of the binary oxide systems involved. On the basis of preliminary studies in the system Sm_2O_3—Fe_2O_3 it is concluded that a 1:1 ideal molecular proportion is probably correct. The intermediate compound has the yttrium chromate structure and a preparation of 1:1 molecular proportion has a liquidus temperature about

TABLE 4. POWDER *X*-RAY DIFFRACTION DATA FOR $YCrO_3$-TYPE COMPOUNDS

hkl	$3Y_2O_3:5Al_2O_3$		$YCrO_3$		$SmCrO_3$		$NdFeO_3$		$SmFeO_3$		$NdScO_3$		$YFeO_3$		$LaScO_3$		$LaInO_3$	
	"*d*"	I/I_0	"*d*"	I/I_0	"*d*"	I/I_0	"*d*"	I/I_0	"*d*"	I/I_0	"*d*"	I/I_0	"*d*"	I/I_0	"*d*"	I/I_0	"*d*"	I/I_0
002	4.24	5																
102	3.70	45	3.80	10			3.885(d)	15	3.867	7	3.98(d)	25			4.07	30		
200	3.68	40	3.754	10	3.84(d)	15			3.83	7								
201	3.36	25																
112	3.32	20	3.389	35	3.43	15	3.478	7	3.445	10	3.56	5	3.427	15	3.63	7	3.707	5
									3.015	2							3.2(d)	VW
003	2.89	3	2.950	10	2.98	2												
103	2.67	40	2.750	35	2.75	25	2.783	20	2.797	25	2.88	20	2.78	20	3.017	15	2.96	25
212	2.62	100	2.67	100	2.675	100	2.738	100	2.72	100	2.825	100	2.694	100	2.867	100	2.903	100
220	2.59	30	2.607	40	2.615	30	2.714	20	2.67	20	2.78	20	2.622(d)	30	2.73	10	2.85	30
113	2.51	25	2.585	20	2.593	20	2.62	5	2.628	2							2.79	5
203	2.26	3	2.485	5													2.72	5
222	2.22	15	2.256	20	2.28	5					2.405	5	2.270	7	2.42	7	2.455	5
213	2.16	25	2.222	12	2.227	10	2.259	7		VW	2.338	5	2.16(d)	7	2.36	15	2.30	5
302	2.12	20	2.143	20	2.2178	15	2.217	10		VW	2.28	10			2.33	20	2.27	15
104			2.125	7	2.146	10	2.18	7		VW	2.211	7	2.108	10	2.24	10		
312	2.05	15	2.094	20	2.113	10	2.15	10		VW								
114	1.996	3	2.049	7	2.06	2												
321	1.972	3	1.998	3														
204	1.859	40	1.895	45	1.912	30	1.94(d)	35	1.933	30	1.977	30	1.920	20	2.025	50	2.053	70
400	1.845	30	1.877	35	1.899	25			1.918	5	1.953	5	1.895	20	1.973	25	2.014	5
214	1.806	20	1.852	20	1.866	10	1.886(d)	15	1.89	2	1.941	7	1.857(d)	15			1.993	10
331	1.694	2	1.838	25	1.855	20			1.873	7							1.87	12
412			1.685	30	1.701	10	1.74(d)	7	1.716	25	1.786	15	1.752	5	1.811	15	1.821	15
224	1.655	10									1.768	18	1.704(d)	20	1.781	15		
											1.727	2			1.666	50	1.698	25
304	1.640	25	1.664	7	1.692	20	1.713	15			1.650(d)	10			1.651	50	1.686	15
314	1.605	10	1.626	10													1.658	45

(d) indicates double reflection.

170° higher than that of the 3:5 composition and about 100° higher than that of the 5:3 composition. That is, there appears to be a maximum on the liquidus curve at a composition corresponding to $SmFeO_3$. Liquidus temperatures in the system Y_2O_3—Cr_2O_3 are too high to permit a similar study of the liquidus curve near $YCrO_3$ with available equipment.

Further work will be required in order to elucidate in detail the relationships among the garnet, perovskite, and $YCrO_3$ structures. It will be noted that perovskite structures give way to garnet and $YCrO_3$ structures as the tolerance factor is decreased below about 0.9; as the tolerance factor is further decreased, that is in combinations of smaller "A" cations with larger "B" cations, we move into a chart area in which cubic structures of the Tl_2O_3 type are obtained in the preparations of 1:1 molecular proportion (Fig. 3). In each case either one or both of the component oxides also has that structure, so that the 1:1 preparation should be considered as a member of a solid solution series rather than as an intermediate compound in the strict sense of the phase rule. In those cases in which both component oxides have the Tl_2O_3 structure, solid solution probably is complete.

At the extreme chart corner where the two combining cations represented are relatively large and of approximately the same effective radius, hexagonal structures of the La_2O_3 type are obtained in 1:1 preparations. At the opposite extreme chart corner, where are represented double-oxide combinations of two relatively small cations of approximately the same radius, structures are either the corundum type or the β-gallia type. In these cases (i.e. for La_2O_3, corundum, and β-gallia type structures) as in the case of the Tl_2O_3 structures discussed above, the structures obtained in 1:1 preparations are of the same type as that of one or both of the component oxides. The single known exception is the low temperature form of $GaAlO_3$ (Hill, Roy, and Osborn, 1952).

It will be noted that double-oxide combinations with trivalent bismuth as the "A" cation are not included in Fig. 3. $BiAlO_3$ and $BiCrO_3$ have been reported as having the perovskite structure (Naray-Szabo, 1943) and that structure would appear to be reasonable from consideration of the ionic radii. It was not found feasible to confirm the structures of double-oxide combinations with bismuth because the volatility of Bi_2O_3 makes it difficult to obtain solid state reactions with Al_2O_3 and Cr_2O_3. An investigation is being made of compounds formed hydrothermally at lower temperatures.

The ionic radius chart (Fig. 3) has not been extended to include boron. The ionic radius of B^{3+} is much smaller than that of Al^{3+} and the structures of double-oxides with boron are quite different. Mixtures corresponding to $LaBO_3$, YBO_3, and $InBO_3$ were prepared by the method used

by Goldschmidt and Hauptmann (1932) and also by our usual methods. The present results confirm those of Goldschmidt and Hauptmann in regard to the formation and crystal structure of $InBO_3$ and $LaBO_3$; both form easily at 1000° C. The structure of $InBO_3$ was found to be of the calcite type with a somewhat larger unit cell than that reported by Goldschmidt. $LaBO_3$ formed by reaction at 600° and at 1000° has the aragonite structure (cell dimensions very similar to those of strontianite); it melts sharply at $1560 \pm 20°$ and crystallizes below that temperature to a high form which has a superficial resemblance to calcite, including similar birefringence and cleavage, but which is biaxial positive and has a powder pattern (Table 5) quite different from those of calcite and aragonite. There is a possibility of some compositional change due to loss of B_2O_3 but this was minimized by using very short heating time at the higher temperatures. No inversions were detected in the low temperature form up to 1050° C. Refractive indices for the high form were determined as: $\gamma(Na) = 1.860 \pm .003$, $\alpha(Na) = 1.820 \pm .003$.

YBO_3 is reported in the literature as having either the calcite structure or the vaterite structure, depending upon the temperature of formation

Table 5. *X*-ray Powder Diffraction Data for New Borates

$LaBO_3$ (high form)		YBO_3	
"*d*"	I/I_0	"*d*"	I/I_0
5.64	7	4.375	30
3.91	20	3.277	100
3.10	100	3.06	10
3.01	90	2.62	60
2.86	5	2.195	10
2.54	7	1.885	35
2.13	10	1.82	25
2.085	3	1.73	20
2.07	2	1.631	7
2.01	15	1.532(d)	15
1.946	5	1.337	5
1.916	15	1.311	2
1.875	3	1.328	2
1.828	7	1.189	10
1.610	5		
1.51	10		
1.378	5		
1.281	5		
1.230	5		
1.207	10		
1.162	7		

(Goldschmidt and Hauptmann, *op. cit.*). The YBO_3 compound obtained in the present investigation exists in only one crystal form from room temperature to its melting point ($1580 \pm 20°$); it has optical characteristics somewhat similar to those of calcite, but giving a positive uniaxial interference figure and an *x*-ray powder pattern (Table 5) which does not correspond to either the calcite type or the vaterite type as given by Brooks, Clark, and Thurston (1951). The refractive indices are $\alpha(\text{Na}) = 1.77 \pm .01$ $\gamma(\text{Na}) = 1.795 \pm .01$.

Mixtures of $CrBO_3$ composition did not yield an intermediate compound. After heating to 1000° C., the *x*-ray diffraction pattern showed the presence of only Cr_2O_3 as a crystalline phase. On prolonged heating (7 days), the B_2O_3 gradually volatilized and the Cr_2O_3 (originally very fine grained) was found to have grown into hexagonal crystals of much larger size (to 0.1 mm. diameter). A similar phenomenon was observed upon heating the $InBO_3$ mixture for a few minutes at 1700° C.; dissociation of the $InBO_3$ compound and volatilization of the B_2O_3, left behind well-formed yellowish brown cubes of In_2O_3. These observations suggest a method for growing the refractory oxides (and possibly some other compounds) into crystals large enough for single-crystal studies.

Discussion of Results

A number of trivalent elements, including some which can exist in trivalent condition as well as in other valence states, were not included in the present study. However, the element combinations which have been studied are sufficiently representative of different ionic radius ratios to form a basis for predicting the probable structures in some cases. Actinium, with ionic radius slightly larger than that of lanthanum, as well as trivalent protoactinium and the trivalent ions of the transuranium elements, all slightly smaller than lanthanum, may form perovskite structures in double-oxide combinations with aluminum, gallium, chromium, and iron.

The 4f elements 63 to 66 inclusive, and trivalent thallium, with ionic radii between those of samarium and yttrium, may form garnet structures in double-oxide combinations with aluminum and gallium, and possibly $YCrO_3$ type structures with chromium and iron. In some cases a garnet structure may be stable at low temperatures and a $YCrO_3$ type structure at higher temperatures. Similar structural relations are possible for the double-oxides of elements 67 to 71 inclusive in combination with aluminum, gallium, chromium or iron. However, the smallest ion of the 4f group may more nearly fulfill size requirements for the formation of Tl_2O_3 type structures in double-oxide combinations with chromium and iron.

Other trivalent ions which have not been mentioned* have ionic radii in a range which suggests that they might form perovskite-type structures in double-oxide combinations with the largest of the "A" cations, e.g. with lanthanum (see Jonker and van Santen, 1948) and cerium. However, the Pauling radii place Sb^{3+} and V^{3+} closer to Sc^{3+} than to Fe^{3+}, that is in a chart area (Fig. 3) in which the $YCrO_3$-type structure would be more likely for combinations with La^{3+} and Ce^{3+}. All of the above suggestions should be qualified to the extent that predictions of probable structures are more likely to be correct for ions which have polarizabilities nearly the same as those of the cations whose double-oxide combinations have been studied, and on which the chart (Fig. 3) is based.

Goldschmidt, in his several publications, considered the importance of radius, polarizability and charge of an ion in determining the positions it could take in specific structures. The influence of ionic radius is discussed and illustrated in all textbooks on crystal chemistry. The present study does not include cations with sufficiently different polarizability to permit conclusions as to the effect of that variable. However, for the first time the effect of ionic charge can be demonstrated clearly; by comparison of Figs. 2 and 3 it can be seen that the extent of perovskite structures is more limited in the combinations of trivalent cations than in combinations of a bivalent and a tetravalent cation. The effect of cation charge ratio upon the lower limit of "t", the tolerance factor for perovskite structures, is as follows:

Compounds (A = larger cation)	Charge ratio, Z_A/Z_B	Lower Limit of "t"
$A^{3+}B^{3+}O_3$	1.0	0.89
$A^{2+}B^{4+}O_3$	0.5	0.77
$A^{+}B^{5+}O_3$	0.2	0.71 to 0.81* (prob. closer to 0.71)

* Bracketed by the "t" values for $NaNbO_3$ (perovskite structure) and $LiNbO_3$ (corundum structure).

The so-called tolerance limits of Goldschmidt are therefore seen to be applicable only to compounds of cations with one combination of charges. Goldschmidt's original perovskite tolerance limits, for example, should be restricted to $A^{2+}B^{4+}O_3$, combinations and cannot be used indiscriminately for different charge combinations without appropriate modification.

Several discrepancies in the older literature have been clarified. For

* e.g. trivalent arsenic, antimony, vanadium, cobalt, and manganese.

example Goldschmidt (1927) listed $YAlO_3$ as having the perovskite structure and that listing has been copied in a number of later publications. Recently Wood (1951) noted the borderline position of $YAlO_3$ on the ionic radius chart between the perovskite structures and the corundum-ilmenite structures and raised the question as to which structure pure $YAlO_3$ would have. The present investigation shows that it has neither of these structures but forms a garnet structure which inverts to a $YCrO_3$ type structure at high temperature. Wood also commented on the anomalous position of $CaCeO_3$ and $CdCeO_3$; it has been shown that these compositions do not have the perovskite structure but contain members of solid-solution series which have the fluorite structure.

Table 6. Preliminary Measurements of Dielectric Constant of Pressed Discs of Some Crystalline Compounds Prepared for the Investigation of Double Oxides of Trivalent Elements*

Preparation Number	Composition	Structure Type	Temperature Degrees C.	Dielectric Constant
104	$LaBO_3$	aragonite	−180	1.6
			25	13.5
			516	34.5
105	$InBO_3$	calcite	−180	3.6
			25	5.5
			562	21.5
63	$CeCrO_3$	perovskite	−180	4.0
			25	85
			165	665
84	$NdCrO_3$	perovskite		n.d.
	(too highly conducting to be measured)			
62	$SmAlO_3$	perovskite	−180	5.1
			25	5.9
			616	33
59	$CeAlO_3$	perovskite	−180	9.0
			25	209
			276	1796
67	$YAlO_3$	garnet solid solution	−180	1.8
			25	7
			467	366

* Measurements of Dielectric Constant by E. Francis and R. Eriks, Physics Department, Pennsylvania State University.

One of the reasons for undertaking a survey of crystal structures of double oxides as a function of ionic radii of the cations was to establish a basis for study of special properties of some of the compounds and the direction of change of properties as a result of substitution of cations of different radius. For example, an investigation is being undertaken of the variation of dielectric constant. Preliminary data for a few of the compounds (Table 6), based upon measurements made by E. Francis and R. Eriks of Dr. R. Pepinsky's laboratory, Pennsylvania State University, indicate that $CeAlO_3$ and $CeCrO_3$ may be of interest as dielectric materials. Both of those compounds have the perovskite structure. It should be emphasized that measurements were made on discs formed by compacting the powdered materials in a pellet press. No correction is made for porosity of the discs and the measurements of dielectric constant may be expected to be lower, as well as less significant, than measurements made on single crystals or crystal slices. Further work is needed in order to locate possible peaks on the curves of dielectric constant versus temperature.

Under contract with the Signal Corps, the investigation of ionic substitutions is being extended to include several other groups of multiple cation combinations than the 3 plus: 3 plus group, as well as some anion substitutions in the place of oxygen. It is believed that accumulation of data on general relationships between crystal structure types and electrical properties will contribute towards a basis for setting up a useful theory regarding the fundamental requirements for high dielectric constant and low power-factor.

Determination of the crystal structures of double oxides also has a bearing on studies of the natural occurrence of some comparatively rare elements. For example, those which form garnet structures in double-oxide combinations with more common elements may be found in appreciable quantity in natural garnets. Many of the new compounds, as well as the binary systems involved, thus offer potentially valuable studies in the fields of geochemistry and mineralogy as well as in the field of ceramic technology.

Acknowledgment

The authors wish to acknowledge the assistance of Merrill R. Shafer in the preparation and thermal analysis of several of the mixtures.

Part of this work was performed under contract to the U. S. Army Signal Corps; Frequency Control Branch, Contract No. DA 36-039 sc 5594.

References

Ahrens, L. H. (1952), The use of ionization potentials. Part I. The ionic radii of the elements: *Geochim. Cosmochim. Acta*, **2,** 155–169.

Goldschmidt, V. M., et al. (1923–1937), Geochemische Verteilungsgesetze der Elemente I–IX: *Skrift. Norske. Vid. Akad. Oslo, I Mat.-Naturv. Kl.*

Goldschmidt, V. M., and Hauptmann, H. (1932), Isomorphie von boraten und Karbonaten: *Nachr. Ges. Wiss. Gott. Math-Phys. Kl.*, 53–72.

Hill, V. G., Roy, Rustum, and Osborn, E. F. (1952), The system alumina-gallia-water: *Jour. Am. Ceram. Soc.*, **35,** 135–142.

Jonker, G., and van Santen, J. H. (1950), Ferromagnetic compounds of manganese with the perovskite structure: *Physica*, **16,** 337.

Larsen, E. S. Jr., and Meyrowitz, R. (1951), Immersion liquids of high refractive index: *Am. Mineral,*. **36,** 746–750.

Matthias, B. T. (1949), New ferroelectric crystals: *Phys. Rev.*, **75,** 1771, and Ferroelectric properties of WO_3: *ibid.*, **76,** 430.

Megaw, H. D. (1946), Crystal structure of double oxides of the perovskite type: *Proc. Phys. Soc. London*, **58,** 133–152.

Naray-Szabo, I. (1943), The structural type of perovskite: *Naturwiss.* **31,** 202–203.

Rankama, K., and Sahama, Th. G. (1949), Geochemistry, University of Chicago Press, Chicago.

Roberts, H. S., and Morey, G. W. (1930), A micro-furnace for temperatures above 1000° C.: *Rev. Sci. Inst.*, **1,** 576–580.

Roberts, S. (1949), Dielectric constants and polarizabilities of ions in simple crystals and $BaTiO_3$: *Phys. Rev.*, **76,** 1215–1220.

Roberts, S. (1951), Polarizabilities of ions in perovskite type crystals: *Phys. Rev.*, **81,** 865–868.

Roy, R., Roy, D. M., and Osborn, E. F. (1950), Stability and compositional relationships among the lithium alumino-silicates, eucryptite, spodumene and petalite: *Jour. Am. Cer. Soc.*, **33,** 152–159.

Stimson, H. F. (1949), The International Temperature Scale: *J. Res. Natl. Bur. Stand.*, **42,** 209–217.

Structure Reports (1951), General Editor, A. J. C. Wilson, Oosthoek, Utrecht.

Wood, E. A. (1951), Polymorphism in potassium niobate, sodium niobate and other ABO_3 compounds: *Acta Cryst.*, **4,** 353–362.

Wyckoff, R. W. G. (1948, 1951), Crystal structures: *Interscience*, New York.

Yoder, H. S., and Keith, M. L. (1951), Complete substitution of aluminum for silicon: the system $3\,MnO \cdot Al_2O_3 \cdot 3SiO_2$—$3Y_2O_3 \cdot 5Al_2O_3$: *Am. Mineral.*, **36,** 519–533.

Zachariasen, W. H. (1928), Untersuchungen uber die kristallstruktur von sesquioxyden und verbindungen ABO_3: *Skrift. Norske. Viden, Akad. Oslo, I. Nat.-Naturv. Klasse*, No. **4,** 1–165.

Manuscript received Sept. 22, 1952

UNIT CELL OF HYDROMAGNESITE

Joseph Murdoch, *University of California at Los Angeles, California.*

Abstract

X-ray study of hydromagnesite crystals confirms the monoclinic character of the mineral, but shows that it is pseudo-orthorhombic in structure. Equator, first and second layer line Weissenberg photographs show that the presently accepted a axis should be doubled. Systematic extinctions show the symmetry to be a near match for $D_2^5(C222_1)$, with a few faint spots unaccounted for. *X*-ray powder photographs can be satisfactorily indexed using the formula for an orthorhombic structure. The unit cell dimensions determined by Weissenberg photographs are in reasonably close agreement with previously determined values, if a_0 is taken as twice the earlier value. These measurements are as follows:

$$a_0 = 18.58 \text{ Å}, \qquad b_0 = 9.06 \text{ Å}, \qquad c_0 = 8.42 \text{ Å}.$$

Typical crystals are pseudo-orthorhombic, due to multiple twinning on {100}, and goniometric measurements are consistent with previous determinations.

Introduction

Previous work on hydromagnesite has shown certain inconsistencies, some writers considering the mineral to be monoclinic, others orthorhombic. An early investigation by J. D. Dana (1) gave a probably monoclinic symmetry with β about 107°. Weinschenk (2) in studying crystals optically, observed multiple twinning and oblique extinction in the sections showing this twinning. He considered the mineral to be monoclinic. Brugnatelli (3) was unable to find any but parallel extinction, and concluded from the morphology and optics that hydromagnesite must be orthorhombic. E. S. Dana (4), p. 304, however, confirmed the monoclinic character of the crystals, but stated that β must be very close to 90°. Goldschmidt (5) in the Winkeltabellen lists it as orthorhombic. Rogers (6) measured some crystal angles under the microscope and calculated others, using minute crystals from Alameda County, California. He observed multiple twinning on {100} with oblique extinction on {010} ($\beta \wedge c = 42° 51'$). From these observations, he concluded that the mineral is definitely monoclinic, owing its orthorhombic aspect to twinning. Assuming Dana's pyramid to be {011}, and taking a small {$h0l$} face as {001}, he calculated β to be 114° 33′ 20″.

Fenoglio (7, 8) made the first x-ray study of hydromagnesite, taking powder photographs, Laue photographs, and rotation photographs about c. From these he derived a rectangular lattice, which he called orthorhombic, space group D_{2h}^1. He recognized the presence of oblique extinction in some sections, but attempted to explain it by twinning on {021}, which would produce the proper obliquity. His diagram to demon-

strate this theory is shown in Fig. 1, together with the optical orientation and twinning plan according to Rogers.

Crystallography

Recently the author received specimens of well crystallized hydromagnesite from Crestmore, California, and it seemed desirable, in view of discrepancies among earlier observations, to attempt a more complete *x*-ray and morphological study of the mineral. The available material included small but well developed crystals, and measurements on the

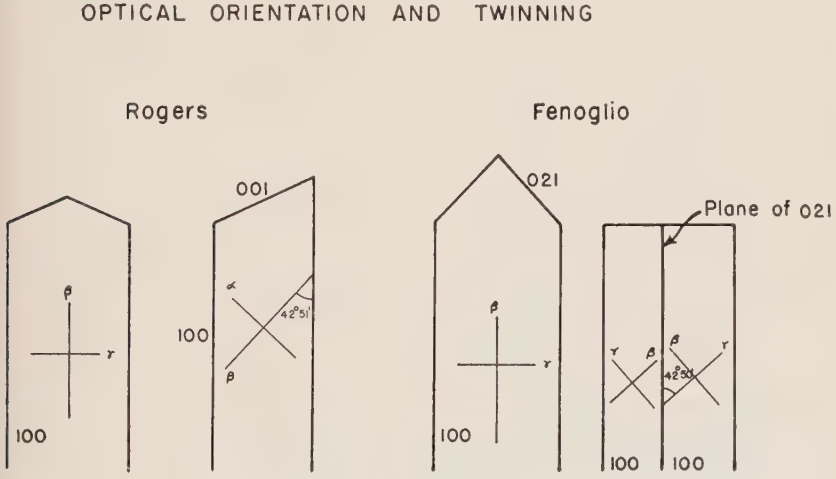

Fig. 1

goniometer gave results which are in reasonable agreement with earlier morphological work. Crystals are of typical lath-like habit, with {100} dominant, {210} usually present, with striations indicating other prisms which were unmeasurable, {111} always present and usually excellent. A few crystals showed {121}, {101} and {201} as well. The following Table 1 shows the angles for these forms as calculated from the *x*-ray pictures, and as measured on the goniometer.

Multiple twinning on {100} as observed by Rogers, is universally present. The twin lamellae are sometimes almost submicroscopic in thickness, so that a true extinction angle is sometimes difficult to measure. However, apparently simple lamellae give an average extinction angle of about 35° on *c* as compared with Rogers' value of 42° 51′. It may be that submicroscopic twinning is responsible for this apparent variation.

TABLE 1

Form	*Calculated*		*Measured* (average)	
	ϕ	ρ	ϕ	ρ
a 100	90°00′	90°00′	90°00′	90°00′
l 210	44°17′	90°00′	44°28′	90°00′
k 101	90°00′	24°23′	88°12′	24°12′ (poor)
d 201	90°00′	42°11′	90°00′	45°12′ (poor)
p 111	26°00′	45°57′	25°43′	45°55′
t 121	13°42′	62°24½′	14°47′	63°30′ (poor)

EQUIVALENT FORMS

Dana	*Rogers*	*Murdoch*
100	100	100
110	110	210
101	001	101
201	101	201
121	011	111
141	021	121
181	041	141

X-RAY STUDY

X-ray powder photographs were taken of selected pure material using copper radiation and nickel filter. The resulting spacings and intensities are shown in the accompanying Table 2, and agree well with Fenoglio's, although showing many more lines than he reported.

"Single" crystal photographs were then taken with the Weissenberg camera, also using copper radiation and nickel filter. These consisted of rotation photographs about [001] of three crystals (for one of these about [010] as well), and equator, first and second layer line pictures, also about [001] and [010]. From these, the translations on *a*, *b* and *c* were measured and calculated from the rotation photographs, and values for a^*, b^* and c^* of the reciprocal lattice averaged from many spacings of the layer line pictures, using direct measurements on the films and graphic determinations on the Schneider constructions of the reciprocal lattice. From these average determinations, the values of a_0, b_0, c_0, and the linear axes, were derived. These values agree reasonably well with Fenoglio's *x*-ray work, and Rogers' morphology. The following Table 3 shows these comparative values.

The pattern in the Schneider constructions from the layer line pictures is orthorhombic, at least within the limits of observation, showing bi-

TABLE 2. HYDROMAGNESITE

X-ray powder photograph data, using Cu radiation, Ni filter

$\frac{d}{n}$	I	hkl	$\frac{d}{n}$	I	hkl
9.18 Å	4	200	1.84 Å	½	830
6.44	4	210	1.82	½	10.1.0
5.79	10	111	1.756	½	624
4.58	½	400	1.74	1	604
4.47	2	020	1.67	½	10.1.2
4.21	2	002	1.65	½	115
4.05	½	220	1.62	3	840
3.81	1	012	1.58	½	10.3.0
3.50	1	212	1.564	1	044
3.31	3	321	1.53	½	505
3.21	½	420	1.50	½	060
3.15	½	511	1.477	½	824, 761
3.09	½	600, 022 (?)	1.448	½	525
2.90	9	222, 610	1.420	½	062
2.84	½	230	1.407	½	006, 715
2.78	½	131 (?) 003 (?)	1.396	½	13.1.1
2.69	3	521	1.385	½	016
2.63	½	113	1.367	½	216
2.50	3	430 (?) 602, 313 (?)	1.330	½	416
2.42	½	612, 711 (?)	1.278	½	606
2.35	½	123	1.257	½	616
2.30	3	800	1.237	½	470
2.20	1	240	1.205	½	117
2.15	5	630	1.176	½	317
2.09	½	004	1.159	½	16.1.0
2.03	½	802, 440	1.113	½	280
1.99	2	042, 812	1.051	½	008
1.966	½	333 (?)	1.021	½	—
1.93	1	242, 632	0.9060	½	—
1.90	½	024, 404	0.8975	½	—
1.86	½	224, 10.0.0			

lateral symmetry, both of distribution and intensities, in all three axial planes. However, distribution of points in the first layer line picture shows that the value of a^* in the reciprocal lattice must be halved, as compared with the value from the equator picture. Furthermore, there are systematic extinctions, which throw the symmetry very nearly into space group D_2^5 ($C222_1$), as contrasted with Fenoglio's determination of D_{2h}^1. The presence of occasional faint spots $\{0k0\}$, $\{h0l\}$, $\{00l\}$, with h, k, and l odd, interfere with perfect matching of the pattern with this space group, and

TABLE 3. CELL DIMENSIONS FROM *X*-RAY MEASUREMENTS

	a	*b*	*c*	
Fenoglio	9.32 Å	8.98 Å	8.42 Å	(orthorhombic)
Murdoch	18.58 Å =9.29×2	9.06 Å	8.42 Å	90°

Axial Elements

	a	*b*	*c*	
Rogers (morphological)	1.1374	1	0.9034	114°0′8″
Fenoglio (*x*-ray)	1.0378	1	0.9376	[90°]
Murdoch (*x*-ray)	2.0508 =1.0254×2	1	0.9293	90°

may well be due to the truly monoclinic structure of the mineral. There are in addition faint superstructure spots which the author has not attempted to interpret.

In view of the apparent monoclinic symmetry of hydromagnesite, as shown by its optical behavior, it is desirable to attempt an explanation of the distinctly orthorhombic aspect of the lattice. The possibility that the mineral might be truly orthorhombic, as suggested by Fenoglio, was first considered. In this case, twinning on a macrodome is required, to produce the observed oblique extinction on {010}. However, it was found by trial that no orthorhombic lattice, tilted to the appropriate angle, could be found which would produce coincidence of points to form a rectangular pattern of the twinned lattices. Accordingly, this possibility may be ruled out.

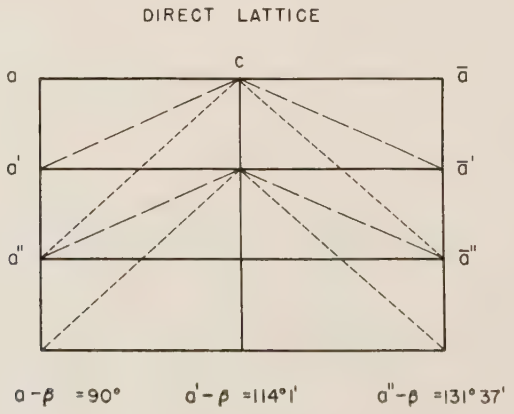

FIG. 2

The other possibility is that the mineral is truly monoclinic, with any value for β which would produce exact, or nearly exact, coincidence of patterns when twinned on {100}. There are of course a number of such values, and three of the more likely are shown in the following Fig. 2. Here a and c are drawn in the proportions of the observed direct lattice, and possible values for β are 90°, 114° 1′ and 131° 37′. Other angles are conceivable, but less and less probable because of the increasing obliquity of the resulting cell. Rogers on morphological grounds selected 114°+, but 90° is equally possible, and in the author's opinion should be chosen, as the simplest way of accounting for both morphological and x-ray characteristics of the mineral.

The writer wishes to acknowledge the assistance of his colleague, Professor George Tunell, in making available x-ray facilities, and in giving valuable counsel in the preparation of this paper. A spectroscopic analysis to determine purity of the material was made possible by research funds from the University of California.

References

1. Dana, J. D., Mineralogical contributions: *Am. Jour. Sci.*, **17,** 78–88 (1854).
2. Weinschenk, E., Weitere Beiträge zur Kenntniss der Minerallagerstätten der Serpentine in der Östlichen Centralalpen: *Zeit Kryst.*, **27,** 559–573 (1897).
3. Brugnatelli, L., Hydromagnesit und Artinit von Amarese (Aostatal): *Rendiconti R. Istituto Lombardo di sci. e. lett.*, 1903, (2^a) **36,** 824–827.
4. Dana, E. S., *System of Mineralogy*, 6th Ed. (1892).
5. Goldschmidt, V., Krystallographische Winkeltabellen.
6. Rogers, A. F., Crystallography of hydromagnesite: *Am. Jour. Sci.*, (5), **6,** 37, (1923).
7. Fenoglio, M., Ricerche sull'idromagnesite: *Periodico di mineralogia* **7,** 1–30) (1936).
8. ———, Ricerche sui Carbonati naturali neutri e bacici di magnesio idrati: *Atti Acad. Lincei*, **24,** 219–221 (1936).

Manuscript received Sept. 15, 1952

STUDY OF ORTHOPYROXENES FROM VOLCANIC ROCKS

Hisashi Kuno, *Geological Institute, Tokyo University, Tokyo, Japan.*

Abstract

Orthopyroxenes from volcanic rocks covering a composition range from bronzite to eulite were studied and the result is compared with the properties of orthopyroxenes from plutonic and metamorphic rocks. Orthopyroxenes crystallized at high temperatures contain from 0.104 to 0.057 Ca in atomic proportion, whereas those crystallized at low temperatures contain less than 0.033 Ca. Pleochroism appears to depend on Ti content. The volcanic orthopyroxenes having compositions about $Mg:Fe^{+2}+Fe^{+3}+Mn=1:1$ show optic angles (2V about X) 7° larger than those of the plutonic and metamorphic rocks. This departure gradually diminishes as the composition becomes either more magnesian or more ferriferous. Unit cell dimensions *a*, *b*, and *c* all increase with Fe^{+2} substituting for Mg. But the *a* and *c* dimensions increase more markedly with Ca substituting for Mg than with Fe^{+2}. Aluminum substituting for Mg causes contraction of the *b* dimension.

Introduction

Orthopyroxenes from volcanic rocks have been less studied than those from plutonic and metamorphic rocks, chiefly because of the difficulty of obtaining pure materials for analysis owing to their fine granularity, close association with clinopyroxenes, and abundance of minute inclusions. However, in orthopyroxenes from plutonic and metamorphic rocks, most of the Ca which was originally contained in the crystals has been exsolved to form lamellae, resulting in the orthopyroxenes of the Bushveld type (Hess and Phillips, 1938). Exsolution of Ti to form ilmenite lamellae was found by Sugi (1951) in diallage, and exsolution blebs or rods of sphene were also described by Hess (1949) in ferrosalite from metamorphic and plutonic rocks. Thin ilmenite lamellae in some orthopyroxenes were probably formed by exsolution. Therefore the plutonic and metamorphic orthopyroxenes have a very narrow range of Ca and perhaps Ti contents after slow cooling and complete adjustment of equilibrium. The volcanic orthopyroxenes have a wider range of Ca, its amount depending on the temperature of crystallization. The effect of Ca on the physical properties of orthopyroxenes can be determined from the study of the volcanic orthopyroxenes.

The result of the present study offers a method for determining the Ca content in orthopyroxenes. The Ca content may be used as a geothermometer.

Another difficulty attached to the study of the volcanic orthopyroxenes is their strong zoning. The writer has never seen unzoned pyroxenes from volcanic rocks. In order to make correlation between the optical constants and the chemical composition of the same specimen, we should determine the exact range of the optical constants and take the mean

values. However, the variation of physical constants with Fe^{+2} content can be known more exactly by studying unzoned pyroxenes from plutonic and metamorphic rocks. This study has been made by Hess (1952).

The writer's study has not yet been completed because of the lack of analyses of ferrohypersthene and eulite (the nomenclature by Poldervaart, 1947) from volcanic rocks. But in view of the difficulty of obtaining such data in the near future, the writer intends to publish the results so far obtained.

The present paper includes 13 analyses of the volcanic orthopyroxenes and 6 analyses of the plutonic and metamorphic orthopyroxenes. Only one of them has not been examined by the writer (eulite from Manchuria described by Tsuru and Henry, 1937). To complete the curves showing the variation of 2V and unit cell dimensions, several unanalyzed pyroxenes were also studied.

Acknowledgments

The separation of the pyroxenes used in this study and a part of the optical determinations were made in the Geological Institute, Tokyo University. The costs of this study and field trips for collecting the materials, together with that of the chemical analyses, were defrayed by the Japanese Government Expenditure for Scientific Research, which is greatly appreciated by the writer.

Another part of the optical determinations and the *x*-ray study were carried out in the Department of Geology, Princeton University, supported by the grant from the Geological Society of America (Grant No. 578-51). The writer wishes to take this opportunity of expressing his acknowledgments to the Geological Society for the grant and to the staff members of the Department of Geology for facilities of using the equipments and for many courtesies received. This study was made in close cooperation with Professor H. H. Hess to whom the writer is greatly obliged for advices in *x*-ray experiments, criticisms of the results, and reading of the manuscript.

Some of the chemical analyses were made by Messrs. Kakuzo Tada and Masa-aki Huzimoto, both of the Research Laboratory of Tokyo-Sibaura Electric Company, through the kindness of Dr. Hideo Inuzuka, the Director of the Laboratory at Mobara. Others were made by Yukio Konishi of the former Central Research Laboratory of the South Manchuria Railway Company at Dairen, and also by Dr. Kozo Nagashima of the Tokyo University of Agriculture and Technology. The writer's cordial thanks are due to Messrs. Tada, Huzimoto, and Konishi, and Drs. Inuzuka and Nagashima.

Finally the writer is obliged to Mr. Ryohei Morimoto of the Earth-

quake Research Institute and to Dr. Goro Asano of the Hurukawa Mining Company for the gifts of some of the pyroxenes used in this study, and also to Mr. Ryohei Ota of the Geological Survey of Japan for free use of the sample and unpublished analysis of hypersthene from Akagi volcano.

Chemical Compositions

The analyses of orthopyroxenes are given in Table 1. The modes of occurrence and localities are shown in Tables 3 and 4, respectively, in which those of unanalyzed pyroxenes are also included.

The general formula for pyroxenes may be written as follows (Hess, 1949):

$$(W)_{1-p}(X, Y)_{1+p}Z_2O_6$$
$$W = Ca^{+2}, Na^{+1}, K^{+1}$$
$$X = Mg^{+2}, Fe^{+2}, Mn^{+2}, Ni^{+2}$$
$$Y = Al^{+3}, Fe^{+3}, Cr^{+3}, Ti^{+4}$$
$$Z = Si^{+4}, Al^{+3}$$

The atomic proportions are calculated on the basis of six oxygen atoms (Table 2). It is assumed that Z positions should be always filled up completely. The result of calculation shows that in most pyroxenes both the Z ions and the sum of the W, X, and Y ions become approximately 2.000, agreeing with the theoretical formula of pyroxenes.

Table 1. Chemical Compositions of Orthopyroxenes

No.	1	2	3	4	5	6	7
SiO_2	57.63	55.73	55.84	54.11	53.17	53.18	52.83
Al_2O_3	1.20	0.93	1.60	1.52	0.45	3.08	2.42
TiO_2	tr.	tr.	0.19	0.19	0.22	0.21	0.29
Fe_2O_3	0.32	0.65	none	none	1.32	0.25	1.53
FeO	3.20	9.30	9.92	15.73	17.18	18.05	18.05
MnO	0.02	0.15	0.15	0.34	0.48	0.41	0.36
MgO	36.07	31.22	30.96	27.03	23.81	23.26	23.05
CaO	0.89	1.80	1.36	1.16	2.67	2.09	1.45
Na_2O	n.d.	0.21	n.d.	n.d.	0.47	n.d.	n.d.
K_2O	n.d.	tr.	n.d.	n.d.	0.00	n.d.	n.d.
H_2O+	n.d.	0.32	n.d.	n.d.	n.d.	n.d.	n.d.
H_2O-	n.d.		n.d.	n.d.	0.21	0.20	n.d.
P_2O_5	none	n.d.	n.d.	n.d.	n.d.	n.d.	n.d.
Total	99.33	100.23	100.02	100.08	99.98	100.73	99.98
Analysts	K. Tada and M. Huzimoto	Y. Kawano and K. Endo	K. Tada and M. Huzimoto	K. Tada and M. Huzimoto	K. Nagashima	T. Kusida	K. Tada and M. Huzimoto

Note: Analysis No. 5 is corrected for 0.5% hematite and recalculated to 100%.

TABLE 1.—*Continued*

No.	8	9	10	11	12	13	14
SiO_2	53.24	53.24	53.32	53.51	53.20	52.07	52.22
Al_2O_3	1.38	1.86	0.88	0.40	1.15	1.70	0.43
TiO_2	0.23	0.38	0.05	0.06	0.13	0.47	0.08
Fe_2O_3	1.05	1.23	0.71	1.50	none	none	0.70
FeO	18.70	19.21	19.91	19.57	21.64	22.65	25.91
MnO	0.85	0.87	1.22	1.05	0.78	0.48	0.83
MgO	23.34	22.18	23.26	23.12	22.50	21.13	18.54
CaO	1.23	0.61	0.74	0.86	0.82	1.55	1.28
Na_2O	tr.	0.35	n.d.	n.d.	n.d.	n.d.	n.d.
K_2O	tr.	0.07	n.d.	n.d.	n.d.	n.d.	n.d.
H_2O+	0.10	n.d.	n.d.	n.d.	n.d.	n.d.	n.d.
H_2O-		n.d.	n.d.	n.d.	n.d.	n.d.	n.d.
P_2O_5	tr.	none	n.d.	n.d.	n.d.	n.d.	tr.
Total	100.12	100.00	100.09	100.07	100.22	100.05	99.99
Analysts	S. Tanaka	G. Kozima and S. Taneda	K. Tada and M. Huzimoto	K. Tada and M. Huzimoto	K. Tada and M. Huzimoto	K. Tada and M. Huzimoto	Y. Konisi

Note: Analysis No. 9 is corrected for 0.8% magnetite and 0.55% apatite, and No. 14 for 0.3% ilmenite, and both recalculated to 100%.

TABLE 1—*Continued*

No.	15	18	19	22	23
SiO_2	50.26	49.43	50.04	45.95	46.56
Al_2O_3	3.13	0.38	1.47	0.90	0.23
TiO_2	0.16	0.17	0.00	0.10	0.03
Fe_2O_3	0.65	0.04	0.08	0.31	0.20
FeO	26.54	34.91	30.07	41.65	48.10
MnO	0.76	1.19	4.88	5.02	0.15
MgO	16.36	12.96	12.54	3.49	3.70
CaO	1.76	0.71	0.63	1.43	0.77
Na_2O	0.24	0.02	0.10	n.d.	0.04
K_2O	0.13			n.d.	
H_2O+	n.d.	n.d.	n.d.	0.65	n.d.
H_2O-	n.d.	n.d.	0.02	0.09	n.d.
P_2O_5	n.d.	n.d.	tr.	n.d.	n.d.
Total	99.99	99.81	99.83	99.59	99.78
Analysts	K. Nagashima	Y. Konisi	Y. Konisi	N. F. M. Henry	Y. Konisi

Note: Analysis No. 15 is corrected for 0.5% hematite, 0.8% ilmenite, and 1.0% apatite and is recalculated to 100%.

Table 2. Atomic Proportions of Orthopyroxenes Calculated on the Basis of 6 Oxygen Atoms

No.	1		2		3		4	
Si	1.970	2.000	1.960	1.998	1.955	2.000	1.948	2.000
Al	0.030		0.038		0.045		0.052	
Al	0.019		0.000		0.022		0.013	
Ti	0.000		0.000		0.006		0.006	
Fe^{+3}	0.008		0.017		0.000		0.000	
Fe^{+2}	0.090		0.272		0.290		0.471	
Mn	0.000	2.009	0.004	2.022	0.004	1.997	0.011	2.006
Mg	1.849		1.648		1.625		1.460	
Ca	0.033		0.068		0.050		0.045	
Na	0.000		0.013		0.000		0.000	
K	0.000		0.000		0.000		0.000	

No.	5		6		7		8	
Si	1.958	1.980	1.931	2.000	1.938	2.000	1.960	2.000
Al	0.022		0.069		0.062		0.040	
Al	0.000		0.062		0.044		0.022	
Ti	0.007		0.006		0.009		0.007	
Fe^{+3}	0.035		0.009		0.040		0.031	
Fe^{+2}	0.528		0.547		0.552		0.575	
Mn	0.015	2.035	0.013	1.989	0.011	1.980	0.027	2.002
Mg	1.315		1.269		1.267		1.291	
Ca	0.104		0.083		0.057		0.049	
Na	0.031		0.000		0.000		0.000	
K	0.000		0.000		0.000		0.000	

No.	9		10		11		12	
Si	1.960	2.000	1.974	2.000	1.980	1.998	1.969	2.000
Al	0.040		0.026		0.018		0.031	
Al	0.044		0.014		0.000		0.022	
Ti	0.011		0.002		0.002		0.004	
Fe^{+3}	0.035		0.018		0.040		0.000	
Fe^{+2}	0.590		0.613		0.604		0.668	
Mn	0.027	1.989	0.038	2.006	0.033	1.995	0.024	1.999
Mg	1.227		1.292		1.283		1.250	
Ca	0.024		0.029		0.033		0.031	
Na	0.027		0.000		0.000		0.000	
K	0.004		0.000		0.000		0.000	

TABLE 2—*Continued*

No.	13		14		15		18	
Si	1.944	2.000	1.992	2.000	1.927	2.000	1.969	1.988
Al	0.056		0.008		0.073		0.019	
Al	0.020		0.010		0.065		0.000	
Ti	0.013		0.002		0.005		0.005	
Fe^{+3}	0.000		0.018		0.018		0.000	
Fe^{+2}	0.706		0.824		0.849		1.159	
Mn	0.016	2.001	0.027	1.997	0.025	1.997	0.040	2.009
Mg	1.183		1.063		0.941		0.774	
Ca	0.063		0.053		0.071		0.031	
Na	0.000		0.000		0.018		0.000	
K	0.000		0.000		0.005		0.000	

No.	19		22		23	
Si	1.976	2.000	1.976	2.000	1.987	1.997
Al	0.024		0.024		0.010	
Al	0.047		0.022		0.000	
Ti	0.000		0.003		0.001	
Fe^{+3}	0.005		0.010		0.005	
Fe^{+2}	0.995		1.491		1.710	
Mn	0.166	1.993	0.183	2.000	0.005	1.996
Mg	0.744		0.224		0.238	
Ca	0.026		0.067		0.035	
Na	0.010		0.000		0.002	
K	0.000		0.000		0.000	

Ca content. As seen from Table 2, the atomic proportion of Ca ranges from 0.104 to 0.057 in Nos. 2, 5, 6, 7, 13, and 15, from 0.053 to 0.045 in Nos. 3, 4, 8 and 14, and from 0.033 to 0.024 in Nos. 9, 10, and 11. The Ca content can be correlated with the temperature of crystallization of the pyroxenes. Thus the pyroxenes Nos. 5, 6, 7, and 13 crystallized in pyroxene andesite (some basaltic andesite) magmas of high temperatures (the pigeonitic rock series of Kuno, 1950); Nos. 3, 4, and 14 in pyroxene andesite and dacite magmas of slightly lower temperatures (the hypersthenic rock series of Kuno, 1950); Nos. 2, 8, and 15 also in pyroxene andesite and dacite magmas but the temperature relations of the magmas are not certain; and Nos. 9, 10, and 11 all in hornblende andesite and dacite magmas of still lower temperatures (the hypersthenic rock series).

The pyroxene No. 5 crystallized during or immediately before the

Table 3. Mode of Occurrence of Orthopyroxenes and References

No.	Mode of occurrence	Reference
1	Main constituent of harzburgite. Few exsolution lamellae.	Kuno, 1941
2	In beach sand. Originally phenocrysts in bronzite andesite.	Kozu and Kawano, 1931
3	Phenocrysts in bronzite andesite.	Kuno, 1947b
4	Phenocrysts in bronzite andesite.	Kuno, 1947b
5	Microphenocrysts in hypersthene-olivine andesite.	Kuno and Nagashima, 1952
6	Phenocrysts in augite-hypersthene andesite.	Ota, 1952
7	Phenocrysts in augite and olivine-bearing hypersthene andesite.	Kuno, 1941
8	Phenocrysts in hypersthene-augite dacite (pumice).	Kuno, 1938
9	Phenocrysts in hypersthene-hornblende dacite (pumice).	Taneda, 1946
10	Phenocrysts in hypersthene-hornblende-quartz dacite (tuff).	Kuno, 1941
11	Phenocrysts in augite-hypersthene-hornblende andesite (tuff).	Kuno, 1941
12	In hypersthene-cummingtonite-hornblende amphibolite. No exsolution lamellae.	Kuno, 1947a
13	Phenocrysts in augite-pigeonite-hypersthene andesite.	Kuno, 1950
14	Phenocrysts in augite-bearing hypersthene dacite.	Unpublished analysis
15	Phenocrysts in augite-bearing hypersthene dacite (obsidian).	Unpublished analysis
16	Phenocrysts in garnet-bearing ferrohypersthene dacite.	No analysis
17	Phenocrysts in ferrohortonolite-ferrohypersthene dacite (obsidian).	No analysis
18	In ferrohypersthene-hornblende gabbro. A little exsolution lamellae.	Unpublished analysis
19	In eulysite or iron-rich hornfels. No lamellae.	Unpublished analysis
20	Phenocrysts in biotite-ferrohypersthene rhyolite (pitchstone).	No analysis
21	Phenocrysts in subcalcic ferroaugite-eulite-fayalite dacite (pitchstone).	No analysis
22	In eulysite or iron-rich hornfels.	Tsuru and Henry, 1937
23	In eulysite or iron-rich hornfels. A little exsolution lamellae. Parting parallel to 100 and 010.	Unpublished analysis

extrusion of the lava. The exceptionally high proportion of Ca in this pyroxene is discussed elsewhere (Kuno and Nagashima, 1952).

The proportion of Ca in the pyroxenes of the pigeonitic rock series agrees with that in orthopyroxenes crystallized from normal basaltic magmas such as those of Stillwater and Bushveld complexes (CaO = 1.65

$\pm 0.3\%$, Hess, 1952). Probably this proportion is normal to the pyroxenes of the pristine basaltic magma whose temperature of crystallization is from 1200° C. to 1000° C. The temperature of basaltic lava of the pigeonitic rock series in Osima volcano, Japan, lies between 1200° C. and 1100° C. (Minakami, 1951). As has been discussed elsewhere (Kuno, 1950), the temperature of crystallization of contaminated magma (the hypersthenic rock series) is lower than that of the pristine basaltic magma.

The proportion of Ca in the pyroxenes from the hornblende-bearing lavas is nearly equal to that in the pyroxenes formed by contact-metamorphism of granitic intrusions (Nos. 12, 19, and 23, Ca = 0.035—0.026) and also to that of the pyroxenes from low-temperature plutonic rocks (Nos. 1 and 18, Ca = 0.033—0.031). In the metamorphic rocks, the orthopyroxenes are associated with cummingtonite, grünerite, and green hornblende. These rocks belong to amphibolite facies. The proportion of Ca in No. 22 is exceptionally high, although the mineral was collected at the same locality as that of No. 19.

The pyroxene No. 1 occurs in serpentinized peridotite which was prob-

Table 4. Localities of Orthopyroxenes

No.	Localities
1	Kamogawa, Tiba Pref.
2	Titi-zima, Bonin Islands.
3	Tyosi, Tiba Pref.
4	Kokubudai, Kagawa Pref.
5	Tengu-zawa, near Hatazyuku, Hakone volcano, Kanagawa Pref.
6	Akagi volcano, Gunma Pref.
7	Tono-mine, near Yumoto, Hakone volcano, Kanagawa Pref.
8	Odawara, eastern foot of Hakone volcano, Kanagawa Pref.
9	Ikaho, Haruna volcano, Gunma Pref.
10	Near Kentyo-zi, Kamakura, Kanagawa Pref.
11	Sitisei-zan, near Tai-pei, north Formosa.
12	Hokizawa, Tanzawa Mountainland, Kanagawa Pref.
13	Hakone-toge, Hakone volcano, Kanagawa Pref.
14	Hirogawara, near Yugawara, Kanagawa Pref.
15	Kaziya, southeastern foot of Hakone volcano, Kanagawa Pref.
16	Northeast of Taguti, Sidara Basin, Aiti Pref.
17	Yosimura, southwestern margin of Sidara Basin, Aiti Pref.
18	Kasimine, near Nizyo-san, southeast of Osaka.
19	Yu-hsi-kou, An-tung-shen, south Manchuria.
20	Kaore, east of Ebi, Sidara Basin, Aiti Pref.
21	Matuki, north of Asio, Totigi Pref.
22	Yu-hsi-kou, An-tung-shen, south Manchuria.
23	Wang-chang-tzu, Je-ho-shen, southwest Manchuria.

ably formed at a temperature lower than that of the ordinary basaltic magma (Hess, 1938). The pyroxene No. 18 occurs in hornblende gabbro closely associated with syn-orogenic granite and is quite different in its petrographic character and mode of occurrence from the normal gabbro.

Probably the orthopyroxenes of these hornblende-bearing igneous and metamorphic rocks and the serpentinized peridotite were formed at temperatures between 900° C. and 600° C.

Hess (1941) postulated that Ca is more soluble in orthopyroxenes at higher temperatures than at lower temperatures. Atlas (1952) demonstrated the relation by his synthetic experiments on the system $MgSiO_3$—$CaMgSi_2O_6$. It is evident that the larger Ca ion can substitute for smaller Mg ion only at high temperatures and the limit of this substitution narrows as the temperature falls.

According to Atlas' diagram, atomic proportion of Ca in enstatite solid solution is 0.115 at 1100° C., which is the maximum limit of solubility in orthopyroxene, 0.050 at 1000° C., and 0.030 at 700° C. These figures agree very closely with the Ca proportion in the natural orthopyroxenes and the inferred temperature of their formation. We may safely conclude that Ca content in orthopyroxenes can be used as a geothermometer.

Al and Mn content. The proportion of Al varies with that of Ca although there are some exceptions. Thus Al is high in the pyroxenes Nos. 6, 7, 13, and 15, whereas it is low in Nos. 10, 11, 14, 18, and 23. In No. 5 Al is low in spite of high Ca.

Mn content is higher in the pyroxenes from hornblende-bearing igneous rocks (Nos. 9, 10, 11, and 18) than in those from the other igneous rocks. It is markedly high in the two pyroxenes (Nos. 19 and 22) from Yuhsi-kou mine which were formed from sedimentary rocks rich in Fe and Mn. The associated magnetite deposit is also rich in Mn and was used as manganiferous iron ore.

Optical Properties

The optical properties are listed in Table 5, together with the atomic ratios $Mg:Fe^{+2}+Fe^{+3}+Mn$ calculated from the analyses. In Fig. 1 $N_xN_zN_z-N_x$, and 2V are plotted against these ratios and the curves showing the variation of the optical constants are drawn. The pyroxenes Nos. 3, 4, 19, and 22 are not used for drawing the curves, because the former two show strong zoning and the latter two are unusually rich in Mn.

The change of the type of dispersion of 2V is also shown in the figure. The true change takes place twice throughout the series (Kuno, 1941), but as the dispersion is written in reference to the acute bisectrix in Table

TABLE 5. OPTICAL PROPERTIES OF ORTHOPYROXENES

No.	1	2	3	4	5	6	7	8
$Mg:Fe^{+2}+Fe^{+3}$ +Mn	94:6	85:15	85:15	75:25	69:31	69:31	68:32	67:33
N_x (mean)	1.660	1.672	1.6755	1.6855	1.691	n.d.	1.696	1.691
N_y (mean)	1.664	1.6765	1.6815	1.6935	1.699	n.d.	1.703	1.701
N_z (mean)	1.669	1.681	1.6865	1.6975	1.703	1.7065	1.708	1.705
Range of N_z	±0.000	±0.005	±0.0095	±0.0215	±0.004	±0.0045	±0.005	±0.005
N_z-N_x	0.009	0.009	0.011	0.011	0.012	n.d.	0.012	0.014
2V (mean)	(+)68°	n.d.	(−)80°	(−)82°.5	(−)63°	n.d.	(−)62°	(−)60°.5
Range of 2V	±0°	n.d.	±13°	±9°.5	±1°	n.d.	±4°	±3°.5
Dispersion	$r>v$	None	$r<v$	$r<v$, $r>v$	$r>v$	n.d.	$r>v$	$r>v$
N_z and corresponding 2V	1.669 (+)68°	1.683 (−)84°	n.d. n.d.	n.d. n d.	1.703 (−)64°	n.d. n.d.	1.708 (−)62°	1.704 (−)61°
Pleochroism	None	None	None	None to weak	Moderate	n.d.	Strong	Moderate

No.	9*	10	11	12	13	14	15	16
$Mg:Fe^{+2}+Fe^{+3}$ +Mn	66:34	66:34	65:35	64:36	62:38	55:45	51:49	?
N_x (mean)	1.6915	1.6955	1.6945	1.693	1.7015	n.d.	n.d.	n.d.
N_y (mean)	1.7005	1.7045	1.7035	1.704	1.7115	n.d.	n.d.	n.d.
N_z (mean)	1.7055	1.7075	1.7075	1.709	1.7145	1.721	1.726	1.735
Range of N_z	±0.0045	±0.0025	±0.0025	±0.001	±0.0025	±0.003	±0.004	±0.006
N_z-N_x	0.014	0.012	0.013	0.016	0.013	n.d.	n.d.	n.d.
2V (mean)	(−)60°.5	(−)63°.5	(−)60°	(−)58°	(−)59°.5	(−)54°.5	(−)52°	(−)54°
Range of 2V	±5°.5	±2°.5	±1°	+1°	±2°.5	±1°	±1°	±1°
Dispersion	$r>v$	$r>v$	$r>v$	$r>v$	$r>v$	$r>v$	None	$r<v$
N_z and corresponding 2V	1.706 (−)62°	1.7075 (−)63°.5	1.706 (−)61°	1.709 (−)58°	1.716 (−)57°.5	1.721 (−)54°.5	1.726 (−)52°	1.737 (−)55°
Pleochroism	Moderate	Moderate	Moderate	Moderate	Strong	Moderate	Weak	Weak

* Optical data except for "N_z and corresponding 2V" by Taneda (1946).

No.	17	18	19	20	21	22*	23
$Mg:Fe^{+2}+Fe^{+3}+Mn$	?	39:61	39:61	?	?	12:88	12:88
N_x (mean)	n.d.	n.d.	n.d.	n.d.	n.d.	1.755	1.7545
N_y (mean)	n.d.	n.d.	n.d.	n.d.	n.d.	1.763	1.7645
N_z (mean)	1.7355	1.7385	1.7345	n.d.	1.7705	1.773	1.7745
Range of N_z	±0.0085	±0.0025	±0.0025	n.d.	±0.0035	±0.000?	±0.0025
N_z-N_x	n.d.	n.d.	n.d.	n.d.	n.d.	0.018	0.020†
2V (mean)	(−)58°	(−)53°	(−)54°.5	(−)65°	(+)89°.5	(+)83°	(+)84°
Range of 2V	±2°	±1°	±0°.5	±3°	±7°.5	±0°?	+1°
Dispersion	$r<v$	$r<v$	$r<v$	$r<v$	$r<v$, $r>v$	$r>v$	$r>v$
N_z and corresponding 2V	1.741 (−)58°	1.7385 (−)53°	1.7345 (−)54°.5	1.751 (−)68°	1.768 (−)83°.5	1.773 (+)83°	1.7745 (+)84°
Pleochroism	Weak	Weak	None	Weak	Strong	Weak?	Moderate

* Optical data by Tsuru and Henry (1937).

† Determined by Hess.

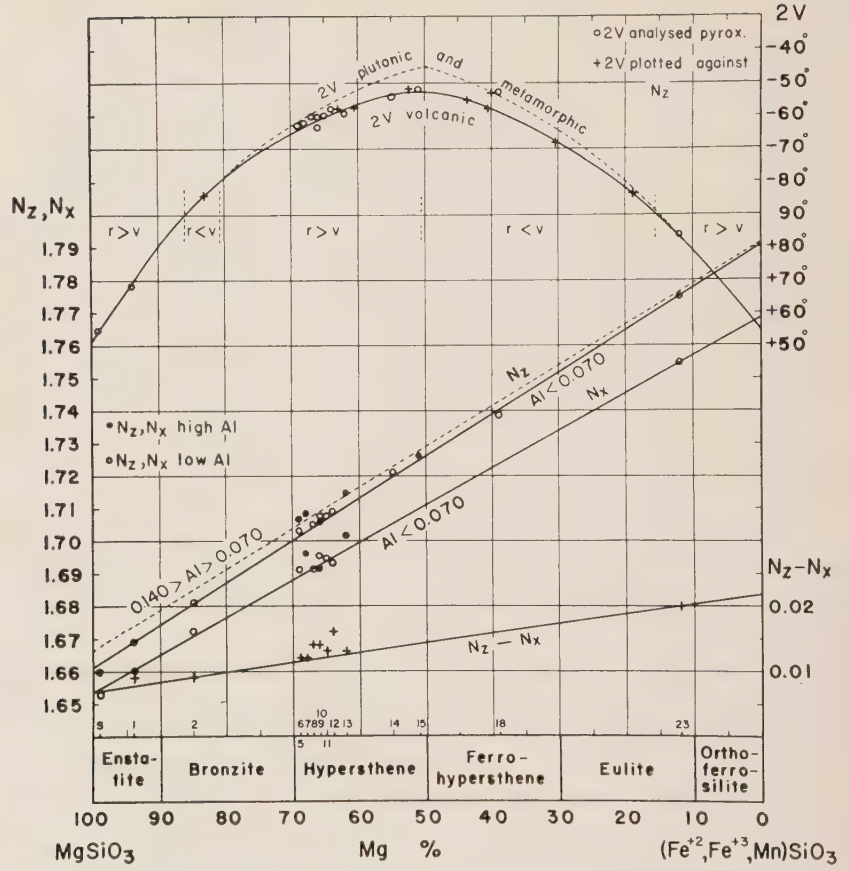

FIG. 1. Variation of optical properties of orthopyroxenes. The numbers in the lower part of the diagram refer to those in Table 1. S—enstatite from Shallowater meteorite.

5, it is shown in the figure as changing also at two points where the 2V curve passes 90°.

Refractive indices. The ranges of the refractive indices were determined on the powders used for the analyses. All the pyroxenes except No. 1 show considerable range of N_z. The error in each determination for the moderately zoned crystals is ± 0.001.

In Fig. 1, points for N_x and N_z of the pyroxenes containing less than 0.070 atomic proportion of Al (both in Si and Mg positions) are shown by open circles. They lie on or very close to a straight line (full lines in Fig. 1). The points for enstatite from Shallowater meteorite (Foshag, 1940) which contains no Al lie a little below the lines. Points for N_x and N_z of the pyroxenes containing 0.140—0.070 Al (solid circles) lie above

the full lines. A dotted line is drawn to show the N_z variation for these aluminous pyroxenes.

Hess (1952) has also drawn the N_z variation curve for the orthopyroxenes of Bushveld type which lies in the middle of the dotted and full lines in Fig. 1. His curve represents N_z variation for orthopyroxenes with medium Al content.

The N_z variation curve given by Poldervaart (1950) nearly coincides with the dotted line.

Mn in orthopyroxenes increases the refractive indices less markedly than Fe^{+2}, as is shown by the lower refractive indices of the manganiferous pyroxene No. 19 than those of No. 18 in spite of their having the same Mg: $Fe^{+2}+Fe^{+3}+Mn$ ratio.

Birefringence. The points for N_z-N_x of the pyroxene No. 23 and the Shallowater enstatite are connected by a straight line. Most of the points for the other pyroxenes lie on or close to this line.

Optic angle. 2V was measured on several crystals of each analyzed pyroxene. The error in each determination for the moderately zoned crystals is $\pm 1°$. The mean values of 2V are plotted in Fig. 1 with open circles.

In order to know the exact variation of 2V of the volcanic orthopyroxenes, several unanalyzed pyroxenes were also studied. N_z and the corresponding value of 2V were measured on one and the same cleavage flake lying on 010 (usually about 0.2 mm. long). The results are given in Table 5. The 2V is plotted against Mg per cent inferred from the corresponding N_z (crosses in Fig. 1).

The points for the volcanic orthopyroxenes lie on a smooth curve (full line in Fig. 1). Hess' (1952) curve for the 2V variation of the orthopyroxenes of Bushveld type (dotted line) lies 7° above the curve for the volcanic pyroxenes at the composition Mg 50, but gradually approaches the latter until the two curves coincide with each other in bronzite and eulite.

Pleochroism. Tables 1 and 5 show that the intensity of pleochroism has no relation to Fe^{+2} or Mn contents. The manganiferous pyroxene No. 19 is colorless. Some relation appears to exist between pleochroism and Ti content.

The strongest pleochroism is seen in the pyroxene No. 13 which has the highest Ti content (0.013). The pleochroism next in intensity is seen in No. 7 which has Ti content (0.009) higher than those of the other pyroxenes except No. 9 (0.011). Nos. 5, 8, 9, 10, 11, 12, 14, and 23 show moderate pleochroism, their Ti contents (except No. 9) varying from 0.007 to 0.001. The colorless pyroxenes (Nos. 1, 2, 3, and 19) have no Ti except No. 3 (0.006).

There may be some exceptions to this rule in the pyroxenes of Bushveld type, because a part of Ti may have been exsolved together with Ca or with Fe^{+2}.

The pleochroism of the two orthopyroxenes are shown below:

Hypersthene No. 13:	Eulite No. 21:
X—pale reddish brown	X—smoky brown
Y—pale greenish brown	Y—pale brown
Z—pale smoky green	Z—smoky green
Absorption X>Z>Y	Absorption Z>X>Y

Unit Cell Dimensions

Unit cell dimensions a, b, and c were determined by a North American Philips x-ray spectrometer, using Fe K_{α_1} radiation. The method was described by Hess (1952) in detail and will not be repeated here. However, instead of using a bakelite slide as described by Hess, the writer used mixture of the powder of the pyroxenes and that of silicon mounted on a glass slide with Duco cement. The correction for the instrument, the thickness of the layer of the sample, and the roughness of its surface was made by reading the known 2θ angles of the reflections from silicon. For the pyroxenes Nos. 16 and 21, the bakelite slides were used. For Nos. 5 and 14, determinations were made on the two different types of slides; the results agreed within 0.001 Å.

The a and b dimensions were determined by the reflections (14, 5, 0), (060), (12, 0, 0), and (650). The average values of these determinations are given in Table 6. The figures include errors usually less than 0.003 Å and rarely ± 0.005 Å. The values are further checked by the reflections (610) and (420).

Table 6. Unit Cell Dimensions (in Å) of Orthopyroxenes

No.	2	5	6	7	8	10
a(observed)	18.281	18.333	18.320	18.326	18.314	18.309
a(calculated)	18.282	18.325	18.321	18.313	18.307	18.303
b(observed)	8.853	8.885	8.884	8.881	8.884	8.890
c(observed)	5.200	5.218	5.215	5.217	5.214	5.211
c(calculated)	5.205	5.220	5.218	5.216	5.213	5.212
Mg:Fe^{+2}:Ca	83:13.5:3.5	67.5:27:5.5	66.5:29:4.5	67.5:29:3.5	67.5:30:2.5	67:31.5:1.5
No.	11	13	14	15	16	21
a(observed)	18.302	18.340	18.337	18.344	18.343	18.429
a(calculated)	18.303	18.323	18.332	18.350	—	—
b(observed)	8.885	8.893	8.920	8.933	8.962	9.016
c(observed)	5.210	5.221	5.220	5.225	5.221	5.249
c(calculated)	5.212	5.219	5.222	5.229	—	—
Mg:Fe^{+2}:Ca	67:31.5:1.5	61:36:3	55:42.5:2.5	50.5:45.5:4	45:55*	17:83*

* Mg:Fe^{+2}+Fe^{+3}+Mn estimated from N_z (mean).

The *c* dimension was obtained by the reflections (004), (502), and (202), using the already known values of *a*. The average values given in Table 6 include errors less than 0.0004 Å. These values were further checked by the reflections (11, 3, 1) and (131).

In Fig. 2 the observed values of *a*, *b*, and *c* are plotted against Mg: $Fe^{+2}+Fe^{+3}+Mn$ calculated from the analyses or estimated from N_z (mean).

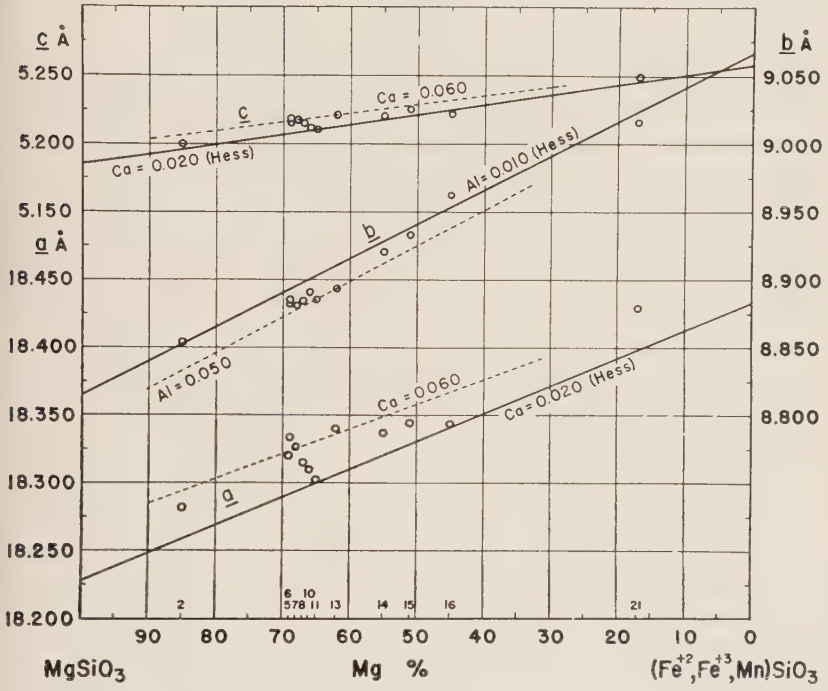

FIG. 2. Variation of unit cell dimensions of orthopyroxenes. The numbers in the lower part of the diagram refer to those in Table 3.

a dimension. The *a* dimension increases with the amount of Fe^{+2} substituting for Mg but more markedly with the amount of Ca substituting for Mg. This is because Fe^{+2} is larger in ionic radius than Mg, but Ca is larger than Fe^{+2}.

The full line in Fig. 2 is a reproduction of the curve given by Hess (1952) showing the variation of *a* dimensions of the pyroxenes of Bushveld type including Nos. 18 and 23. The last two pyroxenes contain only 0.031 and 0.035 Ca respectively, yet they show a little exsolution lamellae. Therefore the full line in Fig. 2 represents the *a* variation for pyroxenes with about 0.020 Ca or with the ratio $Mg+Fe^{+2}:Ca=99:1$.

The points for the volcanic pyroxenes all lie above this line and the amount of departure from this line is proportional to the Ca content of the pyroxenes. Thus the pyroxenes Nos. 10 (Ca = 0.029) and 11 (Ca = 0.033) lie fairly close to the full line, whereas No. 5 (Ca = 0.104) is most removed from the line. A line representing the a variation for pyroxenes with 0.060 Ca or $Mg+Fe^{+2}:Ca = 96:4$ is drawn with a dotted line.

The a dimension of any orthopyroxene may be calculated approximately from the following formula:

$$a = \{(O—Mg) \times l + (O—Fe^{+2}) \times m + (O—Ca) \times n - (O—Mg) \times 100\} \times 0.0396 + 18.228 \text{ Å}$$

where l, m, and n are atomic per cent of Mg, Fe^{+2}, and Ca of the given pyroxene respectively, (O—Mg), ($O—Fe^{+2}$), and (O—Ca) are the interatomic distances between oxygen and Mg, Fe^{+2}, and Ca ions respectively, and 18.228 Å is the a dimension of enstatite ($Mg: Fe^{+2}:Ca = 99:0:1$) obtained from the full line in Fig. 2. The interatomic distances used here are as follows: (O—Mg) = 2.1 Å, ($O—Fe^{+2}$) = 2.15 Å, (O—Ca) = 2.3 Å.

The atomic per cent $Mg: Fe^{+2}:Ca$ of the analyzed pyroxenes and the calculated a for these compositions are shown in Table 6. The calculated values agree fairly closely with the observed values.

b dimensions. The b dimension increases with the amount of Fe^{+2} but decreases with the amount of Al substituting for Mg, because Fe^{+2} is larger than Mg but Al is smaller than Mg.

In Fig. 2 is reproduced the line given by Hess (1952) showing the b variation for orthopyroxenes with about 0.010 Al in Mg position, including the pyroxenes Nos. 18 and 23.

Most of the volcanic pyroxenes contain larger amounts of Al in Mg position, so that the points lie generally below the line. A dotted line is drawn to show the b variation for pyroxenes containing 0.050 Al in Mg position.

c dimension. This also increases with the amounts of Fe^{+2} and Ca substituting for Mg, but the rate of increase is smaller than that in a dimension. The full line in Fig. 2 shows the c variation for pyroxenes with 0.020 Ca, whereas the dotted line for those with 0.060 Ca.

The c dimension of the analyzed pyroxenes can be calculated from the following formula:

$$c = \{(O—Mg) \times l + (O—Fe^{+2}) \times m + (O—Ca) \times n - (O—Mg) \times 100\} \times 0.0142 + 5.185 \text{ Å}.$$

The result of calculation (Table 6) shows a close agreement with the observed values.

Discussion of the Result

The present study indicates that the refractive indices and unit cell dimensions of the volcanic orthopyroxenes vary with the chemical compositions entirely in the same way as found in the orthopyroxenes of the Bushveld type. These physical constants show straight line variations if they are plotted against the atomic ratio Mg: $Fe^{+2}+Fe^{+3}+Mn$, provided the proportion of Ca and Al is constant.

The effects of Fe^{+2}, Ca, and Al on the unit cell dimensions can be explained as due to the difference of their ionic radii from that of Mg for which they substitute.

The only difference between the volcanic orthopyroxenes and those of Bushveld type is found in the variation of 2V according to Mg per cent. Even this might be a result of the difference of Ca content between the two groups (Hess, 1952). It is also possible that the order-disorder relation in the orthopyroxene structure causes this difference. In order to decide whether this difference is related to Ca content, it is necessary to study volcanic orthopyroxenes about Mg50 but with low Ca content.

We can determine Mg per cent of orthopyroxenes by measuring N_z. Then by measuring the *a* and *b* dimensions, we can find Ca and Al content of that crystal.

It will be interesting to determine Ca content of orthopyroxenes crystallized in recent lavas whose temperatures are actually measured.

References

Atlas, L. (1952), The polymorphism of $MgSiO_3$ and solid-state equilibria in the system $MgSiO_3$—$CaMg\ Si_2O_6$: *Jour. Geol.*, **60,** 125–147.

Foshag, W. F. (1940), The Shallowater meteorite: a new aubrite: *Am. Mineral.*, **25,** 779–786.

Hess, H. H. (1938), A primary peridotite magma: *Am. Jour. Sci.*, **35,** 321–344.

——— (1941), Pyroxenes of common mafic magmas: *Am. Mineral.*, **26,** 515–535; 573–594.

——— (1949), Chemical composition and optical properties of common clinopyroxenes, part I: *Am. Mineral.*, **34,** 621–666.

——— (1952), Orthopyroxenes of the Bushveld type, ion substitutions and changes in unit cells dimensions: *Am. Jour. Sci.*, Bowen's Volume, 173–187.

———, and Phillips, A. H. (1938), Orthopyroxenes of the Bushveld type: *Am. Mineral.*, **23,** 450–456.

Kozu, S., and Kawano, Y. (1931), Bronzite from Titi-zima, Bonin Islands: *Jap. Ass. Mineral. Petro. Econ. Geol., Jour.*, **6,** 273–276.

Kuno, H. (1938), Hypersthene from Odawara-mati, Japan: *Imp. Acad. Tokyo, Proc.*, **14,** 218–220.

——— (1941), Dispersion of optic axes in the orthorhombic pyroxene series: *Imp. Acad. Tokyo, Proc.*, **17,** 204–209.

——— (1947 *a*), Hypersthene in a rock of amphibolite facies from Tanzawa Mountain land, Kanagawa Prefecture, Japan: *Jap. Acad., Proc.*, **23,** 114–116.

——— (1947 *b*), Two orthopyroxenes from the so-called bronzite-andesite of Japan: *Jap. Acad., Proc.*, **23,** 117–120.

——— (1950), Petrology of Hakone volcano and the adjacent areas, Japan: *Geol. Soc. Am., Bull.*, **61,** 957–1020.

———, AND NAGASHIMA, K. (1952), Chemical compositions of hypersthene and pigeonite in equilibrium in magma: *Am. Mineral.*, **37** (1000–1006).

MINAKAMI, T. (1951), On the temperature and viscosity of the fresh lava extruded in the 1951 Oo-sima eruption: *Earthq. Res. Inst., Bull.*, **29,** 487–498.

OTA, R. (1952), Petrographic study on the Akagi volcano lava: *Geol. Surv. Japan*, Rept. No. 151, 33–40.

POLDERVAART, A. (1947), The relationship of orthopyroxene to pigeonite: *Mineral. Mag.* **28,** 164–172.

——— (1950), Correlation of physical properties and chemical composition in the plagioclase, olivine, and orthopyroxene series: *Am. Mineral.*, **35,** 1067–1079.

SUGI, K. (1951), Diallage and its inclusion in gabbroic rock from Ayabe, Tanba: *Fac. Sci., Kyusyu Univ., Rep. Sect., Geol.*, **3,** 1–5.

TANEDA, S. (1946), Hypersthene from Haruna volcano: *Geol. Soc. Japan, Jour.*, **52,** 61–64.

TSURU, K., AND HENRY, N. F. M. (1937), An iron-rich optically-positive hypersthene from Manchuria: *Mineral. Mag.*, **24,** 527–528.

Manuscript received July 18, 1952.

SMITHSONITE FROM BROKEN HILL MINE, RHODESIA*

Cornelius S. Hurlbut, Jr., *Harvard University, Cambridge, Massachusetts.*

Abstract

Well-formed crystals of smithsonite, erroneously labeled calcite, have been found on old specimens from Broken Hill Mine, N. W. Rhodesia. The crystals are in two distinct habits. New forms observed are: $B\{12\cdot 8\cdot \bar{2}0\cdot 1\}$, $X\{7\cdot 4\cdot \bar{1}\bar{1}\cdot 2\}$, $j\{21\cdot 7\cdot \bar{2}8\cdot 12\}$, $Y\{25\bar{7}3\}$. Spectrographic analysis on crystals of Type 1 gives impurities MgO = 0.1, CaO = 0.001; type 2: MgO = 0.5, FeO = 0.4, CaO = 0.05, CdO = 0.05, PbO = 0.1. G. Type 1 = 4.424; Type 2 = 4.405. For both types nO = 1.850, nE = 1.623 ± 0.002.

In 1950 when the quarters of Economic Geology at Harvard were changed from one building to another, many specimens came to light that had not been seen in many years. Mr. Richard Gaines, who was in charge of the moving, came across four beautifully crystallized specimens from Broken Hill Mine, N. W. Rhodesia, labeled "Cerussite and Calcite."

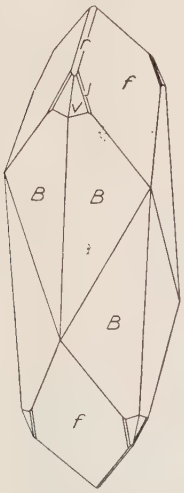

Fig. 1

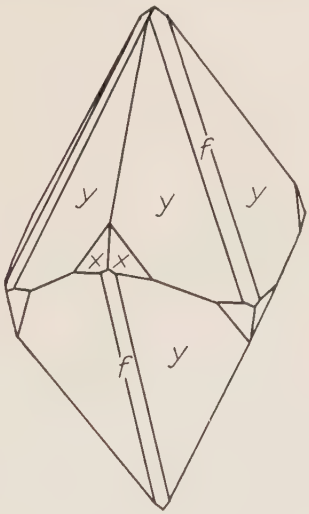

Fig. 2

Smithsonite, Broken Hill Mine, N.W. Rhodesia.

The well-formed colorless and transparent "calcite" proved to be smithsonite.

Morphology. Smithsonite crystals have been described from the Broken Hill Mine by Spencer (1908) and Mountain (1926). Spencer's

* Contribution No. 344. Department of Mineralogy and Petrography, Harvard University, Cambridge, Massachusetts.

crystals were small and showed the forms v $\{21\bar{3}1\}$ and s $\{05\bar{5}1\}$. Mountain's crystals were larger, 7 millimeters long, with the single form f $\{02\bar{2}1\}$.

The new material displays two distinct habits, neither of which is similar to the habits of the crystals previously described. Both types show new forms. Type 1 is represented by a single specimen and Type 2 by three specimens. The single specimen, about 5 centimeters square, is coated with many sharp, well-defined crystals ranging from 1 to 10 millimeters in length. The habit of these crystals is shown in Fig. 1. The large scalenohedron faces, B, are of a new form $\{12.8.\bar{2}0.1\}$. They show brilliant reflections and give a remarkable constancy of angular measurements. The form j $\{21.7.\bar{2}\bar{8}.12\}$, also new, is represented only by small faces which are not found on all crystals. Other forms present are r $\{10\bar{1}1\}$, f $\{02\bar{2}1\}$ and v $\{21\bar{3}1\}$.

Three specimens are coated with crystals of similar habit showing the forms represented in Fig. 2. The crystals are intergrown with one another and it is difficult to obtain a single individual for goniometric measurements. A new form, y $\{25\bar{7}3\}$, dominates the crystals and its faces are usually striated parallel to the intersection with f $\{02\bar{2}1\}$. Another new form, X $\{7.4.\bar{1}\bar{1}.2\}$, is present on some crystals. On one specimen there is a crown-like growth, about one centimeter in diameter, all part of a single crystal, as shown in Fig. 3. Around the girdle of this crystal are small spherical masses of siderite.

Weissenberg photographs of the Type 1 smithsonite give the unit cell dimensions, $c_0 = 14.96$ kX, $a_0 = 4.65$, which are in very close agreement with those given in the seventh edition of Dana's *System of Mineralogy*.

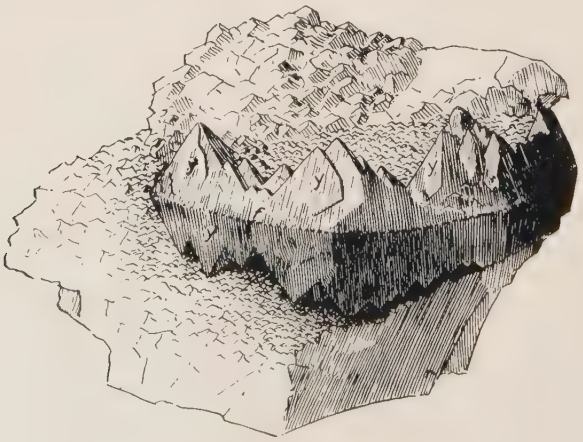

FIG. 3. Type 2, Smithsonite.

TABLE 1. SMITHSONITE ANGLE TABLE

Smithsonite—$ZnCO_3$
Hexagonal—R; hexagonal scalenohedral
$a:c=1:0.8063$; $\alpha=103°28'$
$p_0:r_0=0.9311:1$; $\lambda=72°20'$

	Form	ϕ	$\rho=C$	A_1	A_2
r	$10\bar{1}1$	30°00′	42°57½′	53°49½′	90°00′
f	$02\bar{2}1$	−30°00′	61°46′	90°00′	40°16′
*B	$12\cdot8\cdot\bar{2}0\cdot1$	6°35′	86°28½′	53°30′	66°21′
*x	$7\cdot4\cdot\bar{1}1\cdot2$	8°57′	77°26′	52°09′	69°29′
v	$21\bar{3}1$	10°53½′	67°54½′	52°39½′	72°20½′
*j	$21\cdot7\cdot\bar{2}8\cdot12$	16°06′	62°56½′	50°05′	77°39′
*y	$25\bar{7}3$	−13°54′	62°42′	46°06′	51°58′

* New forms.

Table 2 gives a summary of the data on which are based the observed new forms.

TABLE 2. SMITHSONITE

Form	ϕ	ρ	Range ϕ	Range ρ	No. of Faces
$12\cdot8\cdot\bar{2}0\cdot1$	6°32′	86°28′	6°27′– 6°37′	86°25′–86°30′	30
$7\cdot4\cdot\bar{1}1\cdot2$	8°51′	77°18′	8°45′– 9°03′	77°10′–77°30′	12
$21\cdot7\cdot\bar{2}8\cdot12$	16°10′	63°02′	15°59′–16°15′	62°52′–63°25′	21
$25\bar{7}3$	−13°48′	62°45′	−13°06′–14°33′	62°35′–63°00′	27

Chemical Composition. Two spectrographic analyses of each type of smithsonite were made by Dr. Harold C. Harrison. The approximate amounts of the impurities found spectrographically are given in Table 3.

The small percentage of impurities in the Type 1 material shows it to be very nearly pure $ZnCO_3$, probably the purest smithsonite reported.

TABLE 3. IMPURITIES IN SMITHSONITE

	Type 1	Type 2
MgO	0.1	0.5
FeO	—	0.4
CaO	0.001	0.05
CdO	—	0.05
PbO	—	0.1

The specific gravity 4.424 of Type 1, as determined by four measurements on the Berman balance, approaches very closely the calculated specific gravity of 4.43. The specific gravity of Type 2 is 4.405. The refractive indices of both types as determined by the immersion method, are the same for sodium light: $n\mathrm{O} = 1.850$ and $n\mathrm{E} = 1.623 \pm 0.002$.

References

Mountain, E. D., *Mineral. Mag.*, **21,** No. 113, 51 (1926).
Spencer, L. J., *Mineral. Mag.*, **15,** No. 68, 35 (1908).

Manuscript received Jan. 23, 1953.

CALCULATION OF POLAR AND DIRECT AXIAL RATIOS AND POLAR AND DIRECT AXIAL ANGLES OF TRICLINIC CRYSTALS FROM INTERFACIAL ANGLES

GEORGE TUNELL, *Department of Geology, University of California, Los Angeles, California.*

ABSTRACT

The polar axial ratios of a triclinic crystal can be calculated by means of the equations:

$$\frac{p_0'}{r_0'} = \frac{l \sin (001 \wedge h0l)}{h \sin (100 \wedge h0l)}, \tag{1'}$$

$$\frac{q_0'}{r_0'} = \frac{l \sin (001 \wedge 0kl)}{k \sin (010 \wedge 0kl)}, \tag{2'}$$

and

$$\frac{p_0'}{q_0'} = \frac{k \sin (010 \wedge hk0)}{h \sin (100 \wedge hk0)}. \tag{3'}$$

The polar axial ratios of some triclinic minerals can thus be obtained as the ratios of the sines of measured interfacial angles. The polar axial angles λ, μ, and ν of a triclinic crystal are by definition the interfacial angles $010 \wedge 001$, $100 \wedge 001$, and $100 \wedge 010$ respectively. The polar axial angles of some triclinic minerals can thus be obtained as measured interfacial angles or as the sums of measured interfacial angles. In the absence of one or more of the necessary faces it will be impossible to measure one or more of the interfacial angles needed for the application of at least two of the equations (1'), (2'), and (3'). The required interfacial angles can then be calculated from measured interfacial angles in some cases by the methods of plane trigonometry, in other cases only by the methods of spherical trigonometry, provided at least 5 interfacial angles have been measured that will permit the solution of certain triangles.

The direct axial ratios of triclinic crystals can be evaluated as the ratios of the sines of certain interzonal angles, as is well known. These interzonal angles are not equal to any interfacial angles in the case of triclinic crystals, but they can be calculated from certain interfacial angles by the methods of spherical trigonometry, and this has been the practice of crystallographers making use of the one-circle goniometer or the contact-hand-goniometer.

The direct axial ratios of triclinic crystals can be calculated more easily in many cases by means of the polar axial ratios and polar axial angles than by means of interzonal angles. The equations necessary for this purpose are derived very simply by the application of the law of sines for spherical oblique triangles.

A simple method of calculation of crystallographic axial ratios and axial angles, and a simple method of determination of Miller indices from measurements of interfacial angles with the one-circle goniometer or with the contact goniometer, are especially needed by mineralogists and geologists whose principal interests are in branches of geologic science other than crystallography but who wish to make some use of crystallographic data in mineral determination. The purpose of this paper is to outline the simplest methods known to the writer of accomplishing these results.

U. OF I.
LIBRARY

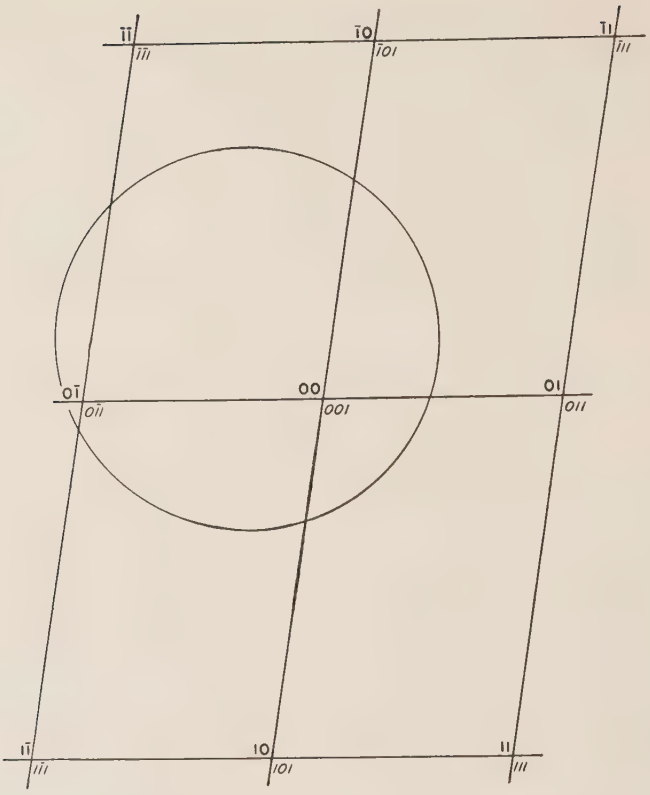

FIG. 1. Gnomonic projection of a triclinic crystal. The figures in roman type are the coordinates in the plane of the gnomonic projection; the figures in italics are the Miller indices.

The Miller indices of crystal faces can usually be determined most easily by the use of the gnomonic projection (Fig. 1) and the polar lattice.[1] This method of indexing faces has been the usual procedure in cases of measurements of coordinate angles by means of the two-circle goniometer, and, as T. V. Barker[2] has pointed out, it can also be readily applied with measurements of interfacial angles by means of the one-circle goniometer or contact goniometer. In order to determine the Miller indices of a face by this method from measurements of interfacial angles, it is best to construct the stereographic pole of the face by the use of a

[1] The polar lattice of the mineralogist is identical in proportions and angles with the reciprocal lattice of the *x*-ray crystallographer, but is not, in general, drawn to the same scale (Palache, C. *Am. Mineral.*, **19**, 108 (1934)).

[2] Barker, T. V. Graphical and Tabular Methods in Crystallography, Thomas Murby & Co., London, 1922, p. 25.

stereonet and then to construct the gnomonic pole from the stereographic pole by means of an auxiliary section (Fig. 2) or by the use of a stereographic-gnomonic protractor. Application of Neumann's gnomonic theorem then permits the indices of the face to be obtained from the

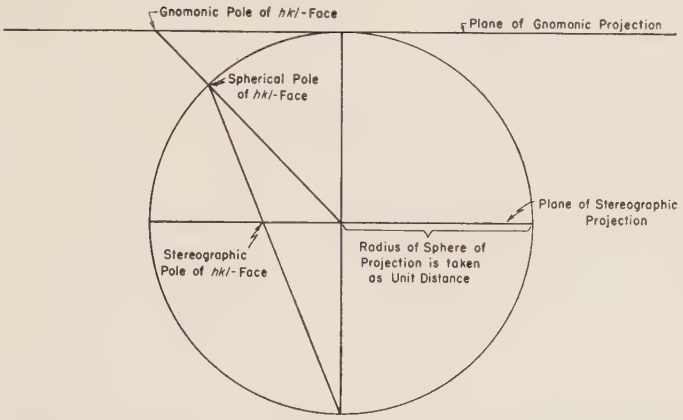

FIG. 2. Construction of the gnomonic pole of a face from its stereographic pole in the case of a triclinic crystal.

coordinates of the gnomonic pole, provided the plane of the gnomonic projection is parallel to two of the polar axes, by the addition of the third coordinate, which is one, and the multiplication of all three coordinates by the smallest factor necessary to convert all fractions, if there are any fractions, into integers. The plane of the gnomonic projection being coincident with the first level of the polar lattice, the face-poles in the gnomonic projection the coordinates of which are integers are nodes of the first level of the polar lattice (Fig. 3); face-poles in the gnomonic projection having one or both coordinates fractional correspond to nodes of higher levels of the polar lattice projected onto the gnomonic plane along the face-normals.

In all crystal systems the polar axial angles are defined as the angles between the edges of a parallelepiped constructed with its edges perpendicular to the faces 100, 010, and 001, and with its body diagonal perpendicular to the face 111, and the polar axial ratios are defined as the ratios of the lengths of the edges of this parallelepiped. The edge perpendicular to the face 100 is designated p_0' in this paper, the edge perpendicular to the face 010 is designated q_0', and the edge perpendicular to the face 001 is designated r_0'; the angle between q_0' and r_0' is designated λ, the angle between p_0' and r_0' is designated μ, and the angle between p_0' and q_0' is designated ν. The polar axial angle λ is thus by

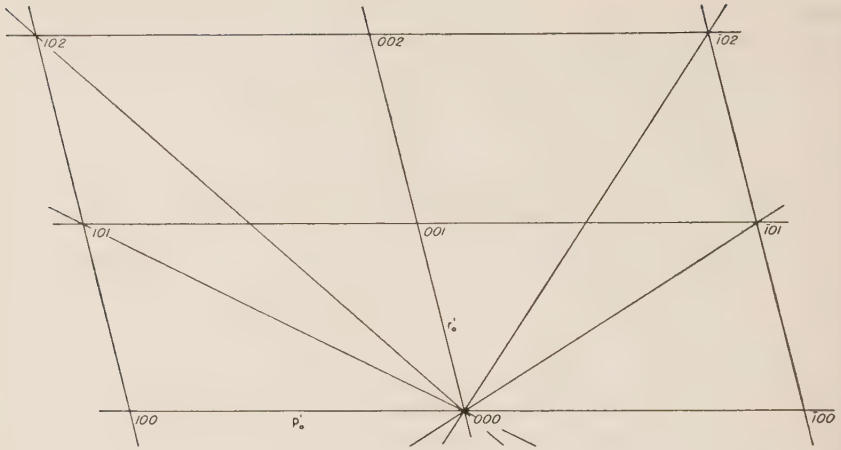

FIG. 3. Section of the polar lattice of a triclinic crystal through the normals to 100 and 001.

definition the angle between the normals to the faces 010 and 001. Likewise the polar axial angle μ is by definition the angle between the normals to the faces 100 and 001, and the polar axial angle ν is by definition the angle between the normals to the faces 100 and 010.

The fundamental relations between polar axial ratios and interfacial angles can be derived very easily. In Fig. 4 let OA represent a line perpendicular to the face 100, OB a line perpendicular to the face 010, and OM a line perpendicular to the face 110 of a triclinic crystal. Then, by

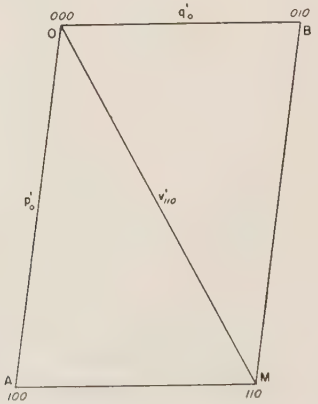

FIG. 4. Relationship of the polar lattice elements p_0' and q_0' of a triclinic crystal to the interfacial angles $100 \wedge 110$ and $010 \wedge 110$.

applying the law of sines for plane triangles to the triangle OBM, we obtain immediately the relation

$$\frac{p_0'}{q_0'} = \frac{\sin \angle BOM}{\sin \angle OMB} = \frac{\sin (010 \wedge 110)}{\sin (100 \wedge 110)},^3 \tag{1}$$

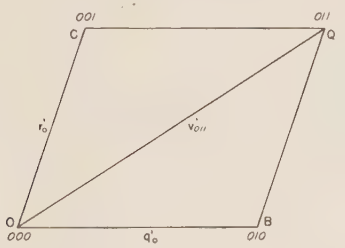

FIG. 5. Relationship of the polar lattice elements q_0' and r_0' of a triclinic crystal to the interfacial angles 010/\011 and 001/\011.

In Fig. 5 let OB represent a line perpendicular to the face 010, OC a line perpendicular to the face 001, and OQ a line perpendicular to the face 011. By applying the law of sines for plane triangles to the triangle OBQ, we obtain the relation

$$\frac{q_0'}{r_0'} = \frac{\sin \angle OQB}{\sin \angle BOQ} = \frac{\sin (001 \wedge 011)}{\sin (010 \wedge 011)}. \tag{2}$$

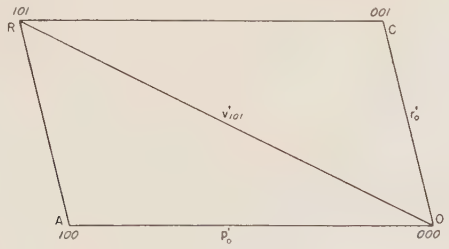

FIG. 6. Relationship of the polar lattice elements p_0' and r_0' of a triclinic crystal to the interfacial angles 100/\101 and 001/\101.

In Fig. 6 let OA represent a line perpendicular to the face 100, OC a line perpendicular to the face 001, and OR a line perpendicular to the face 101. By applying the law of sines for plane triangles to the triangle OCR, we obtain the relation

[3] Goldschmidt, V. Einleitung in die formbeschreibende Krystallographie, Julius Springer, Berlin, 1887, p. 102.

$$\frac{p_0'}{r_0'} = \frac{\sin \angle COR}{\sin \angle CRO} = \frac{\sin (001 \wedge 101)}{\sin (100 \wedge 101)}. \tag{3}$$

Thus, the polar axial ratios can be calculated from the four interfacial angles 100/\010, 100/\001, 100/\101, 100/\110, or from the four interfacial angles 100/\010, 001/\010, 100/\110, 010/\011, or from the four interfacial angles 100/\001, 010/\001, 100/\101, 010/\011 in the most general case, that of the triclinic system.

If the face 110 is not present on the crystal, but some face $hk0$ is present in the zone containing the faces 100 and 010, the ratio of p_0' to q_0' can be obtained by the use of the equation

$$\frac{hp_0'}{kq_0'} = \frac{\sin (010 \wedge hk0)}{\sin (100 \wedge hk0)}. \tag{1'}$$

Likewise, if the face 011 is not present on the crystal, but some face $0kl$ is present in the zone containing the faces 010 and 001, the ratio of q_0' to r_0' can be obtained by the use of the equation

$$\frac{kq_0'}{lr_0'} = \frac{\sin (001 \wedge 0kl)}{\sin (010 \wedge 0kl)}. \tag{2'}$$

Similarly, if the face 101 is not present on the crystal, but some face $h0l$ is present in the zone containing the faces 100 and 001, the ratio of p_0' to r_0' can be obtained by the use of the equation

$$\frac{hp_0'}{lr_0'} = \frac{\sin (001 \wedge h0l)}{\sin (100 \wedge h0l)}. \tag{3'}$$

Hence if the forms {100}, {010}, {001}, and either one $\{h0l\}$-form and one $\{0kl\}$-form, or one $\{h0l\}$-form and one $\{hk0\}$-form, or one $\{0kl\}$-form and one $\{hk0\}$-form are present on the crystal, all the polar axial ratios and polar axial angles of a triclinic crystal can be obtained by the measurement of five interfacial angles and the calculation of two quotients of sines of measured angles. One or another of these combinations of forms is a combination of common forms of the following triclinic minerals: babingtonite, amblygonite, wollastonite, axinite, and tarbuttite, and this method could thus be used to calculate the polar axial ratios and polar axial angles of crystals of these minerals.

If various other combinations of forms are present, the calculation of all the polar axial ratios and polar axial angles of a triclinic crystal can still be accomplished very simply by the application of the equations of plane trigonometry. This is possible, for example, if the forms {001} and {010} and two $\{hk0\}$-forms, one $\{0kl\}$-form, and one $\{h0l\}$-form are present (a combination of forms that is commonly found on triclinic as well as on monoclinic feldspar crystals).

It is not possible, of course, to calculate all the polar axial ratios and polar axial angles from measured interfacial angles of triclinic crystals

in all cases without the solution of any spherical triangle. Thus, for example, if only the forms {100}, {010}, {110}, {011}, {011} were present, it would be necessary to solve two oblique spherical triangles in order to calculate all the polar axial ratios and polar axial angles[4] from measurements of the interfacial angles.[5]

The direct crystallographic elements of a triclinic crystal are the interaxial angles, α, β, γ, and the axial ratios, a/b and c/b. The direct axial ratios and axial angles can be calculated from the interfacial angles; in some cases, however, the direct axial ratios can be calculated more easily from the polar axial ratios and polar axial angles.

The derivation of the equations needed for the calculation of the direct crystallographic elements of a triclinic crystal from measurements of interfacial angles has been given in several treatises[6] and is as follows.

[4] Since only the relative dimensions of the polar lattice are fixed by measurements of interfacial angles, the scale on which the polar lattice is drawn in morphological work is arbitrary. In investigations of crystals with the two-circle goniometer, the plane of the gnomonic projection has been constructed tangent to the projection sphere, the length of the radius of this sphere being taken equal to unity. Elements of the polar lattice drawn on this scale have been called "projection elements" by V. Goldschmidt and those who have made use of his methods of calculation, and have been designated by letters with primes by them. Elements of the polar lattice drawn on the smaller scale on which the length of the element normal to the face 001 is taken as equal to unity have been called "polar elements" by Goldschmidt and those who have made use of his methods, and have been designated by letters with subscript zeros by them. In this paper, where the scale is that of the "projection elements," the phrase "polar lattice elements" is used rather than "polar elements," since, in the terminology of Goldschmidt and those who have made use of his methods, "polar elements" are based on the scale on which the length of the element normal to the face 001 is taken as equal to unity. It is clear, however, that both Goldschmidt's "projection elements" and his "polar elements" are elements of polar lattices that differ only in scale.

[5] As Barker and others have stated, greater accuracy is usually obtainable with measurements of coordinate angles made by means of a two-circle goniometer than with measurements of interfacial angles made by the use of a one-circle goniometer. In the investigation of complex crystals there is also an important saving of time and labor when the two-circle goniometer is used. The very simple fundamental relations between interfacial angles and polar elements as well as the simple fundamental relations between interzonal angles and direct elements need to be understood by students of mineralogy, however, even if they intend to proceed to the more complicated methods permitting the calculation of the most accurate values of the crystallographic elements from measurements of the coordinate angles with the two-circle goniometer. Moreover, measurements of interfacial angles made with the one-circle goniometer or with the contact goniometer are important in determinative work.

[6] Cf. Liebisch, T., Grundriss der physikalischen Krystallographie, Veit & Comp., Leipzig, 1896, pp. 21–22, Tutton, A. E. H., Crystallography and Practical Crystal Measurement, Macmillan and Co., London, 1922, Vol. 1, p. 111, Peacock, M. A., in Technique of Organic Chemistry, Edited by A. Weissberger, Interscience Publishers, New York, 1949, Vol. 1, Second Edition, Part 1, pp. 1005–1006.

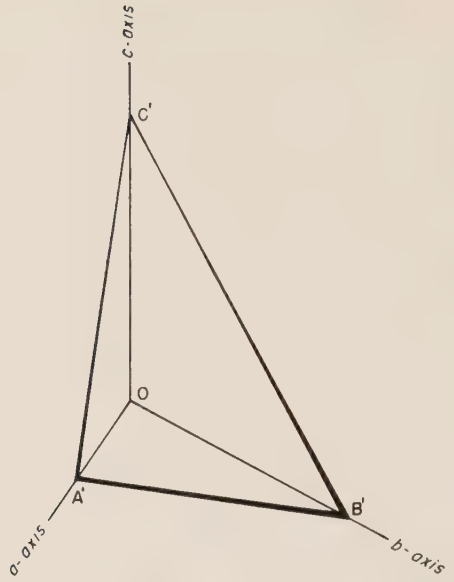

FIG. 7. Relationship of the unit plane 111 to the unit distances along the a-axis, b-axis, and c-axis in the case of a triclinic crystal.

In Fig. 7 the plane $A'B'C'$ represents the plane chosen as the unit plane 111. The ratios of its intercepts on the three crystallographic axes are consequently the axial ratios, that is,

$$\frac{\overline{OA'}}{\overline{OB'}} = \frac{a}{b} \tag{4}$$

and

$$\frac{\overline{OC'}}{\overline{OB'}} = \frac{c}{b}. \tag{5}$$

By applying the law of sines for plane triangles to the triangle $OA'B'$, one obtains immediately

$$\frac{\overline{OA'}}{\sin \angle OB'A'} = \frac{\overline{OB'}}{\sin \angle OA'B'}, \tag{6}$$

and, combining equations (4) and (6), one has

$$\frac{a}{b} = \frac{\sin \angle OB'A'}{\sin \angle OA'B'}. \tag{7}$$

Now the angle $OB'A'$ is the angle between the zone-axis OB' (which is the zone-axis of the zone including 100 and 001) and the zone-axis $A'B'$ (which is the zone-axis of the zone including 111 and 001). Also

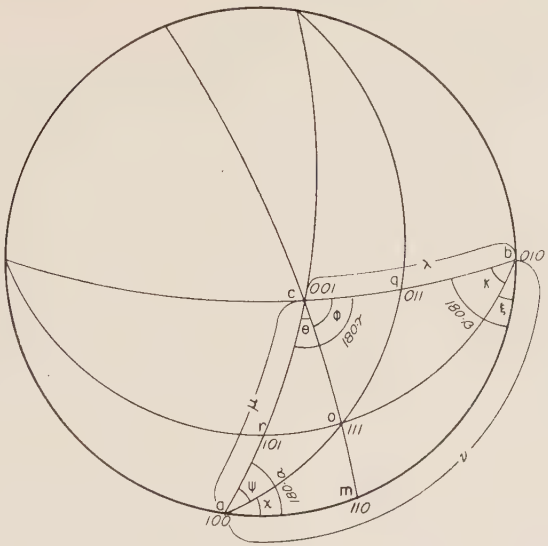

Fig. 8. Relationships of the principal interfacial and interzonal angles in the stereographic projection of a triclinic crystal. The points *a*, *b*, and *c* are the stereographic poles of the faces 100, 010, and 001 respectively (the points *a*, *b*, and *c* are not the stereographic projections of the points in which the *a*-axis, *b*-axis, and *c*-axis intersect the sphere of projection in the case of a triclinic crystal). The *a*-axis, *b*-axis, and *c*-axis are not drawn in the figure; they are perpendicular to the great circles *bqc*, *cra*, and *amb* respectively.

the angle θ in the stereographic projection of the crystal faces (Fig. 8) is the angle between the zone including 100 and 001 and the zone including 111 and 001. Therefore $\theta = \angle OB'A'$. Furthermore the angle $OA'B'$ is the angle between the zone-axis OA' (which is the zone-axis of the zone including 010 and 001) and the zone-axis $B'A'$ (which is the zone-axis of the zone including 111 and 001). And, the angle ϕ in the stereographic projection (Fig. 8) is the angle between the zone including 010 and 001 and the zone including 111 and 001. Therefore $\phi = \angle OA'B'$. Hence, by substituting $\sin\theta$ for $\sin \angle OB'A'$ and $\sin\phi$ for $\sin \angle OA'B'$ in equation (7), one obtains

$$\frac{a}{b} = \frac{\sin\theta}{\sin\phi}. \tag{8}$$

Similarly, by applying the law of sines for plane triangles to the triangle $OB'C'$, one obtains

$$\frac{\overline{OC'}}{\sin \angle OB'C'} = \frac{\overline{OB'}}{\sin \angle OC'B'}, \tag{9}$$

and combining equations (5) and (9), one has

$$\frac{c}{b} = \frac{\sin \angle OB'C'}{\sin \angle OC'B'}. \tag{10}$$

Now the angle $OB'C'$ is the angle between the zone-axis OB' (which is the zone-axis of the zone including 100 and 001) and the zone-axis $C'B'$ (which is the zone-axis of the zone including 100 and 111). Also the angle ψ in the stereographic projection (Fig. 8) is the angle between the zone including 100 and 001 and the zone including 100 and 111. Therefore $\psi = \angle OB'C'$. Furthermore the angle $OC'B'$ is the angle between the zone including 100 and 010 and the zone including 100 and 111. And the angle χ in the stereographic projection (Fig. 8) is the angle between the zone including 100 and 010 and the zone including 100 and 111. Therefore $\chi = \angle OC'B'$. Hence, by substituting $\sin \psi$ for $\sin \angle OB'C'$ and $\sin \chi$ for $\sin \angle OC'B'$ in equation (10), one obtains

$$\frac{c}{b} = \frac{\sin \psi}{\sin \chi}. \tag{11}$$

By means of equations (8) and (11) the direct axial ratios of a triclinic crystal can be calculated from the interzonal angles θ, ϕ, ψ, and χ. These interzonal angles must themselves be calculated from the measured interfacial angles by application of the equation of spherical trigonometry giving the angle of an oblique spherical triangle in terms of the three sides.

The interaxial angles, α, β, γ, of a triclinic crystal are the supplements of the angles of the spherical triangle abc (Fig. 8),

$$\alpha = 180^\circ - \angle bac, \tag{12}$$

$$\beta = 180^\circ - \angle abc, \tag{13}$$

$$\gamma = 180^\circ - \angle acb. \tag{14}$$

Thus α, β, and γ can be calculated from the measurements of the interfacial angles $100 \wedge 010$, $100 \wedge 001$, and $010 \wedge 001$, which are the sides of this spherical triangle. By applying the standard formula of spherical trigonometry giving an angle of an oblique spherical triangle in terms of the three sides[7] one obtains

$$\sin \frac{\angle bac}{2} = \sqrt{\frac{\sin (s-\mu) \sin (s-\nu)}{\sin \mu \sin \nu}}, \tag{15}$$

where $s = (\lambda + \mu + \nu)/2$. Hence, making use of equation (12), one has

$$\sin \frac{180^\circ - \alpha}{2} = \sqrt{\frac{\sin (s-\mu) \sin (s-\nu)}{\sin \mu \sin \nu}} \tag{16}$$

and, finally,

[7] This standard formula is to be found in text-books of spherical trigonometry.

$$\cos\frac{\alpha}{2} = \sqrt{\frac{\sin(s-\mu)\sin(s-\nu)}{\sin\mu\sin\nu}}. \tag{17}$$

In an analogous way one can prove that

$$\cos\frac{\beta}{2} = \sqrt{\frac{\sin(s-\lambda)\sin(s-\nu)}{\sin\lambda\sin\nu}} \tag{18}$$

and

$$\cos\frac{\gamma}{2} = \sqrt{\frac{\sin(s-\lambda)\sin(s-\mu)}{\sin\lambda\sin\mu}}. \tag{19}$$

Instead of calculating the direct axial ratios of a triclinic crystal from interfacial angles, one can compute them more easily in some cases from the polar axial ratios and polar axial angles by means of the well known equations[8]

$$\frac{a}{b} = \frac{q_0'\sin\lambda}{p_0'\sin\mu}, \tag{20}$$

and

$$\frac{c}{b} = \frac{q_0'\sin\nu}{r_0'\sin\mu}. \tag{21}$$

These equations can be readily derived by application of the law of sines for oblique spherical triangles. In Fig. 8 the angle *am* is the angle between the face 100 and the face 110,

$$\angle am = 100 \wedge 110, \tag{22}$$

also the angle *mb* is the angle between the face 110 and the face 010,

$$\angle mb = 110 \wedge 010. \tag{23}$$

Applying the law of sines for oblique spherical triangles to the triangle *amc*, one obtains

$$\frac{\sin\theta}{\sin\angle am} = \frac{\sin\angle amc}{\sin\angle ac} \tag{24}$$

and applying the same law to the triangle *bmc*, one obtains

$$\frac{\sin\phi}{\sin\angle mb} = \frac{\sin\angle bmc}{\sin\angle bc}. \tag{25}$$

Now $\angle amc + \angle bmc = 180°$, since *amb* is an arc of a great circle. Therefore

$$\sin\angle amc = \sin\angle bmc. \tag{26}$$

Substituting this value for $\sin\angle bmc$ in equation (25), one obtains

[8] Cf. Palache, C., *Am. Mineral.*, **5**, 81 (1920), Goldschmidt, V., Kursus der Kristallometrie, Gebrüder Borntraeger, Berlin, 1934, p. 135, Hermann, C., Editor, Internationale Tabellen zur Bestimmung von Kristallstrukturen, Bd. 1, Gebrüder Borntraeger, Berlin, 1935, p. 68.

$$\frac{\sin\theta}{\sin\angle am}\sin\angle ac = \sin\angle amc = \frac{\sin\phi}{\sin\angle mb}\sin\angle bc. \tag{27}$$

Since $\angle am = 100 \wedge 110$ and $\angle mb = 110 \wedge 010$ and $\angle ac = \mu$ and $\angle bc = \lambda$, we have

$$\frac{\sin\theta}{\sin\phi} = \frac{\sin\lambda}{\sin\mu}\,\frac{\sin(100 \wedge 110)}{\sin(010 \wedge 110)}, \tag{28}$$

and, making use of equations (1) and (8), one obtains finally

$$\frac{a}{b} = \frac{q_0'}{p_0'}\,\frac{\sin\lambda}{\sin\mu}.^{9} \tag{29}$$

Equation (21) is readily derived in an analogous way.

Acknowledgment

The author is indebted to the late Dr. F. E. Wright and to Professor Joseph Murdoch for kindly reading the manuscript of this paper and offering constructive suggestions.

[9] Equations (20) and (21) can be derived very simply from the definitions of the reciprocal lattice vectors. The derivation given in this paper can, however, be used by those who have not studied the methods of vector analysis, and may also be of value to mineralogists who are familiar with the derivation by means of vectors, since it brings out certain fundamental morphological relations.

Manuscript received Jan. 6, 1953.

INTERTRACIAL ANGLES AS INDICATORS OF OPTICAL AND DIMENSIONAL ORIENTATION OF SOME MONOCLINIC CRYSTALS IN RANDOM SECTIONS

E. den Tex, *The University of Melbourne, Victoria, Australia.*

Abstract

A Universal Stage method is presented to construct the location of dominant zone axes in random sections of crystals from the orientation of the indicatrix and the values of apparent dihedral angles (hereinafter called intertracial angles) as compared with corresponding true angles. It applies to monoclinic crystals with known axial elements, identifiable faces or cleavages and known crystallographic orientation of the optic axial plane; such as the majority of pyroxenes and hornblendes. Applicability, advantages and limitations of the method are discussed. It appears suitable for petrofabric analysis, giving sufficiently accurate results for all orientations. Special reference is made to aegirine-augite in a pseudomassive alkaline trachyte.

Introduction

The optical orientation, more specifically the extinction angle $Z\wedge c$ of monoclinic pyroxenes and amphiboles having the optic axes situated in (010), has been the subject of a number of papers during the last twenty years.

Strictly speaking, direct observation of the extinction angle in 010 is limited to sections parallel to c with inclinations of 010 at less than 40° to the section, so as to enable its correct adjustment perpendicular to the microscope axis on the universal stage. If the latter operation is impossible, $Z\wedge c$ may be read from the stereographic projection. In all cases where c is not parallel to the section, the traces of $hk0$ planes in the section are not parallel to c and should therefore be discarded as a direct reference for $Z\wedge c$ in 010.

The above limitations are responsible for the methods developed for indirect computation of the extinction angle from universal stage measurements. In a review, Turner (1942) has indicated the limitations and the range of error of the better known procedures, at the same time suggesting variations to overcome some of the former (1940) and reduce some of the latter obstacles (1942). Special attention was given to errors resulting from vertical adjustment of crystallographic reference planes, due to imperfect development, low inclination to the section, difference in R.I. between section and hemispheres and its impact on aberration of the rays in inclined positions of the section. Preference was shown by Turner for the use of selected sections with Nemoto's (1938) procedure of computing crystallographic references from postulated symmetry relations between the indicatrices of twinned crystals.

From the crystallographic point of view, application of universal stage methods to identification of crystal faces and to measurement of interfacial angles in the stereographic projection was presented by Nieland (1932) and by Gilbert and Turner (1949) respectively, whilst Donnay and O'Brien (1954) described a microscopic procedure for the determination of axial elements from apparent interedge angles as well as for crystal identification from interzonal or apparent interzonal angles in independent sections. However, the latter treatment applies to oriented sections only and does not consider the optical orientation of the crystal.

To determine lineations and foliations of hornblende crystals in schists and gneisses Schmidt (1928) and Wenk (1936) used the intersection of *hk*0 planes as a means of locating *c*, a method improved by Burri (1931) through construction of [001] as pole of a great circle containing the poles of *hk*0 planes. Thus universal stage stereography was applied to the field of dimensional orientation as treated statistically by petrofabric analysis. Schmidt also drew the attention to the lack of accuracy in his method for sections subparallel to *c* where often only one (110) cleavage is present at low inclination to the section (*op. cit.*).

In the course of a structural analysis of a number of alkali-trachytic domes in the Macedon district, near Melbourne, it proved desirable to the present author to microscopically determine a possible lineation of aegirine-augite "phenocrysts" with dominant [001], which were too small to be effectively measured in the hand specimen.

For this purpose the optical orientation of each individual crystal was determined from oriented thin sections by means of the universal stage. The axis (*c*) of the dominant zone [001] being the crystallographic direction to constitute a possible lineation, its location was derived from the extinction angle $Z \wedge c$ in 010. Use of the location of *c* in petrofabric analysis, excluded the possibility of selecting favourable sections which, moreover, may be rare in slides of a certain orientation.

Apart from these considerations calling for special precautions against errors and for careful selection of slides with regard to the major structural features, the exact vertical adjustment of crystallographic reference planes was severely hampered by their often imperfect development, their sometimes low inclination to the section and, above all, by the clouded to almost opaque appearance of many sections subparallel to *c* due to strong absorption and alteration (cf. Fig. 4).

However, nearly all sections did show well developed crystal faces whose identification was aided by fairly regular cleavage traces. Although, at first, it seemed possible to use these faces for vertical adjustment, their corroded condition—further impaired by granular alteration

products—precluded accurate adjustment as already experienced by Nieland (1932). On the other hand, the traces of faces and cleavages in the plane of section could usually be located within $\frac{1}{2}$ degree (cf. Donnay and O'Brien, 1945, p. 597). The angles between these traces in the plane of section, the apparent dihedral angles or intertracial angles as they will be referred to in this paper, give an indication of the inclination—if any—of the crystal with respect to the section. Knowing from the orientation of the indicatrix, the position in space of one crystallographic plane, 010, the possible locations of *c* are restricted to this plane, generally resulting in only one such location to produce the specific intertracial angles, although it should be realized that an equal but opposite inclination of *c* in 010 produces corresponding supplementary angles (cf. Fig. 3, *A*3 and *B*5). Special conditions apply when 010 is perpendicular to the section giving rise to the same intertracial angles for equal but opposite inclinations of *c* (cf Fig 3, *A*2 and *B*4), unless the section is further specified as either perpendicular to *c* showing true dihedral angles between all traces of *hk*0 planes (cf. Fig. 3, *A*1) or parallel to *c*, when all traces of *hk*0 planes are parallel (cf. Fig. 3, *B*1–3). The other orientations perpendicular to 010 give the only cross-sections ambiguous with respect to the location of *c* in 010 owing to the fact that the twofold axis of symmetry *b* lies in the plane of section. The result of this is that dihedral angles of 90°, such as (010)$\wedge$(100) and (010)$\wedge$(001) are preserved throughout rotation and that others such as (010)$\wedge$(110) and (010)$\wedge(\bar{1}10)$ are changed in the same sense retaining the symmetry of outline of a section perpendicular to *c*. These sections require a special treatment as will be shown below.

Geometry

It may be useful to visualize the geometrical relations of the problem before offering a stereographical solution.

The orientation of a crystal in space may be described by two intersecting faces; each of which may, in turn, be fixed by two non-parallel lines in it. The latter description can be used to determine the principal sections of the indicatrix, of which ZX coincides with 010 in the case of aegirine-augite. Other crystallographic planes, however, are merely limited in orientation by containing one line, i.e. their trace in the section. Nevertheless, in the monoclinic system *h*0*l* planes such as (100) and (001), which are parallel to [010], are completely fixed in orientation when their trace in any section not parallel to *b* and the direction of *b* have been determined. Moreover, for any monoclinic pyroxene or amphibole the angle between the (110) planes and *b* is constant, the value for aegirine-augite being approximately 46°30′. This means that they are

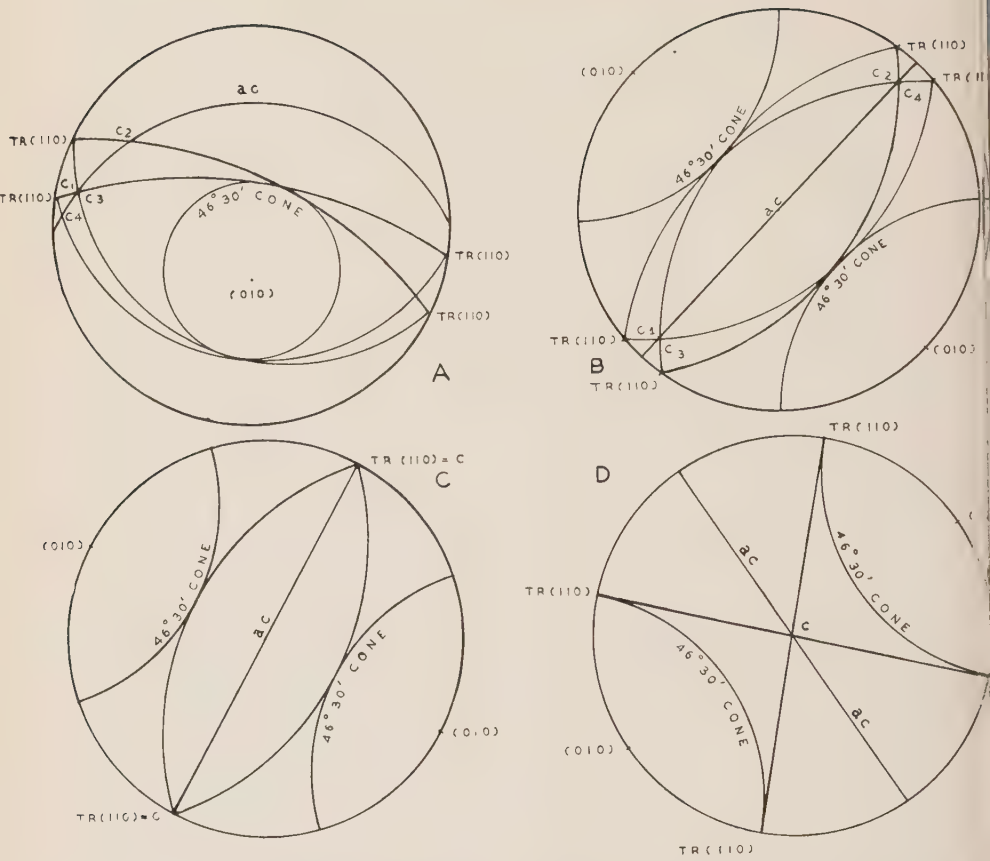

FIG. 1. Stereographic projections of the geometrical relations in an aegirine-augite crystal between the *b* axis and the (110) crystallographic planes as described by their traces in the plane of section. In the general case (*A*) there are four possible planes tangent to the 46°30′ cone about *b*, two of which have a common intersection in the *ac*-plane. In sections ⊥ 010 generally two common intersections in the *ac*-plane are offered by the four planes (*B*). Sections ‖*c* (*C*) and sections ⊥*c* (*D*) have only two possible (110) planes and only one common intersection in the *ac*-plane.

tangential planes to a cone with apical angle of 46°30′ about *b* intersecting the sectional trace in the apex. The stereographic projections of Fig. 1 are in the plane of the section and designed to show the geometrical relations between (110) traces in the section and the cone about *b* with its apex in the centre of the projection, where all directions in the crystal intersect. From the general case, figured in 1*A*, it is evident that there is a maximum of two tangential planes that will simultaneously pass through a particular (110) trace in the section. As there are generally

two (110) traces present, this results in a maximum of four possible orientations of the (110) planes of which commonly only one pair, belonging to different traces, will constitute a [001] zone by common intersection in 010, thus satisfying the symmetry requirements.

However, two common intersections of different (110) planes in 010 may be available resulting in two possible locations of *c*, when the cone axis *b* bisects the angle between the (110) traces. This happens only in sections perpendicular to 010 where the twofold axis of symmetry lies in the plane of section so that both pairs of (110) planes contact the cone along opposite lines (cf. Fig. 1*B*).*

Two sections perpendicular to 010 have only one possible pair of (110) planes tangent to the cone about *b*, caused by either mutual coincidence of (110) traces at right angles to the cone axis (cf. Fig. 1*C*) or by coincidence of different (110) traces with the cone (cf. Fig. 1*D*). The former condition is common to all sections of the *c* zone where parallelism of *hk*0 traces obviates the necessity of constructing *c*, the latter applies to sections at right angles to the (110) form and hence perpendicular to *c*.

Stereographic Construction

These principles may now be applied to the actual location of *c* in the stereographic projection.

First of all, plotting of the indicatrix on the Wulff net is performed in the conventional manner using the plane of section as the surface of projection. 010 and the orientation of Z within it are established from measurements on the universal stage. The inner stage is then set horizontal and the traces of relevant faces and cleavages (with their directions averaged if identical) are successively set parallel to the N-S. cross-hair, the angular positions being read from the arc of the inner stage. The traces, representing intersections of crystallographic planes with the section, are now plotted. They all lie on the primitive circle (cf. Fig. 2*A*). All *h*0*l* planes can be constructed as great circles through *b* and their trace in the section, if these do not happen to coincide. To facilitate the construction of other structural elements, such as planes of the (110) form, a second projection of the crystal may then be plotted from the first by a rotation designed to bring *b* = Y at the centre (cf. Fig. 2*B*). The trace directions of the crystallographic planes are marked on the upper hemi-

* Actually sections parallel to *b* through monoclinic crystals have a planar point group symmetry (*C*2*l*) containing a centre and 2 lines of symmetry which are the *h*0*l* and 0*k*0 traces. As *c* is confined to 010, the crystal symmetry is satisfied in positions symmetrical to a vertical plane through the *h*0*l* trace. For similar reasons of symmetry all planes of the (110) form are interchangeable as far as they serve for the location of *c* in 010.

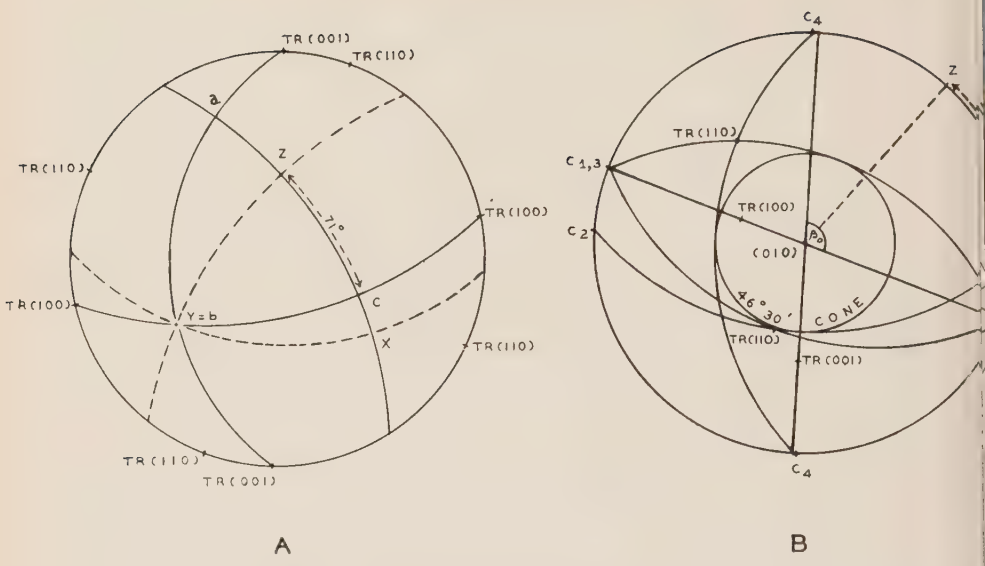

FIG. 2. Stereographic constructions of the extinction angle $Z \wedge c$ from the orientation of the indicatrix and from the traces of crystallographic planes in a section through an aegirine-augite crystal. In *A* the *c* axis is found by construction of *h0l* planes and their intersection in *ac*, using the initial projection on the plane of section. *B* is a projection of the same crystal on the *ac* plane, plotted from *A*, in which the construction of (110) planes tangent to a 46°30′ cone about *b* is greatly facilitated.

sphere with their appropriate Miller indices and the prefix *TR*.

Either trace of the (110) form, by rotations about *b* 180° apart, falls on opposite 46°30′ great circles from the centre, representing a tangential plane to the corresponding cone about *b*, reproduced by the symmetry in 010. Also, if more than 46°30′ radially from *b*, either (110) trace has two possible locations on each 46°30′ great circle resulting in two different tangential planes and therefore generally in two possible locations of *c* in 010. The same applies to the other (110) trace, but from the four possible locations of *c* thus produced at least one of the latter should be shared with the former to satisfy the symmetry of the form. Failure to do so implies lack of accuracy in orientation and construction and may be overcome by adhering to the mean location between the 2 most nearly coinciding orientations resulting from different traces. A further check may be available in the trace of any *h0l* plane in 010. In Figs. 1*A* and 2*B* the correct location of *c* is shown by $c_1 = c_3$. However, c_2 may also coincide with c_4 (cf. Fig. 1*B*) when a series of steps can be taken to decide which is the correct location by:

(i) Reading the alternative extinction angles $Z \wedge c_1 = c_3$ and $Z \wedge c_2 = c_4$ from the primitive circle graduation and comparing the values so obtained with the range of extinction

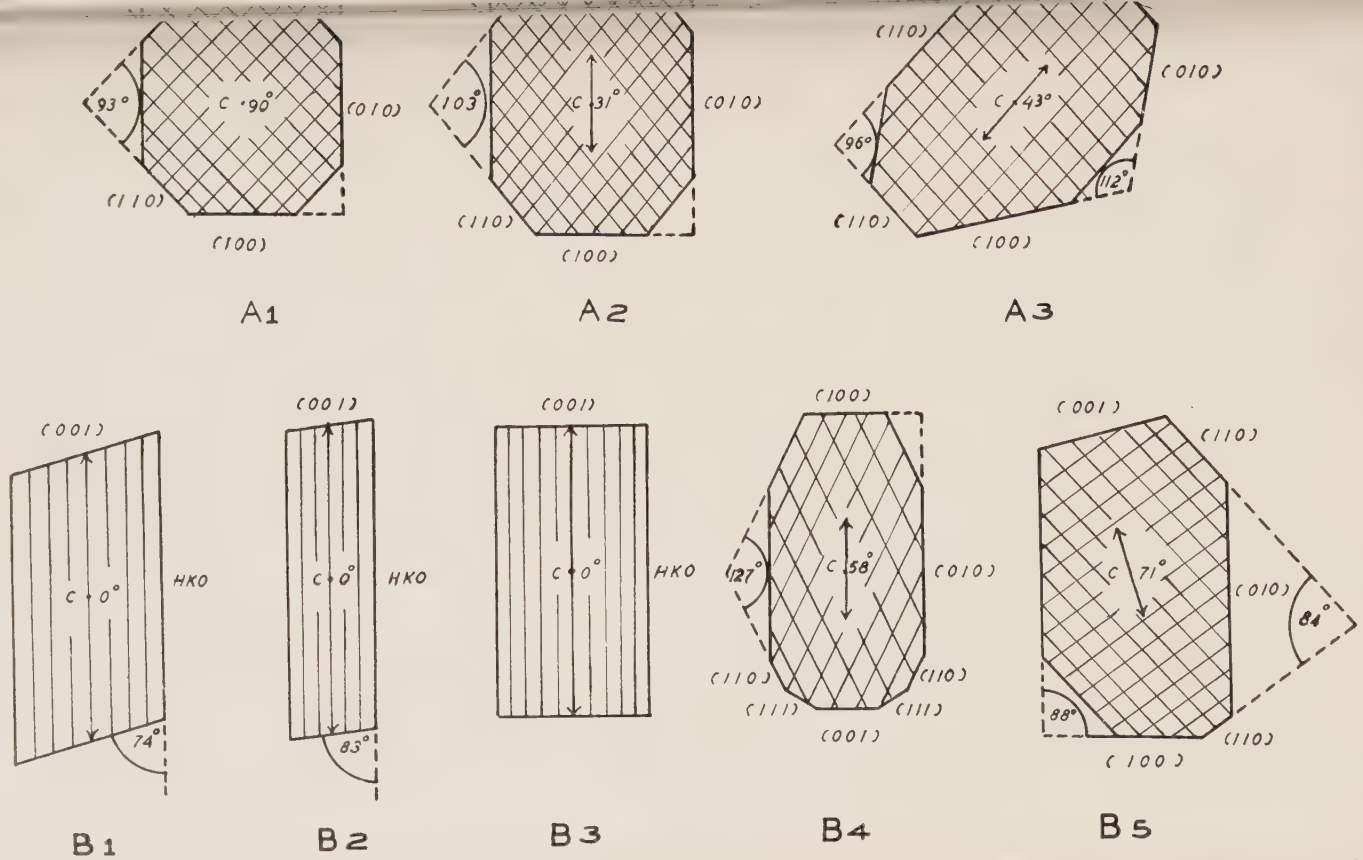

FIG. 3. Ideal sections of an aegirine-augite crystal typical of the treatment required for recognition of their orientation. Possible directions and inclinations of c to the section are indicated as well as some of the relevant intertracial angles. Symbols refer to the schedule of typical sections given in the text. Ambiguity of orientation in A_3 and B_5 will cease to exist once the sense of inclination of (010) is established. Axial elements: $(110) \wedge (\bar{1}10) = 87°$; $\beta = 74°$.

angles given by any of the better text books for the species under consideration Failure of elimination necessitates:

(ii) Gauging the sense of inclination to the section of at least one of the (110) planes. This is done in the conventional universal stage manner and is a much safer operation than the exact vertical adjustment as pointed out by Schmidt (1928, p. 206). The sense of inclination of c in 010, as derived from these data, is indicated by an arrow from the centre of the initial projection along the ac radial and is subsequently rotated to a corresponding position along the primitive circle of the second projection.

Finally there may be either no alternative great circles to suit each trace (cf. Fig. 1*D*) or no difference between traces (cf. Fig. 1*C*) both resulting in a unique location of c, perpendicular or parallel to the section respectively.

Schedule of Typical Sections

The general procedure of stereographic construction may now be supplemented by a practical subdivision of monoclinic pyroxene-amphibole sections according to the treatment required for recognition of their orientation.

c being the dominant zone axis sought, the sections may be roughly divided into:

(*A*) those $\perp$ or sub $\perp$ to c, being approximately octagonal in outline;

(*B*) those $\parallel$ or sub $\parallel$ to c, being approximately rectangular or parallelogram shaped in outline.

In each case the forms of faces are identified as far as possible by their relations to the characteristic (110) cleavages and to (010) as determined by means of the indicatrix. Preference is given to $hk0$ planes as direct indicators of c in 010.

(*A*) In this division three types of sections may be recognized as to require a different treatment. These are:

(1) *Those $\perp$ to c,* which are easily recognized by true dihedral angles between all traces of $hk0$ planes. For petrofabric purposes all adjustment and plotting may be dispensed with. Plotting of the indicatrix is necessary for the determination of $Z \wedge c$, whereby the principal section of the indicatrix coinciding with 010 should be vertical and c in the centre of the initial projection.

(2) *Those $\perp$ to 010, sub $\perp$ to c* may be distinguished from those $\perp$ to c by true dihedral angles of 90° between 100 and 010 but apparent dihedral angles between the traces of other planes such as 110 and $\bar{1}10$, whilst the principal section of the indicatrix coinciding with 010 appears to be vertical in the initial projection. Location of c depends on the traces of (110) planes.

(3) *Other sections sub $\perp$ to c* do not reveal any true dihedral angles between $hk0$ traces unless $\perp$ to 100. Location of c is obtained by construction of 100 in the initial projection through b and its trace in the section. An alternative is available in the construction of (110) planes, which may be used as an unequivocal check on the location of c for steep inclinations of 010 to the section (cf. Fig. 4*A*).

(*B*) Sections parallel or subparallel to *c* may be subdivided into five types according to the treatment required:

(1) *Those* ∥ *to 010* are recognized by perfect parallelism of *hk*0 traces combined with a cardinal orientation of the indicatrix which has the principal section coinciding with 010 horizontal. True dihedral angles are enclosed between the traces of all *h*0*l* planes. The trace of any *hk*0 plane in the section gives the location of *c*. Z/*c* is read from the arc of the microscope stage.

(2) *Those* ∥ *to c, sub* ∥ *to 010* are identified by parallelism of *hk*0 traces with the principal section of the indicatrix coinciding with 010 inclined at less than 40° to the section. They are treated in essentially the same way as B_1 provided 010 is set horizontal for reading Z/*c*.

(3) *Those* ∥ *to c,* ⊥ *or sub* ⊥ *to 010* constitute a case similar to B_2 with the exception that 010 cannot be set parallel to the microscope stage for direct measurement of Z/*c*. It may be read, however, from the great circle connecting Z and the *hk*0 trace in the initial projection.

(4) *Those* ⊥ *to 010, sub* ∥ *to c* are not essentially different from those mentioned under A_2 but subparallelism of *hk*0 traces may prove to be confusing, in which case *hkl* traces, if identifiable, can be used to advantage.

(5) *Other sections sub* ∥ *to c* are similar to those sub ⊥ to *c* the treatment and recognition of which are given under A_3. However, the 001 trace is now more likely to appear alongside that of 100 or even as the only *h*0*l* trace available. As both may be used for the location of *c* in this type of section, care should be taken to correctly identify the faces they represent. If both are present they will be seen to make different angles with 010 whereby the 001 trace is characterized by absence or shorter development of adjoining (110) traces compared with those near the 100 trace (cf. Fig. 4*B*). If only (001) or (100) traces are present, they will be parallel and the relevant face giving rise to a subparallel location of *c* is represented (cf. Fig. 4*C*).

Applicability, Advantages and Limitations

The proposed method is applicable to random sections of crystals with known axial elements, identifiable faces or cleavages, and known crystallographic orientation of one principal section of the indicatrix, commonly the optic axial plane, as provided by the majority of monoclinic pyroxenes and hornblendes. It is virtually independent of the degree of perfection and preservation of faces and cleavage planes, because the crystallographic reference planes are described by their trace directions in the horizontal plane of section and their relation to a principal section of the indicatrix only. Once the orientations of the two measured principal sections of the indicatrix have been corrected on the Fedorov or Hallimond (1950) nomograms for errors due to tilt of the section on vertical adjustment, no more errors of this type are introduced in the construction of crystallographic reference planes. Especially for low inclinations of the latter to the section the accuracy of construction is thus improved while time consuming corrections are reduced to a minimum.

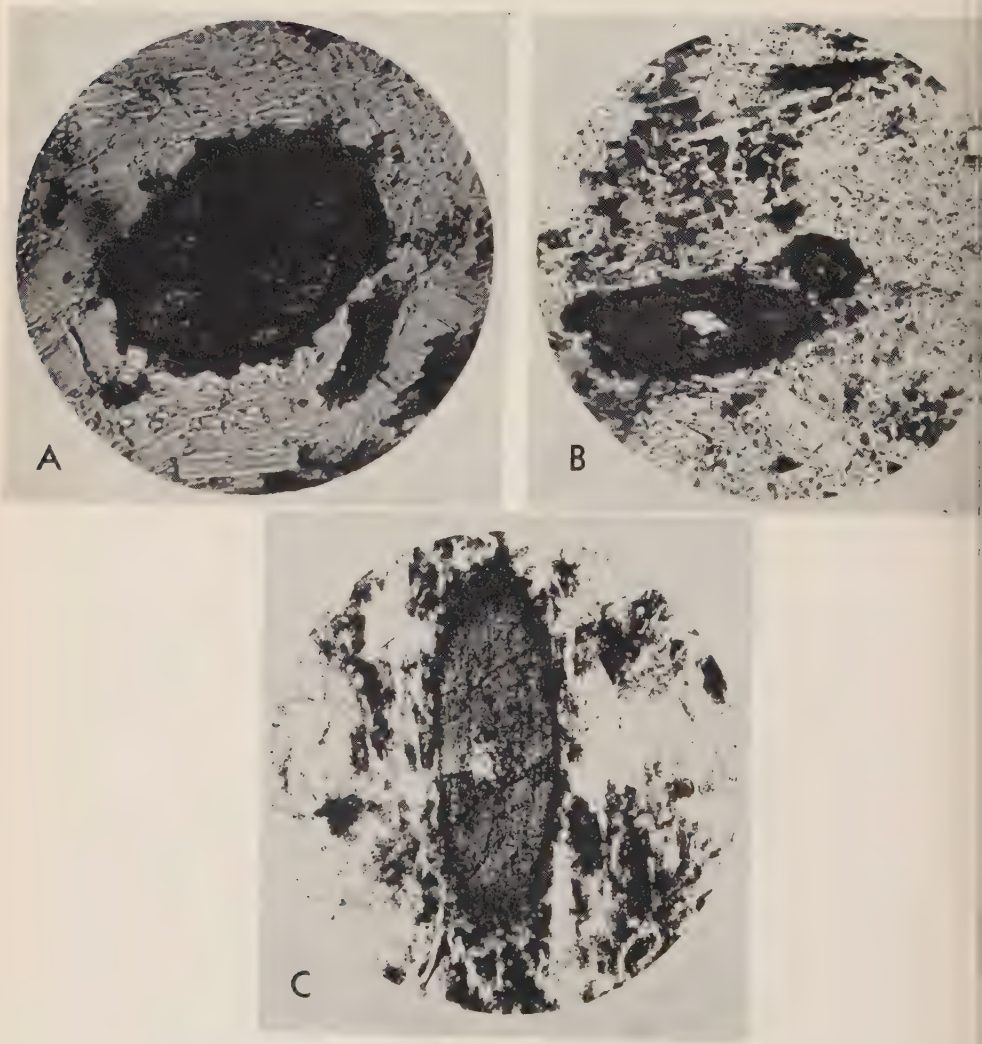

FIG. 4. Three photomicrographs of general orientations as shown by the outline of aegirine-augite phenocrysts in selected sections of alkaline trachytes from the Macedon district, Victoria. Identification of planes is aided by the presence of traces of one (110) cleavage in *A*, of 001, 010 and 100 faces in the larger phenocryst in *B*, and of (001) and (100) partings in *C*. *A* conforms to A_3, *B* and *C* to B_5 of the schedule. *C* is nearly parallel to 010. Lin. mags: *A* and *B*, 350; *C*, 100.

Generally c may be located within 2° in 010 if the relevant traces can be adjusted with an accuracy of $\frac{1}{2}°$. This may not be possible for low inclinations of the relevant planes to the section as is often the case with $hk0$ faces and cleavages in sections of monoclinic pyroxenes and hornblendes subparallel to c. However, this effect is countered by the only slight change in location of c brought about by a specific variation of trace direction in these sections as compared with that due to the same cause in sections subperpendicular to c, where the $hk0$ traces are usually adjustable within less than $\frac{1}{2}°$. Also, in the latter type of section, there is a greater variety of identifiable $hk0$ traces offering a close check on the location of c (cf. Fig. 1*C*, *D*; 3*A*, *B*; 4). This constancy of error within 2° for all orientations makes the method especially suitable for statistical treatment of dimensional orientation as used in the petrofabric analysis of rocks for possible lineations provided by monoclinic pyroxenes and hornblendes. For individual crystals the extinction angle or optical orientation, indicating the chemical composition, should be determined by means of the most accurate pertinent method.

The principal limitation of the proposed method is set by the requirement of identifiable faces or cleavages. Thus the mineral under consideration should be of idiomorphic development throughout the slide unless at least two characteristic and identifiable cleavages are available as in the monoclinic pyroxenes and hornblendes. In the latter minerals the identification of faces is greatly facilitated by the presence of either or both (110) cleavages. Idiomorphic development may be rare, but in certain extrusive and hypabyssal rocks a lineation can be restricted to the phenocrysts. Idioblastic development of amphiboles is, on the other hand, a common feature.

Schmidt (1928) applied predetermined extinction angles from selected sections to the optical orientation of unfavourable sections once the sense of inclination of (110) and c were established. For quick, though rough results in microscopic dimensional lineation, universal stage work is made superfluous by adapting Lowe's method (1946) of correlating average apparent lineations to use in oriented sections. However, $Z \wedge c$ may vary for individual crystals, whilst apparent lineations may be too faint to be recognized by visual averaging of elongations.

It is indeed very likely that lineations suggestive of the mode of emplacement are to be found in apparently massive igneous rocks by petrofabric analysis of selected specimens, whereby individual location of dominant zone axes will add to accuracy with very little extra effort as shown above. Results of this nature will be discussed in a separate paper.

Use of the 5 axes universal stage is not essential, but it may be helpful in identifying sections subparallel to ZX with the aid of the Berek-Dodge

procedure as advocated by Emmons (1943), especially when the optic axial angle is suspected to be rather small and Bx_a subhorizontal.

Acknowledgment

The author is greatly indebted to Dr. C. M. Tattam, Associate Professor of Geology in the University of Melbourne, and to Dr. J. McAndrew, Officer of C.S.I.R.O. Mineragraphic Section, Melbourne, for critical reading of the manuscript and valuable suggestions.

References

Schmidt, W. (1928), Zur Regelung Zweiachsiger Mineralien in Kristallinen Schiefern: *N. Jahrb. Min., A*, **57,** 203–222.

Burri, C. (1931), Zur Bestimmung der Auslöschungsschiefe Monokliner Hornblenden und Augiten auf (010) mittels beliebiger Schnitte: *Schweiz. Min. Petr. Mitt.*, **11,** 285–289.

Nieland, H. (1932), Zur Bestimmung von Auslöschungsschiefe und Kristallformen mittels des Drehtisches nach Fedorow: *Centralbl. Min., A*, 215–218.

Wenk, E. (1936), Zur Genese der Bändergneise von Ornö Huvud: *Bull. Geol. Inst. Univ. Upsala*, **26,** 59–60.

Nemoto, T. (1938), A new method of determining extinction angles of monoclinic minerals, especially pyroxenes and amphiboles by means of random sections: *Journ. Fac. Sc. Hokkaido Imp. Univ.*, IV, **4,** 108–112.

Turner, F. J. (1940), Note on determination of optic axial angle and extinction angle in pigeonites: *Am. Mineral.*, **25,** 821–825.

Turner, F. J. (1942). Determination of extinction angles in monoclinic pyroxenes and amphiboles: *Am. Jour. Sc.*, **240,** 571–583.

Emmons, R. C. (1943), The Universal Stage with 5 axes of Rotation: *Geol. Soc. Am. Memoir*, **8,** 28–39.

Donnay, J. H. F. and O'Brien, W. A. (1945), Microscope goniometry: *Jour. Ind. Eng. Chem., An. Ed.*, **17,** 593–597.

Lowe, K. E. (1946), A graphic solution for certain problems of linear structure: *Am. Mineral.*, **31,** 425–434.

Gilbert, Ch. M., and Turner, F. J. (1949), Use of the Universal stage in sedimentary petrology: *Am. Jour. Sc.*, **247,** 3–7.

Burri, C. (1950), Das Polarisationsmikroskop: Basel, Birkhäuser Verl., 151 159, 272–279, 286–293.

Hallimond, A. F. (1950), Universal stage methods: *Mineral. Mag.*, London, **83,** 12–22, 77–80.

Sabine, P. A. (1950), Optical properties and composition of acmitic pyroxenes: *Mineral. Mag.*, **29,** 120–122.

Manuscript received Oct. 10, 1952.

ON CLOUDED PLAGIOCLASE

ARIE POLDERVAART AND ARTHUR K. GILKEY*

ABSTRACT

Various theories to account for clouded plagioclase are reviewed. Observations indicate that the particles causing this effect may consist of different minerals, and that many minerals, besides plagioclase, may show clouding. It is suggested that in clouded minerals there are minute surfaces of physical discontinuity which provide adequate passages for diffusion of material into and out of the crystals. In intermediate plagioclases these surfaces may consist of internal phase boundaries in the unmixed feldspar. Slight clouding is probably due to exsolution of iron present in the feldspar lattice at the time of its formation, but more intense clouding is believed to be the result of the migration of iron and other elements into the crystal after its formation. The geological significance of clouded plagioclase is discussed and it is shown that such feldspars cannot be used as sole criteria for thermal metamorphism.

INTRODUCTION

There are many records in the literature of peculiarly clouded plagioclases. The phenomenon is due to the presence of numerous minute dark particles distributed throughout the crystals. These microlites consist of one or more minerals which sometimes can be recognized with difficulty (seldom with certainty) under the microscope. Clouding may be slight or very pronounced, rendering crystals nearly opaque. The particles are described as dust-like specks, short rods, or thin, hair-like growths and needles. They vary from sub-microscopic dimensions to one-tenth of a millimeter or more in diameter, but enclosures large enough to be identified with ease under medium powers of magnification are generally not included in the phenomenon of clouded feldspars.

Clouding of this type is different from the turbidity so frequently shown by feldspars upon weathering or hydrothermal alteration, and caused by the development of small flakes of kaolinite or sericite. It is also different from the phenomenon seen in so-called "gefüllte" feldspars in which the microlites consist of clinozoisite and sericite (Christa, 1931; Cornelius, 1935). The different types of turbidity are easily distinguished optically, and it would avoid confusion if the adjective "clouded" be reserved for the phenomenon described here.

The geological significance, origin, and nature of clouded feldspars has been the subject of speculation. Various opinions expressed in the literature are reviewed in the present paper, additional observations are made, and further suggestions offered concerning clouding in plagioclase and other minerals.

* Department of Geology, Columbia University, New York. N. Y.

The authors wish to thank Mr. J. Anthony Denson of the United States Geological Survey for his cooperation in taking the photomicrographs included in this paper.

Previous work

In an important contribution, MacGregor (1931) attributed clouding of plagioclase to thermal metamorphism. He thought that the minute particles which produce clouding probably consist of iron ore, and believed that later heating results in exsolution of iron originally contained in the plagioclase in solid solution. He noted that clouded plagioclase crystals often have clear margins which are also more sodic. Consequently he believed that the solubility of iron in plagioclase decreases rapidly towards the sodic end of the series. Feldspar analyses also show almost twice as much iron oxide in oligoclase-anorthite than in albite or potash feldspars. MacGregor considered that clouding of plagioclase marks low-grade thermal metamorphism of pre-existing feldspar, which with higher temperatures recrystallizes to clear plagioclase.

MacGregor's interpretation of clouded feldspars has been accepted by many petrologists; so much so that the occurrence of clouded plagioclase in a rock is now sometimes cited as "evidence" for the rock having been subjected to thermal metamorphism. Thus Bailey (1952, p. 303) remarks that "*all* the many Scourie dykes examined are metamorphosed, for *all* which have not suffered more obvious reconstruction have clouded feldspars."

However, the literature by no means shows general agreement with MacGregor's conclusions. Grout (1933, p. 1014) found clouded plagioclase in hornfels xenoliths in gabbros of Minnesota and pointed out that "in the Minnesota rocks the feldspars are newly generated from clay minerals, so that the cloudiness is not due to an attack upon old feldspars and certainly is not a sign that the unaltered rock was a feldspathic igneous rock."

Joplin (1935) criticized in particular MacGregor's opinion that clouding is an exsolution phenomenon. Anderson (1937, p. 65–7) found that "in the rocks of the northern Inyo Range, the potassic feldspars are as strongly clouded as are the plagioclase feldspars, and only the albite is relatively clear." He suggested that clouding may represent a forward migration of iron, sometimes of country-rock origin, through the pre-existing formations. Reynolds (1946, p. 435–6) noted that desilicated and basified rocks are commonly characterized by clouded lime-soda feldspars and concluded that "further investigation may show clouding of felspars, when present, to be a useful criterion in the recognition of rocks, produced by the basification of pre-existing types."

Williamson (1936, p. 149) pointed out that plagioclase crystals having a clouded core and clear rim do not always show a compositional change at the junction of interior and mantle. Shand (1945, p. 262) also found that the clear marginal parts of a plagioclase crystal may yet have the same composition as the dusty cores.

Little is known of the solubility of iron in plagioclase, and neither iron-albite nor iron-anorthite has been synthesized. However, experimental work has been done on iron-bearing potash feldspars (Faust, 1936; Rosenqvist, 1951). It is now generally believed that to a limited extent Fe^{+3} may substitute for Al^{+3} in the feldspar lattice, and that the iron would probably exsolve upon slow cooling as hematite or magnetite lamellae. Ramberg (1949, p. 30) in a footnote stated that the greenish brown color of plagioclase in the granulite facies "is due to absorption of about 0.5 per cent FeO and Fe_2O_3 in the feldspar lattice"—"probably the high P-T conditions of the granulite facies enable iron to enter the feldspar lattice provided that the chemical potential or vapor tension of Fe in the rocks is high enough." Finally, Herz (1951, p. 985) found that finely crushed plagioclase with clouded cores and clear margins from the Baltimore gabbro, Maryland, could be separated with a Franz separator into a least magnetic fraction of sodic plagioclase free from inclusions, and a more magnetic fraction of calcic, clouded plagioclase.

Examples of clouding in plagioclase of volcanic rocks have also been found. Cloudy zones in plagioclase phenocrysts of pyroxene-andesites from Hakone volcano were observed by Kuno (1936; 1950) and attributed by him to mixing of two different magmas. Bentor (1951, p. 535) found similar plagioclase phenocrysts in the Quaternary volcanics of the Chaîne des Puys and believed the phenocrysts "formed by a process of auto-resorption, during which the fluid magma breaks through the roof of the magma chamber, formed by a holocrystalline plutonic facies of the same magma." In both cases the particles producing the cloudy zones consist of glass and of minerals other than plagioclase found also as constituent minerals of the rocks. It is therefore believed that this type of clouding is produced by the incorporation of foreign particles through rapid growth of the plagioclase. Consequently the cloudy zones in plagioclase phenocrysts of volcanic rocks are different from the clouded plagioclase described in the present paper.

Present Observations

The writers studied a large number of different examples of clouded feldspars and as a result are able to confirm and add to observations made by previous workers. The relations of clouded plagioclase are here summarized.

1. Plagioclase of large gabbroic intrusions, such as the Bushveld, Namaqualand, Stillwater, Sudbury, Baltimore, and Cortlandt plutons is frequently slightly and sometimes even strongly clouded. The particles causing this effect may be extremely small and clouding may be so slight as to escape notice in cursory examinations of thin sections.

2. Plagioclase may show slight or medium clouding, even when there is no evidence of subsequent thermal metamorphism. Several authors have given examples of older rocks with clouded plagioclase occurring in regions where there are no younger intrusives (e.g., Wiseman, 1934; Poldervaart and von Backström, 1949). The conclusion drawn from equivalent examples by MacGregor (1931) is that the presence of clouded feldspar indicates later regional heating of the rocks, even when no younger intrusions can be found in the area. At Khale (Bechuanaland Protectorate) Poldervaart (1952) found a Karroo diabase sheet which shows clouded plagioclase near the chilled upper contact, although the feldspar of both the central diabase and the granitic country rock at the contact is clear. There are again no younger intrusives in this area. An assumption of post-Karroo regional heating of the rocks is extremely unlikely and does not explain the observed variations in clouding of plagioclase in different parts of the sheet.

3. Feldspar-bearing coronites invariably contain clouded plagioclase (Shand, 1945, p. 262). Feldspar-bearing meteorites, likewise, contain clouded plagiocalse (H. H. Hess, personal communication). Members of the charnockitic suite of rocks often, but not invariably, contain clouded feldspar, as well as blue quartz (Quensel, 1951). Basic dikes cutting charnockites and other Basement rocks of southern Mysore *all* contain clouded plagioclase, although probably several ages of dike-intrusion are involved. The equivalent dikes of northern Mysore contain clear feldspar (Ch. Pichamuthu, personal communication).

4. Clouding is not confined to plagioclase only, but has been observed in apatite, spinel, olivine, rhombic and monoclinic pyroxene, potash feldspars, quartz, biotite, hornblende, garnet, and even in calcite and serpentine. Platy or needle-like opaque inclusions of a larger size (schiller, sagenite, etc.) are more common in ferromagnesian minerals, but the dust-like particles which cause clouding can also be found and exactly reproduce the features of clouded plagioclase described here. In thin sections of blue quartz clouding appears as a yellow turbidity, believed by Jayaraman (1938; 1939) to be due to the presence of colloidal TiO_2.

5. The particles producing clouding may vary greatly in size, sometimes within the same host. When large enough to be identified, it is frequently noted that they consist of other minerals such as biotite (Groves, 1935), spinel (Shand, 1945), rutile (MacGregor, 1931), hornblende, or garnet, as well as opaque ore.

FIG. 1. Magnetite-ilmenite ore, Sanford Lake, Adirondack Mountains, New York. Clouded plagioclase crystal with irregular trails. ×15.

FIG. 2. Magnetite-ilmenite ore, Sanford Lake, Adirondack Mountains, New York. Clouded plagioclase crystal with trails. Note cleared incursions with larger microlites extending inward from unclouded periphery. ×25.

6. The particles appear to be rod-shaped rather than spherical, and small specks are probably cross sections of rods. Even the smallest particles seem to be elongated when viewed with high magnifications.

7. The orientation of the rods is somewhat variable. The smallest particles are apparently randomly distributed throughout the host-crystal, but their seeming lack of orientation may be the result of their smaller size. Larger particles are oriented either parallel to albite composition planes (Reynolds, 1936, p. 341), or are aligned in at least three, and probably four sets which intersect the albite twin planes (Williamson, 1936, p. 149). Apparently both types of orientation have not been found in the same rock.

8. The distribution of the particles is also irregular. Clouding may be evenly distributed throughout the host crystal. Frequently narrow irregular trails of clear or less turbid feldspar may be seen in the clouded crystals (Figs. 1, 2). These trails pursue a course entirely unrelated to the morphological directions of the host mineral, branch and bifurcate freely, and coalesce in slightly larger, clear patches. Sometimes the trails are studded at irregular intervals with larger enclosures of various minerals (Fig. 2), but this is not always the case. In other instances, different densities of clouding within the same crystal may form a highly irregular pattern (Fig. 3).

9. Clouded feldspars do not invariably have clear margins. The "clear"

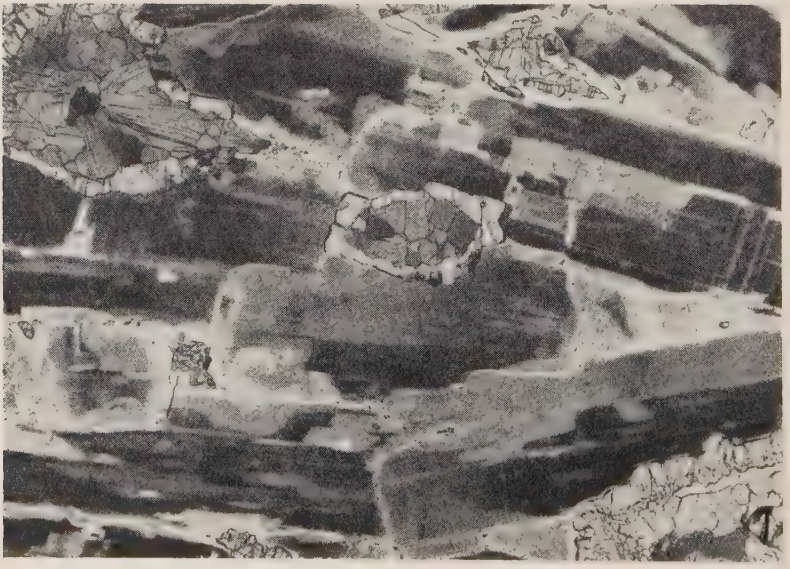

Fig. 3. Metagabbro, Adirondack Mountains, New York. Densely and irregularly clouded plagioclase mostly with narrow, clear rims. ×25.

FIG. 4. Metagabbro, Gore Mountain, New York. Plagioclase clouded with spinel and garnet particles, larger in the marginal portions than in the cores. ×70.

mantles, when present, may actually be devoid of inclusions, or may contain fewer and larger enclosures than the clouded cores (Fig. 4), thus creating an impression of greater purity, although probably containing the same total amount of foreign material as the clouded cores. In some cases clouding actually increases in density toward the margin, despite a narrow, clear outer zone. In coronites clouded plagioclase crystals often show corroded outlines and are surrounded by olive green, greenish brown, or brown hornblende. The outer portions of the plagioclase may be clear, or clouding may persist to the periphery, or it may actually extend some distance into the surrounding hornblende (Fig. 5); all three instances having been observed in the same rock, and even in different marginal portions of the same crystal. Where clouding extends into the surrounding hornblende the particles are often slightly larger in the hornblende than in the plagioclase. Moreover, the rods maintain the same orientation in the hornblende coronas as in the enclosed plagioclase, regardless of the disposition of the former in relation to the latter mineral.

10. Demarcations between clouded and clear portions of crystals are not confined to planes of chemical discontinuity in the host mineral. Such demarcations may occur at twin composition planes, or along boundaries which mark a temporary halt in the crystallization of the host mineral. The latter boundaries often coincide with sudden variations in composi-

FIG. 5. Coronite, eastern Quebec. Corroded plagioclase crystal with spinel and opaque ore particles which extend into the surrounding hornblendic corona. ×30.

tion, but the former do not. The demarcations appear sharp with low or medium magnifications, but with high magnifications they can be seen to consist of narrow zones in which there is a rapid, but gradational decrease in concentration of the minute enclosures. Whether or not there is a compositional difference, clouded crystals frequently show a decrease in clouding intensity towards their margins, and this peripheral clearing does not appear to be related to either chemical or physical differences in the plagioclase of the turbid and clear portions.

11. Larger inclusions of foreign minerals (e.g., quartz) or of newly-formed minerals (e.g., garnet) in clouded plagioclase may or may not be surrounded by narrow, clear rims. In the case of newly-generated garnet in plagioclase of a coronite (Fig. 6), it may be noted that there is a concentration of minute opaque particles immediately surrounding the garnet enclosure, though a narrow clear strip may be present between the garnet and the nearly opaque plagioclase. Similar features may be observed in enclosures of opaque ore in pyroxenes or other ferromagnesian minerals. Here too there is no evidence of any physical or chemical discontinuity between the clear and the clouded portions of the host mineral.

12. Time appears to play a major role in the production of clouded feldspars. Country rocks at the immediate contact of diabase intrusions are heated to a higher temperature than those occurring at contacts of granitic plutons, yet the authors know of no case of small diabase intru-

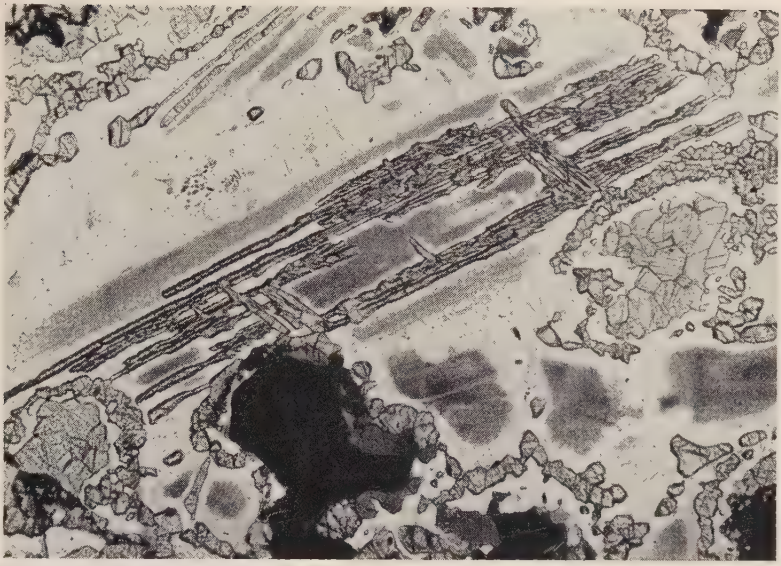

FIG. 6. Coronite, Essex County, New York. Newly-generated garnet in partly clouded plagioclase crystal. Clouding is concentrated around the garnet, but generally there is a narrow, cleared zone between the garnet and the clouded feldspar. ×25.

sions having produced clouding in the plagioclase of the adjacent rocks by thermal metamorphism only. This appears to hold no matter what the composition is of the plagioclase. However, assimilation of argillaceous material by diabase magmas produced hypersthenic rocks which frequently contain newly-generated, clouded plagioclase (cf. Walker and Poldervaart, 1941).

ORIGIN OF CLOUDING MATERIAL

There appear to be two contrasting views with regard to the origin of the particles producing clouding in plagioclase and other minerals. According to one view the material composing these particles was incorporated in the crystal at the time of its formation, while the second theory holds that the material was introduced into the crystal some time after its formation. It may be stated here that in the opinion of the present writers both theories are probably correct and supplement one another.

Slight clouding of plagioclase, such as observed in many gabbroic intrusives, is probably caused by exsolution of foreign ions in the plagioclase lattice upon slow cooling. Most likely a large proportion of these foreign ions consists of Fe^{+3} substituting for Al^{+3} in the lattice, but undoubtedly other ions such as Fe^{+2} and Mg^{+2} are also present. However,

it appears to the writers somewhat unreasonable to assume that intense clouding of plagioclase which renders crystals almost opaque, is due to exsolution of iron and other ions originally contained in the lattice. Whatever the solubility of iron in plagioclase, it is not likely to be more than a fraction of a per cent. Reliable analyses of clear plagioclase from volcanic rocks, in which the foreign ions are presumably not exsolved, also do not show more than at most 0.5 per cent total iron.

Bowen (1948) has ably summarized the case against diffusion through crystals in noting that (1) the threshold temperature for appreciable diffusion is approximately 0.8–0.9 T (Eitel, 1929), where T is the absolute melting temperature of the silicate, (2) the crystallization temperature of minerals in polycomponent systems such as magmas is far below that of the individual phases, and hence probably also below the diffusion threshold temperature, (3) the coefficient of diffusion for solid silicates is of the order 10^{-9}–10^{-10} cm^2/sec., while that of "dry" silicate melts is roughly 10^{-6}–10^{-7} cm^2/sec., and the temperature diffusion coefficient is about 10^{-2} cm^2/sec.; hence heat dissipation would normally prevent any appreciable diffusion in crystals and (4) zoned crystals should become uniform upon diffusion of ions through their lattice; the presence of zoning therefore indicates that diffusion through the lattice of the zoned crystal did not occur.

Objections could probably be raised against these arguments (Goldsmith, 1952), but the weight of the evidence does not favor diffusion of extraneous ions through the feldspar lattice as being the cause for intense clouding of plagioclase. On the other hand, the evidence does indicate that the material which produces clouding in plagioclase is extraneous and only migrated into the crystals after their formation. Other examples, such as the replacement of plagioclase by almandine garnet starting in the feldspar core (Fig. 6), also indicate that extraneous material can and does diffuse into already-formed crystals. This is the main conclusion of the present writers, but in seeking to explain how this material migrated into the plagioclase crystals they can only offer suggestions, in the hope that this will stimulate further experimental work.

Cleavage planes probably provide openings of relatively large size which freely permit outside solutions to penetrate the crystal. Deposition of and replacement by other minerals along cleavage planes prove that solutions do penetrate crystals along these passages. Subboundaries have been observed in metals (Guinier, 1950, pp. 402–440) and similar phenomena may be present also in silicates, representing potential passages for diffusion of slightly smaller separation than cleavage planes. If present in silicates, block structures (Freudenthal, 1950) may provide potential passages for diffusion of comparable or smaller separation.

Transformations of the so-called disordering type (Buerger, 1948) result in the production of innumerable small surfaces of physical discontinuity, each the size of a few unit cell surfaces. Intermediate plagioclases are at low temperatures mixtures of low-albite and anorthite; two phases which are evenly, and probably more or less symmetrically distributed throughout the crystal in layers a few unit cells large (Cole, Sörum, and Taylor, 1951). Along the mutual boundaries of these two phases there probably exists a state of high disorder, and such "internal phase boundaries" may provide a great many potential passages for diffusion, allowing for extremely intimate penetration of the crystal. Owing to this high degree of disorder, the internal phase boundaries may show features comparable to the surface boundaries of the crystal, rather than the bulk material.

Surface effects are still very imperfectly understood, yet present evidence indicates that they may play a major role in such important geological processes as diagenesis, metasomatism, metamorphism, and weathering (Verhoogen, 1948). Experiments show that "monomolecular films" have properties different from those of the corresponding solids and more nearly like those of the liquids. Lichtenecker (1942) found that surface melting of metal layers 10^{-4} cm. thick occurs at temperatures much lower than the true melting temperature. Adam (1941) noted that melting of thin films is rarely sharp but occurs gradually over a melting interval. Most significant to the present discussion, Beischer (1950) found that surface diffusion coefficients of stearic acid on mica are "greater than the values normally found for volume diffusion coefficients of substances in solids. They are of the magnitude of diffusion coefficients in liquid diffusion media" (1952, p. 683).

It would seem from these observations that (1) in unmixed minerals, such as intermediate plagioclases, there are innumerable surfaces of physical discontinuity present, more or less regularly distributed throughout the crystals, (2) the material along these boundaries is probably highly disordered and may show effects comparable to crystal surfaces rather than bulk material, (3) surface properties are different from those of bulk material and more nearly like those of the corresponding liquids, (4) surface melting occurs at lower temperatures than the true melting of the equivalent bulk material, while measured coefficients of surface diffusion are appreciably higher than those of the corresponding solids. Thus it seems at least plausible for material to diffuse into crystals along these potential passages, in preference to diffusion through the crystal lattice. Nor is it necessary for zoned crystals to become uniform when diffusion takes place along internal phase boundaries. Whether these passages are large enough to accommodate water molecules, or diffusion

is in the "solid state" is not known, but the solution of this problem is not essential to the present discussion.

Experimental work carried out so far has been mainly concerned with solid diffusion of ions through crystal lattices, in the absence of water (cf., Rosenqvist, 1951; Verhoogen, 1952; Jensen, 1952). These experiments have shown that ionic diffusion in crystals is controlled by both ionic size and electrostatic charge. The influence of electrostatic charge appears to be especially marked and Verhoogen found that large K^{+1} ions diffuse more rapidly through quartz plates than small bivalent or trivalent ions such as Mg^{+2}, Fe^{+2}, Al^{+3}, or Fe^{+3}. On the other hand, in clouded feldspars it is apparent that diffusion affected especially these smaller ions of high valency. Coefficients of diffusion found experimentally so far also seem too low to account for clouded feldspars. The present writers suggest that possibly higher values might be obtained if the experiments were repeated under high water vapor pressures. It may be significant that Bowen and Tuttle (1950, p. 500) found that unmixing in K-Na feldspars at elevated temperatures is accelerated when the crystals are maintained under high water vapor pressures.

The size of the particles in clouded plagioclase is clearly many times that of the suggested internal phase boundaries. Possibly upon crystallization of the introduced material along the larger conduits ions were drawn from the smaller passages, or perhaps the growing microlites enlarged the smaller passages.

Replacement of one mineral by another from the core outwards, instead of from the periphery inwards (Fig. 6), and the intimate penetration achieved in associations of synantectic minerals in symplektites may also be explained by the occurrence of minute division surfaces within unmixed crystals and migration of extraneous ions along these potential passages.

Petrology of Clouded Plagioclase

Given a sufficiently high temperature level for diffusion, ions will migrate principally down concentration gradients, but other effects, notably thermal convection-diffusion (Wahl, 1946) may also prevail. Temperature probably also governs which ions are predominant in the solutions at any particular time. Iron apparently migrates at rather low temperatures, while the predominance of Fe^{+2} or Fe^{+3} is probably determined by such factors as temperature, initial rock-composition, hydrogen ion concentration at any particular stage, etc. With an adequate temperature level, sufficient time, and in the presence of water, a fluid phase relatively rich in iron will be developed in the rocks.

In any particular crystal of intermediate plagioclase the iron concen-

tration along the internal phase boundaries and other surfaces of greater separation will be lower than that of the surrounding pore fluid, hence iron will tend to migrate along these potential passages into the crystal, and will continue to do so until some degree of equilibrium has been attained in the iron concentration of the pore fluid of the rock and that existing within the division surfaces of the crystal. Other ions will also tend to establish equilibrium by migrations into and from the crystal, but it is assumed that iron is the principal migratory constituent under the postulated conditions.

With a subsequent decrease in temperature, iron will crystallize from the pore fluid, perhaps as magnetite. The iron present along the internal phase boundaries and other surfaces of greater separation within the plagioclase crystal also crystallizes as magnetite, since there is equilibrium between the interior and exterior of the crystal. Likewise, hematite, spinel, garnet, biotite, rutile, or hornblende are formed *inside* the crystal if they happen to crystallize at the same time from the pore fluid *exterior* to the crystal. The fact that enclosures of clouded plagioclase, when large enough to be recognized, invariably are the same as minerals occurring outside the plagioclase crystals indicates some degree of equilibrium between exterior and interior of the crystals, and would seem to militate against the formation of the clouding particles by exsolution.

Within the minute division planes of the plagioclase crystal the iron ions are used up in the formation of numerous magnetite rods. The relatively rapid decrease in iron concentration of the pore fluid upon crystallization of magnetite may result in iron again diffusing out of the plagioclase crystal, but both the time factor and the interior crystallization of magnetite inhibit complete clearing of the plagioclase. Thus only the peripheral parts of the crystal become clear, while the larger part remains clouded. The above explanation assumes that concentration gradient is the dominant driving force for ionic diffusion. Other factors may also be important, and chemical potential, especially, may play a role, as suggested by Jensen (1952).

From these considerations the geological implications of clouded plagioclase may be postulated. Clouding occurs in unmixed plagioclases of intermediate composition, and intense clouding has not been observed in either albite or anorthite.* Conditions for clouding of plagioclase in a rock are (1) the existence of an adequately high temperature for a sufficient length of time, (2) the presence of an aqueous pore fluid, and (3) the presence of iron-bearing minerals in the original rock. These conditions are often realized in thermal metamorphism, but both the time factor and the amount of iron present in the original rock may be insufficient,

* Slight clouding in the end-members of the series is probably due to exsolution.

while there may also be insufficient water available for the formation of a medium for diffusion. It should also be noted that an "excess" of water would promote recrystallization of plagioclase in preference to clouding. In such cases thermal metamorphism does not produce clouded feldspars in the rocks. Regional metamorphism may likewise result in clouding of plagioclase if the requisite conditions are fulfilled. Clouding of plagioclase in the basic dikes of the north-west Highlands and southern Mysore is probably due to regional, rather than thermal metamorphism. A prolonged iron-rich deuteric phase in basic intrusives, as might result from magmatic incorporation of water and pelitic material upon emplacement, may also produce clouding of pre-existing or newly-formed plagioclase which cannot then be attributed to later thermal or regional metamorphism. The writers believe that the absence of strongly clouded plagioclase from basic intrusives not affected by later metamorphism is primarily due to a combination of unfavorable factors such as relatively rapid crystallization of iron ore, slow unmixing of plagioclase, and relative brevity of the deuteric stages. Clouded plagioclase clearly cannot form the sole criterion for thermal or regional metamorphism

Conclusions

Clouded feldspars are often found in thermal metamorphic aureoles, but plagioclase of thermally metamorphosed rocks is not invariably clouded, even when crystals are of original feldspar, nor is clouding of plagioclase confined to rocks subjected to thermal metamorphism. It follows that clouding of plagioclase cannot be used as a criterion for thermal metamorphism.

Slight clouding may be the result of exsolution of iron dissolved in the plagioclase crystal at the time of its formation. More intense clouding cannot reasonably be expected to be due to exsolution. The evidence indicates that such clouding is produced by diffusion of extraneous material into the crystal after its formation. Strong clouding is only observed in intermediate plagioclases, and crystals of this composition are at low temperatures extremely fine-grained mixtures of low-albite and anorthite.

Unmixing of a uniform plagioclase is considered to produce innumerable minute surfaces of physical discontinuity throughout the crystal, and these surfaces are believed to provide potential passsages for diffusion of material. The properties of the internal division surfaces are regarded as comparable to those of monomolecular films, for which experimental evidence indicates much higher coefficients of diffusion than are estimated for the bulk material. Thus the rate of diffusion along these passages is probably considerably higher than experimentally determined diffusion rates through crystal lattices.

Clouding is most common in plagioclase, but the same effects may be encountered in apatite, spinel, olivine, pyroxenes, amphiboles, micas, quartz, potash feldspars, garnet, calcite, and serpentine. The particles which produce clouding generally consist of opaque ore, but other minerals such as spinel, garnet, biotite, hornblende, and rutile may also be present in clouded minerals.

The requisites for plagioclase clouding are (1) elevated temperature for a prolonged period, (2) presence of water, and (3) supply of iron from the original rock. These conditions may or may not be realized in thermal or regional metamorphism. Frequently they are met, especially when basic rocks, normally of high iron content, are metamorphosed, but clouded feldspars are rarely found in metamorphosed arkoses poor in iron. Clouding of plagioclase may also be caused by extended iron-rich deuteric activity in basic intrusives, which often results from earlier assimilation of pelitic material and water by the magma.

References

Adam, N. K. (1941), The physics and chemistry of surfaces, London, Oxford Univ. Press.

Anderson, G. H. (1937), Granitization, albitization, and related phenomena in the northern Inyo Range of California-Nevada: *Geol. Soc. Am., Bull.*, **48**, 1–74.

Bailey, Sir Edward (1951), in written contribution to Sutton, J., and Watson, J. (1951), The pre-Torridonian metamorphic history of the Loch Torridon and Scourie areas in the northwest Highlands, and its bearing on the chronological classification of the Lewisian: *Geol. Soc. London, Quart. Jour.*, **106**, 241–307.

Beischer, D. E. (1950), Electronic radiography by transmission using radioactive monolayers: *Science*, **112**, 535–536.

——— (1952), Melting phenomena of a surface of monomolecular thickness: *Science*, **115**, 682–684.

Bentor, Y. K. (1951), On the formation of cloudy zones in plagioclases: *Schweiz. Min. Petr. Mitt.*, **31**, 535–552.

Bowen, N. L. (1948), The granite problem and the method of multiple prejudices: *Geol. Soc. Am., Mem.* **28**, 79–90.

———, and Tuttle, O. F. (1950), The system $NaAlSi_3O_8$-$KAlSi_3O_8$-H_2O: *Jour. Geol.*, **58**, 489–511.

Buerger, M. J. (1948), The rôle of temperature in mineralogy: *Am. Mineral.*, **33**, 101–121 (pres. addr.).

Christa, E. (1931), Das Gebiet des oberen Zemmgrundes in den Zillertaler Alpen: *Jour. Geol. Bundesanst. Wein*, **81**, 533–636.

Cole, W. F., Sörum, H., and Taylor, W. H. (1951), The structures of the plagioclase feldspars, I: *Acta Cristall.*, **4**, 20–29.

Cornelius, H. P. (1935), Zur Deutung gefüllter Feldspäte: *Schweiz. Min. Petr. Mitt.*, **15**, 4–30.

Eitel, W. (1929), Physikalische Chemie der Silikate, Leopold Voss, Leipzig.

Faust, G. T. (1936), The fusion relations of iron-orthoclase: *Am. Mineral.*, **21**, 735–763.

Freudenthal, A. M. (1950), The inelastic behavior of engineering materials and structures: John Wiley and Sons, New York.

Goldsmith, J. R. (1952), Diffusion in plagioclase feldspars: *Jour. Geol.*, **60**, 288–291.

GROUT, F. F. (1933), Contact metamorphism of the slates of Minnesota by granite and by gabbro magmas: *Geol. Soc. Am. Bull.*, **44,** 989–1040.

GROVES, A. W. (1935), The charnockite series of Uganda, British East Africa: *Geol. Soc. London, Quart. Jour.*, **91,** 150–207.

GUINIER, A. (1950), in Imperfections in nearly perfect crystals: John Wiley and Sons, New York.

HERZ, N. (1951), Petrology of the Baltimore gabbro, Maryland: *Geol. Soc. Am., Bull.*, **62,** 979–1016.

JAVARAMAN, N. (1938), The colour of the blue quartz of the charnockites of South India, and of the opalescent quartz-gneiss of Mysore: *Current Sci. Bangalore,* **6,** 381–383.

——— (1939), The cause of colour of the blue quartzes of the charnockites of south India and of the Champion gneiss and other related rocks of Mysore: *Indian Acad. Sci., Proc.*, **9,** 265–285.

JENSEN, M. L. (1952), Solid diffusion of radioactive sodium in perthite: *Am. Jour. Sc.*, **250,** 808–821.

JOPLIN, G. A. (1935), A note on the origin of basic xenoliths in plutonic rocks, with special reference to their grain-size: *Geol. Mag.*, **72,** 227–234.

KUNO, H. (1936), Petrological notes on some pyroxene-andesites from Hakone volcano with special reference to some types with pigeonitic phenocrysts: *Jap. Jour. Geol. Geogr.*, **13,** 107–140.

——— (1950), Petrology of Hakone volcano and the adjacent areas, Japan: *Geol. Soc. Am., Bull.*, **61,** 957–1020.

LICHTENECKER, K. (1942), Das Oberflächenschmelzen in einer Schichten 10^{-3} bis 10^{-4} mm.: *Zeits. Elektrochem.*, **48,** 601–604.

MACGREGOR, A. G. (1931), Clouded feldspars and thermal metamorphism: *Min. Mag.*, **22,** 524–538.

POLDERVAART, A. (1952), Karroo dolerites and basalts of the eastern Bechuanaland Protectorate: *Geol. Soc. S. Africa, Trans.*, **55,** 125–130.

———, AND VON BACKSTRÖM, J. W. (1949), A study of an area at Kakamas (Cape Province): *Geol. Soc. S. Africa, Trans.*, **52,** 433–495.

QUENSEL, P. (1951), The charnockite series of the Varberg district on the southwestern coast of Sweden: *Ark. Min. Geol.*, **1,** 227–332.

RAMBERG, H. (1949), The facies classification of rocks: A clue to the origin of quartzofeldspathic massifs and veins: *Jour. Geol.* **57,** 18–54.

REYNOLDS, D. L. (1936), The two monozonitic series of the Newry Complex: *Geol. Mag.*, **73,** 337–364.

——— (1946), The sequence of geochemical changes leading to granitization: *Geol. Soc. London, Quart. Jour.*, **102,** 389–446.

ROSENQVIST, I. TH. (1951), Investigations in the crystal chemistry of silicates. III. The relation haematite-microcline: *Norsk. Geol. Tidsskr.*, **29,** 65–76.

SHAND, S. J. (1945), Coronas and coronites: *Geol. Soc. Am. Bull.*, **56,** 247–266.

VERHOOGEN, J. (1948), Geological significance of surface tension: *Jour. Geol.*, **56,** 210–217.

——— (1952), Ionic diffusion and electrical conductivity in quartz: *Am. Mineral.*, **37,** 637–655.

WAHL, W. (1946), Thermal diffusion-convection as a cause of magmatic differentiation, Part I: *Am. Jour. Sci.*, **244,** 417–441.

WALKER, F., AND POLDERVAART, A. (1941), The Hangnest dolerite sill, S. A.: *Geol. Mag.*, **78,** 429–450.

WILLIAMSON, W. O. (1936), Some minor intrusions of Glen Shee, Perthshire: *Geol. Mag.*, **73,** 145–157.

WISEMAN, J. D. H. (1934), The central and south-west Highland epidiorites: A study in progressive metamorphism: *Geol. Soc. London, Quart. Jour.*, **40**, 354–417.

Manuscript received Jan. 24, 1953

"MR. ARTHUR K. GILKEY died August 10, 1953, in the unsuccessful attempt of the Third American Alpine Club Karakoram Expedition to climb K-2 in the Himalayas. It was a great shock to all who were privileged to know him to hear of his tragic death. As a student of geology Art Gilkey showed exceptional promise. He had completed a brilliant study on the Zuni uplift in New Mexico under the sponsorship of Professor Walter H. Bucher for his Ph.D. thesis, which he was to defend after his return from the Himalayan Expedition. His keen interest in and awareness of geologic problems was also manifest throughout the work for the present paper. All of us here at Columbia University had the highest regard for him, both as a man and as a geologist. His death leaves us with a deep sense of loss. He was a good friend and a fine man, whom I am proud to have known.

Arie Poldervaart"

THE DISTRIBUTION OF ALUMINUM IN THE TETRAHEDRA OF SILICATES AND ALUMINATES

WALTER LOEWENSTEIN, *Max Lowenstein & Cia., São Paulo, Brazil.*

ABSTRACT

In crystals of silicates and aluminates the distribution of aluminum in the centers of tetrahedra is not entirely at random, but must obey certain restrictions not easily understood on the basis of the Pauling electrostatic valence rule. Whenever two tetrahedra are linked by one oxygen bridge, the center of only one of them can be occupied by aluminum; the other center must be occupied by silicon, or another small ion of electrovalence four or more, e.g. phosphorus. Likewise, whenever two aluminum ions are neighbours to the same oxygen anion, at least one of them must have a coordination number larger than four, that is, five or six, towards oxygen. These rules explain the maximum substitution of 50% of the silicon in three-dimensional frameworks and plane networks of tetrahedra by aluminum. For 50% substitution, rigorous alternation between silicon and aluminum tetrahedra becomes necessary; this explains the experimental fact that the unit cell of anorthite has double the size of that of albite. Agreement of several known structures with these rules is shown. One exception is explained.

INTRODUCTION

One of the most important features of the modern theory of silicates is the double rôle of aluminum, which can substitute for silicon in tetrahedra, and, on the other hand, function as an independent cation with coordination number five or six towards oxygen. Substitution of aluminum for silicon in tetrahedra was formerly considered to be entirely random and of infinite extent, and this view is presented even in modern text-books, e.g. by Evans (1). Although it was shown by Machatschki (2) in the structure of haüynite, and by Barth (3) in the structure of microcline, that at least in some cases the substitution of aluminum for silicon is not a random one, random substitution as a rule with possible exceptions was accepted by most authors. Thus, when the difference in the size of the unit cells of albite and anorthite was found by Taylor, Darbyshire and Strunz (4), it was attributed to a possible different coordination around the sodium and calcium ions, and not to a difference in the distribution of aluminum ions in the centers of tetrahedra. Also the well-known fact that in all known cases of substitution of silicon by aluminum in condensed tetrahedra the maximum substitution is 50% seems so far not to have been duly accounted for or explained. It clearly indicates alternation of silicon and tetrahedral aluminum positions.

THE OXYGEN BRIDGES

The Pauling electrostatic valence rule does not explain why an oxygen bridge between aluminum tetrahedra should be excluded. In fact, it

would attribute to the oxygen one and a half electrostatic bonds, leaving one half to be satisfied by some other cation. The third of Pauling's rules (5) is more helpful in making the restriction comprehensible: it expresses the tendency of polyhedra around cations with small coordination number not to share elements with each other. Reciprocally, if elements are shared, but alternative structures with higher coordination numbers are possible, these should have higher stability. The condition that this effect is especially large when the radius ratio approaches the lower limit of stability of the polyhedron is clearly satisfied for aluminum with tetrahedral coordination. This effect of the radius ratio is particularly important for understanding the possibilities of existence of oxygen bridges between tetrahedra, even under conditions where the electrostatic valence rule is not satisfied. Thus, phosphate tetrahedra condense in pyrophosphates and metaphosphates, and also the anhydride P_4O_{10}, consists of four condensed tetrahedra, linked by oxygen atoms to which two and a half electrostatic bonds must be attributed. Sulfate tetrahedra condense in pyrosulfates, and probably in one of the forms of the anhydride, and in this case three electrostatic bonds must be attributed to the oxygen bridge. In perchloric anhydride, Cl_2O_7, three and one half electrostatic bonds pertain to the oxygen linking the tetrahedra. In these cases, the cations become successively smaller from aluminum to silicon and phosphorus, and then remain substantially of the same size.

In the structure found by Keggin (6) for phosphotungstic acid, subsequently established also for silicotungstic, borotungstic and metatungstic acid, four oxygen atoms link the central tetrahedron of the anion to three tungsten octahedra condensed in these same oxygens. The electrostatic valence bonds that must be attributed to these oxygen anions are respectively three and one half for metatungstic, three and three quarters for borotungstic, four for silicotungstic, and four and one quarter for phosphotungstic acid. Here, clearly, the limit of stability is reached; no sulphotungstic acid of analogous structure, though formally possible, is known. In all these cases, the radius ratio permits easy accommodation of the cations in the anion polyhedra, and where two possible numbers of coordination exist, the higher one is preferred; thus, boron is surrounded by a tetrahedron, not a triangle; hydrogen in the central tetrahedron has its maximum coordination of two; and hexavalent tungsten has its maximum coordination of six towards oxygen. These enhanced numbers of coordination account for the stability of the bridges, and electrostatic valence becomes of minor importance, since neutrality of the whole is maintained.

Similarly, the oxygen bridge between two aluminum ions has stability only when at least one of them has the enhanced coordination of five

or six, and, as a consequence, no two aluminum ions can occupy the centers of tetrahedra linked by one oxygen. Also in this case, it is of no consequence that electrostatic valence seems not to exclude the possibility of neighboring aluminum tetrahedra. The unfavorable radius ratio determines the instability of such a configuration.

The contradiction between the third Pauling rule and the electrostatic valence rule in its application to elements shared by anion polyhedra is only apparent. In reality, it must be assumed that in polyhedra with enhanced number of coordination the central atom or cation has a certain freedom of position and does not contact simultaneously all the surrounding anions. If one of these is shared with a polyhedron around another cation, the cation with enhanced number of coordination will be displaced by repulsion from the other cation, increasing its distance from the bridge anion, and thus weakening the electrostatic bond.

Structures with Aluminum of Four and Five or Six Coordination Towards Oxygen

In the structure of $12\,CaO \cdot 7Al_2O_3$, investigated by Büssem and Eitel (7), less than half of the aluminum ions occupy the centers of tetrahedra, the others have higher, probably five, coordination towards oxygen. In corundum, Al_2O_3, the aluminum occupies the centers of octahedra, while the metastable Al_2O_3, investigated by Hägg and Söderholm (8, 9), has a defective spinel structure, with alternating tetrahedral and octahedral positions and some vacant sites. No known structure of Al_2O_3 contains an excess of tetrahedral cations, or only such cations.

Only tetrahedral aluminum ions are, however, found in $KAlO_2$, investigated by Barth (10). This compound has a cristobalite structure, with potassium ions localized in the space between twelve oxygen anions. No alternative structure with coordination number of aluminum higher than four seems to be geometrically possible. This compound also does not conform strictly to the Pauling rules: the polyhedra around potassium share faces with each other, and with the tetrahedra around aluminum. The great distance between potassium and oxygen, 3.19 Å, permitting easy accommodation of the potassium ion in the oxygen polyhedron, offers an explanation for this exception to the rules.

Structures of Silicates

In kyanite, Al_2SiO_5, aluminum has sixfold coordination towards oxygen, silicon fourfold coordination. The structure, determined by Náray-Szabó, Taylor and Jackson (11), contains isolated silicon tetrahedra and oxygen anions. In andalusite, as determined by Taylor (12), coordination of aluminum is fivefold, of silicon fourfold. In sillimanite, investigated

by Taylor (13), half of the aluminum atoms occupy centers of octahedra, the other half centers of tetrahedra condensed with alternating silicon tetrahedra. The rational formula is $Al(AlSiO_5)$. The structure of mullite, $Al_6Si_2O_{13}$, also investigated by Taylor, is similar, but not identical. Its formula suggests it to be possibly, but not necessarily, an exception to the established rule.

In sheet structures of aluminum and silicon tetrahedra, maximum substitution of silicon by aluminum is 50%. This maximum is attained in the calcium micas, e.g. margarite, $CaAl_2(OH,F)_2(Al_2Si_2O_{10})$.

In three-dimensional frameworks of tetrahedra, 50% substitution of silicon by aluminum occurs in haüynite, $Na_2Ca_4(Al_6Si_6O_{24})(SO_4)_2$, the structure of which was determined by Machatschki (2), and in anorthite, $Ca(Al_2Si_2O_8)$, investigated by Taylor, Darbyshire and Strunz (4). In haüynite, alternation between silicon and aluminum tetrahedra was determined, and since the anorthite structure is very similar, it should also contain alternating silicon and aluminum tetrahedra. This explains why the anorthite unit cell has double the size of the albite cell. Albite, $Na(AlSi_3O_8)$, must be considered a defect structure in which no difference in the positions of aluminum and silicon can be detected. This defectiveness does not exist in anorthite. In spite of the difference in the size of the unit cell, the two minerals must be considered isomorphous. In the compositions with more than 50% anorthite, half of the positions in the centers of tetrahedra become prohibited for aluminum, which distributes statistically over the other half. The structure is still a defective one, for the aluminum positions are in part occupied by silicon; but this should be considered rather a substitution of aluminum of anorthite by silicon than of silicon by aluminum. In pure anorthite, no defectiveness of this type occurs, and the intensities of x-ray reflections due to the double cell become maximal.

Conclusions

The Pauling electrostatic valence rule admits exceptions for anions shared by polyhedra with enhanced number of coordination. The reason for these exceptions is the influence of the radius ratio upon the stability of structures, accounted for in the third of Pauling's rules. For the same reason, anion bridges between polyhedra with lowest possible number of coordination, though formally possible according to the electrostatic valence rule, must be expected to be unstable whenever alternative structures with higher numbers of coordination in a part of the polyhedra are possible. Substitution of aluminum for silicon ions in silicates is therefore not an entirely random one.

Since non-random distribution of aluminum atoms in the centers of tetrahedra explains the difference in the size of the unit cells of albite

and anorthite, and the transition between both is gradual, the classical concept of isomorphism of the plagioclase feldspars should not be altered in spite of x-ray data.

Note: A summary covering the above subject was presented at the monthly meeting of the São Paulo Group of the Sociedade Brasileira de Geologia on September 17, 1952, and at the Annual Meeting of the Society at Pôrto Alegre, on November 4, 1952.

References

1. Evans, R. C.: An Introduction to Crystal Chemistry, Cambridge (1939), p. 225.
2. Machatschki, E.: *Zbl. Min. Geol. Pal.*, (A) 136 1934; *Z. Krist., Strukturbericht* **III,** 546.
3. Barth, T. F. W.: *Am. J. Sci.* (5) **27,** 273 (1934).
4. Taylor, W. H., Darbyshire, J. A., & Strunz, H.: *Z. Krist.* (A), **87,** 464 (1934).
5. Pauling, L.: *J. Am. Chem. Soc.*, **51,** 1010 (1929).
6. Keggin, J. F.: *Proc. Roy. Soc. London* (*A*) **144,** 75 (1934); *Z. Krist., Strukturbericht* **III,** 463.
7. Büssem, W., & Eitel, A.: *Z. Krist.* (*A*), **95,** 175 (1936).
8. Hägg, G.: *Nature,* **135**, 874; *Z. Krist., Strukturbericht* **III,** 338.
9. Hägg, G., & Söderholm, G.: *Z. phys. Chem.* (*B*), **29,** 88 (1935).
10. Barth, T. F. W.: *J. Chem. Physics*, **3,** 323 (1935).
11. Náray-Szabó, St., Taylor, W. H., & Jackson, W. W.: *Z. Krist.*, **71,** 117 (1929).
12. Taylor, W. H.: *Z. Krist.*, **71,** 205 (1929).
13. Taylor, W. H.: *Z. Krist.*, **68,** 503 (1928).

Manuscript received Jan. 22, 1953

STRUCTURAL VARIATIONS OF SOME KAOLINITES IN RELATION TO DEHYDRATED HALLOYSITE

HAYDN H. MURRAY, *Indiana University and Geological Survey.**

ABSTRACT

A selected series of kaolin clay minerals was examined using *x*-ray powder diffraction techniques to show structural variations. Differential thermal analysis curves were run, using these same kaolin clay minerals to see if any relationship could be established between the *x*-ray data and the *DTA* curves. The results show that there is a relationship for all the samples studied with the exception of dehydrated halloysite.

INTRODUCTION

Investigations of the structure of kaolinite have shown that there are structural variations within the kaolinite unit layer and variations in the stacking of these layers, one upon the other (1).

The structural determinations on the kaolin minerals selected for this study were accomplished using *x*-ray powder diffraction data. The kaolin minerals were classed according to their degree of crystallinity. The degree of crystallinity is defined to include the disorder within the crystallographic unit layer and the stacking variations of the unit layers. Differential thermal analysis curves were run using samples which were identical to those used for the *x*-ray powder photographs. The *DTA* curves were then analyzed to see if there were any significant features which could be used to relate these curves to the degree of crystallinity as determined from *x*-ray data.

The following kaolinite clays were investigated: a kaolin from Gordon, Georgia; a flint clay from Montgomery County, Missouri; a flint clay from Soldier, Kentucky; a ball clay from Whitlock, Tennessee; a kaolin clay from Union County, Illinois; a fireclay from Mexico, Missouri; and an underclay from Grundy County, Illinois. In addition to these kaolinite clays, a halloysite clay from Gardner Mine Ridge in Lawrence County, Indiana, was included because it is generally considered to be a member of the kaolin clay mineral group even though it has many different characteristics.

X-RAY DIFFRACTION STUDIES

The most comprehensive study on randomness in the structure of some kaolin clay minerals was that done by Brindley and Robinson (1). They established that differences could be detected on *x*-ray powder photographs, and used to indicate randomness in layer orientation and struc-

* Portion of thesis submitted in partial fulfillment of the requirements for the degree of Doctor of Philosophy in Geology to the Graduate College of the University of Illinois, 1951.

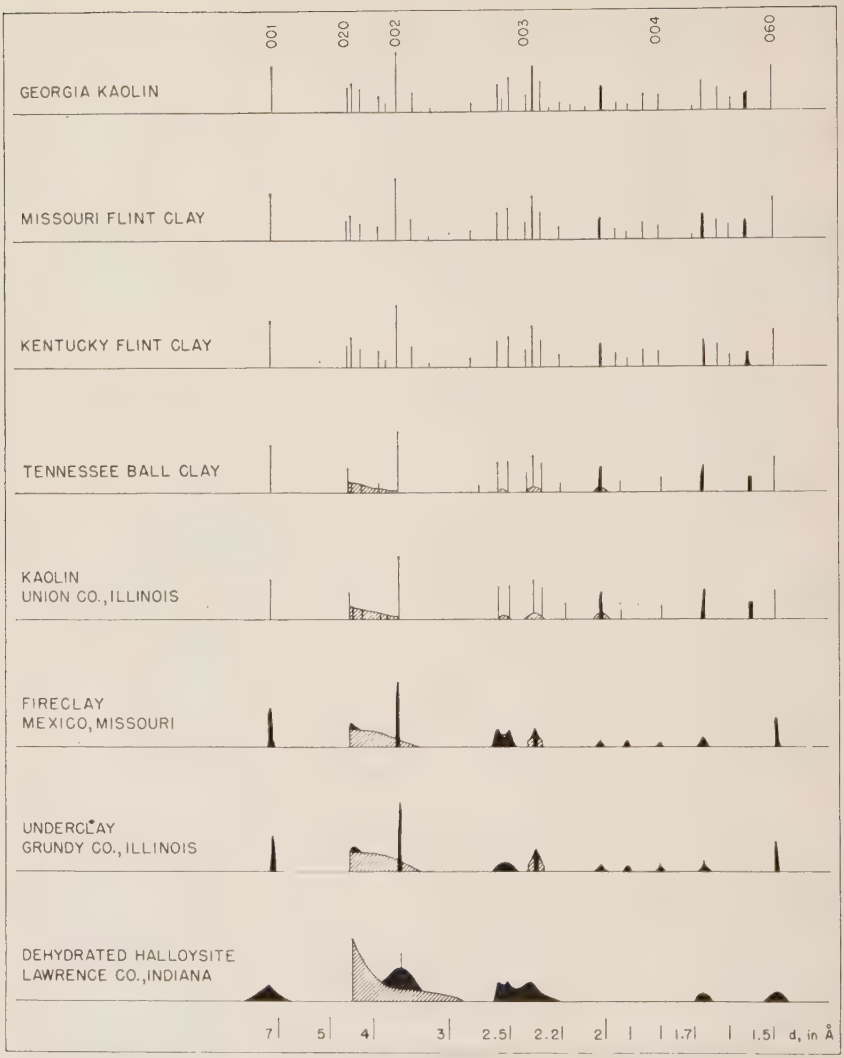

FIG. 1. Diagrammatic representation of x-ray photographs of some kaolin minerals. (Intensities estimated.)

tural variations in kaolin clay minerals. The criteria used by Brindley and Robinson and some additional features found by the author were used to determine the relative degree of crystallinity of the kaolinites and dehydrated halloysite used in this investigation. The halloysite was dehydrated in order that it would have approximately the same basal spacing as kaolinite. The x-ray powder diffraction patterns of the kaoli-

nites and halloysite were obtained with a North American Philips x-ray unit. The samples were ground, dried, and then packed into a wedge-type sample holder. A powder camera with a diameter of 14 cm. was used and the specimens were exposed to nickel filtered Cu radiation for 4.5 hours at 35 KV and 18 ma.

The following major differences, noted on the x-ray powder photographs, were used as criteria to determine the degree of crystallinity:

(1) Sharpness of the reflections.
(2) Number of reflections.
(3) Slight change in the basal spacing.
(4) Resolution of closely spaced reflections.
(5) Absence of certain reflections.

Each of these criteria will be discussed in the following paragraphs.

The x-ray reflections on some of the photographs were very sharp and distinct and on others the reflections were broad, fuzzy bands. The relative sharpness of the reflections from the clays studied are shown diagrammatically in Fig. 1. The x-ray reflections of the three clays at the top of the diagram are sharp and distinct. Some of the reflections of the kaolinite in the Tennessee ball clay and the Union County kaolin become fuzzy and broad. The x-ray reflections on the bottom three photographs of the diagram are all relatively broad and diffuse. It is realized that sharpness of reflections is also dependent on particle size and orientation. The samples were not oriented and the sizes of particles were very similar, so that these factors had little, if any, effect.

The number of x-ray reflections which appear on a photograph serve as an indicator of the degree of crystallinity. The reflections which can be indexed out through the (060) reflection on the x-ray photograph of Georgia kaolin amount to a total of 31. Only 8 reflections appear on the x-ray photograph of the dehydrated halloysite. The other kaolinites have an intermediate number of reflections, the number of reflections decreasing from the top to the bottom photograph shown diagrammatically in Fig. 1.

Slight variations in the basal spacings of the clays used in this study were detected and may indicate to some extent the degree of crystallinity. The (001) spacing for the Georgia kaolinite and the two flint clays was 7.18 Å. The (001) basal spacing of both the Tennessee ball clay kaolinite and the kaolinite in the Union County kaolin was 7.20 Å., and for the kaolinite in the Missouri fireclay and the Grundy County underclay was 7.30 Å. The basal spacing of the dehydrated halloysite was 7.42 Å. This shows that there is a general increase in the (001) basal spacing progressing from the Georgia kaolin to the dehydrated halloysite as shown in Fig. 1 and Table 1. This slight increase in basal spacing could be the

TABLE 1. "*d*" VALUES OF SOME KAOLIN MINERALS IN ANGSTROM UNITS

Brindley and Robinson	*I*	Ga. (soft)	*I*	Flint Mo.	*I*	Flint Ky.	*I*	*hkl*	Tenn. Ball Clay	*I*	Union Co. Kaolin	*I*	Fireclay Mo.	*I*	Grundy Co. Underclay	*I*	Dehydrated Halloysite	*I*
7.15	10	7.18	VS	7.18	VS	7.18	VS	001	7.20	VS	7.20	VS	7.30	VS	7.30	VS	7.42	VS
4.453	4	4.50	S	4.49	M	4.50	M	020	4.55	S	4.48	S	4.49	S	4.49	S	4.47	VS
4.349	6	4.41	S	4.41	S	4.43	S	$1\bar{1}0$										
4.170	6	4.21	S	4.23	M	4.23	M	$11\bar{1}$										
4.120	3							$1\bar{1}\bar{1}$										
3.837	4	3.87	M	3.87	M	3.91	M	$02\bar{1}$	3.95	W								
3.734	2	3.76	W			3.76	W	021										
3.566	10	3.62	VS	3.61	VS	3.61	VS	002	3.59	VS	3.58	VS	3.58	VS	3.56	VS	3.63	VS
3.365	4	3.42	M	3.43	M	3.41	M	111										
3.138	2	3.13	W	3.13	W	3.15	W	$11\bar{2}$										
3.091	2							$11\bar{2}$	3.09	W								
2.748	2	2.76	W	2.75	W	2.76	W	022										
2.553	8	2.56	S	2.55	S	2.57	S	$20\bar{1}$, $1\bar{3}0$, 130	2.56	S	2.55	S	2.57	M	2.56	M	2.56	M
2.521	4	2.52	M					$13\bar{1}$, $1\bar{1}2$	2.52	S	2.49	S	2.50	M				
2.486	9	2.48	S	2.50	S	2.49	S	$1\bar{3}1$, 200, 112									2.48	M
2.374	7	2.38	M	2.42	M	2.41	M	003	2.42	M								
2.331	10	2.36	VS	2.37	VS	2.36	S	$20\bar{2}$, $1\bar{3}1$	2.36	S	2.35	S	2.35	M	2.37	M	2.35	M
2.284	9	2.32	S	2.31	S	2.31	M	$1\bar{1}3$, $13\bar{1}$	2.29	S	2.30	S						
2.243	1	2.26	W					$13\bar{2}$, 040										
2.182	3	2.20	W	2.21	M	2.22	W	201, $1\bar{3}2$, $2\bar{2}0$	2.21	W	2.20	W	2.21	W				
2.127	2	2.13	W					$02\bar{3}$, 041							2.13	W		
2.057	1	2.08	W	2.01	S	2.05	M	023, $2\bar{2}2$										
1.985	7	1.99	S	1.96	W	1.96	W	$20\bar{3}$, $1\bar{3}2$	1.97	S	1.99	S	2.00	W	2.00	W		
1.935	4	1.95	W					221, 132										
1.892	2	1.92	W	1.91	W	1.90	W	113, $13\bar{3}$	1.92	W	1.90	W	1.90	W	1.90	W		
1.865	1							042										
1.836	4	1.86	M	1.86	M	1.85	M	$1\bar{3}3$, 202, $22\bar{3}$										
1.805	1							$11\bar{4}$, $2\bar{2}3$										
1.778	5	1.79	M	1.80	M	1.80	M	004	1.80	M	1.79	M						
1.704	1							$2\bar{2}2$										
1.682	2	1.68	W	1.69	W			$1\bar{5}0$, $24\bar{1}$, $31\bar{1}$										
1.659	8	1.66	S	1.67	S	1.67	S	$24\bar{0}$, $20\bar{4}$, $1\bar{3}3$	1.66	S	1.67	S	1.68	M	1.67	W	1.67	W
1.616	6	1.62	M	1.62	M	1.63	M	$24\bar{2}$, 133, 310	1.63	M	1.62	M						
1.581	4	1.58	M	1.58	M	1.58	W	$15\bar{2}$, $13\bar{4}$										
1.539	5	1.52	M	1.54	M	1.54	M	241, $1\bar{1}4$, $13\bar{4}$										
1.486	9	1.48	S	1.49	S	1.49	S	060, $33\bar{1}$, $33\bar{1}$	1.50	S	1.48	S	1.49	S	1.49	S	1.48	M

consequence of : (*a*) the presence of an occasional water layer between the unit layers of the kaolinites with the poorer degrees of crystallinity, and/or (*b*) disorder in the unit layer or stacking variations in the kaolin unit layers which would be expected to be greater in the samples with the lower degree of crystallinity.

The resolution of the closely spaced reflections on an *x*-ray powder photograph of a kaolinite can be used to indicate the degree of crystallinity. The closely spaced reflections on a powder photograph of a kaolinite with a good degree of crystallinity are well resolved as exemplified by the reflections adjacent to the (020) and the (003) reflections on the top three diagrams of Fig. 1. These closely spaced reflections become hazy and indistinct on the diagrams of Tennessee ball clay and the Union County kaolin and are completely merged on the bottom three diagrams of Fig. 1.

Many reflections are absent on the *x*-ray photographs of kaolinites with a poor degree of crystallinity. This criteria is related to the total number of reflections which appear, but there are certain reflections which are cut out by the displacements of the kaolin layers and so need separate discussion. An explanation for the absence of certain reflections has been advanced by Brindley and Robinson (2). The (OH) groups in the kaolin layer are arranged at regular intervals along the *b*-axis, this distance being equal to $b_0/3$. This means that if one of two adjacent layers is displaced along the *b*-axis by an integral multiple of $b_0/3$, the two sheets will still be oriented with the same relationship to each other. If the displacement is not an integral multiple of $b_0/3$, then all reflections are cut out except those with a k index of 0, 3, 6 · · · . Random displacements result in broad, diffuse reflections (2).

The broad, diffuse reflections may also be explained in a different manner. The hydroxyl groups in the basal plane of the kaolin layer are arranged in three straight lines each trending 120° from the other (Fig. 2). Each hydroxyl group is an equal distance from the adjacent hydroxyl which lies in the same plane and this distance is equal to $b_0/3$. This means that in addition to displacements of $nb_0/3$, some layers may be rotated 120° relative to the adjacent layer without changing the relationships of the hydroxyl groups to the oxygen atoms of the adjacent layer. The positions of the aluminum atoms, however, would be changed, which could cause many reflections to be very diffuse, and the combination of displacement and rotation would cause broad band-like reflections.

The above *x*-ray data indicate that there is considerable structural variation in the kaolinites and dehydrated halloysite. Figure 1 shows the kaolinites and dehydrated halloysite in the relative order of their degree of crystallinity based on *x*-ray data, with Georgia kaolin having the highest degree of crystallinity and dehydrated halloysite the lowest.

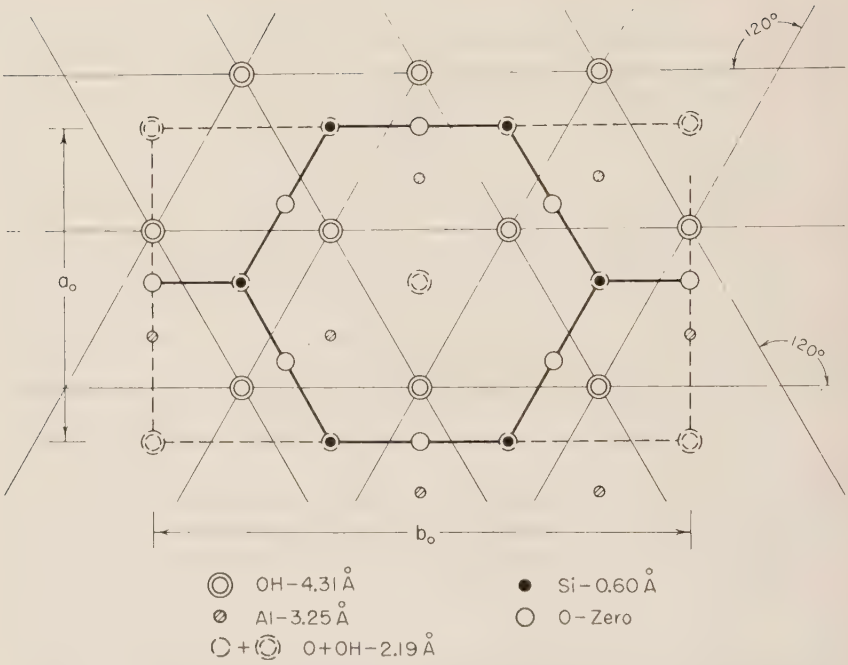

FIG. 2. Diagrammatic representation of the kaolin layer projected on the (001) plane showing the three possible directions along which the O—OH relationship of the adjacent layer could be satisfied.

Dehydrated halloysite, according to *x*-ray data, has the lowest degree of crystallinity of any of the samples studied since the unit layers are randomly oriented with respect to each other. This is significant because the criteria for dehydrated halloysite based on differential thermal analysis do not agree with the *x*-ray data.

Differential Thermal Analyses

It has been suggested that the crystallinity of a kaolinite is indicated by differential thermal analysis curves (3). In order to further test this suggestion, differential thermal analyses were made using the same kaolin clays as were used in the *x*-ray studies. The results obtained using the differential thermal analysis curves could then be compared with the results of the *x*-ray determinations.

The thermal apparatus used was similar to that described by Grim and Rowland (4). Great care was taken to pack the sample into the sample block in the same manner each time an analysis was run and also to keep the weight of sample constant.

No general criteria based on differential thermal analysis curves which

could be used for all kaolinites to determine the relative degree of crystallinity have been indicated previously. Grimshaw et al. (5) have indicated that in kaolins, there is a variation in the temperature of the peak of the endothermic reaction which can be correlated with the degree of crystallinity. Impurities affect the *DTA* curve, as has been shown by Gruver, Henry, and Heystek (6). Recently Bramao et al. (7) have correlated the shape of the main endothermic peak on the *DTA* curve of the kaolin minerals with particle size and degree of crystalline perfection. In addition to the characteristics of the main endothermic peak, other criteria have been used in this study. By recording a variety of measurements and observations, it was hoped that an evaluation of them all would give a relative degree of crystallinity for the kaolins. The measurements and observations which were used are as follows:

(1) The temperature range and the size of the endothermic reaction associated with the loss of the lattice water. Temperature range means the difference in temperature between the points at which the reaction begins and ends. The size refers to the distance of the peak from the base line of the thermal curve.

(2) The peak temperature of the endothermic reaction.

(3) The slope of the curve between the point at which the endothermic reaction ends and the point at which the exothermic reaction begins.

(4) The temperature range between the endothermic peak and the exothermic peak.

(5) The presence of a slight endothermic reaction immediately preceding the exothermic reaction.

(6) The temperature range and size of the exothermic reaction.

(7) The peak temperature of the exothermic reaction.

The temperature range of the endothermic peak should be an indication of the degree of crystallinity, since it would seem that the lattice water would be more tightly bonded in the better crystalline kaolinites than the poorly crystalline ones. More energy would be needed to break the bonds holding the structural water in the lattice and, consequently, the temperature range, temperature, and size of this peak would be greater for the kaolinites with a high degree of crystallinity. The thermal curves (Fig. 3) reveal that the endothermic peak is very useful in determining the crystallinity of a kaolinite. The data in Table 2 show that in general the values for the temperature range, temperature of the peak, and the size of the peak are higher for the kaolinites which are shown to have the higher degrees of crystallinity by *x*-ray data. The major exception is dehydrated halloysite which has higher values than one would expect since *x*-ray data showed it to have a poor degree of crystallinity.

The kaolinites with the highest degree of crystallinity and the dehydrated halloysite reveal an upward sloping curve between the endothermic and the exothermic reactions and also a small endothermic break just before the exothermic peak (Fig. 2 and Table 2). This may mean that all the lattice water has not been ejected and that a structural

reorganization is taking place. The final endothermic break may be a breakdown of the newly forming structure. It would seem that an upward sloping curve and a small endothermic break before the exothermic peak is an indication of a high degree of crystallinity. The major exception between the x-ray data and the use of this criterion is again dehydrated halloysite.

The values for the temperature range between the endothermic and the exothermic peaks do not appear to give any indication of the degree of crystallinity (Table 2).

TABLE 2. VALUES USED TO CLASSIFY THE KAOLIN MINERALS

(all temperatures are degrees centigrade)

Kaolinite*	Temp. range end. peak	Temp. at peak	Size of peak	Slope (°)	Temp. range between peaks	End. react. before exo.	Range exo. peak	Temp. at peak	Size of peak
1	310	595	$4\frac{1}{2}''$	15°	375	strong	30	970	6″
2	290	580	$5\frac{1}{2}''$	14	385	strong	40	965	$5\frac{1}{4}''$
3	300	580	$3\frac{1}{4}''$	8	370	none	60	950	$6\frac{1}{2}''$
4	270	580	$4\frac{1}{4}''$	7	375	weak	60	955	$6\frac{3}{4}''$
5	170†	570	$3\frac{1}{2}''$	0	390	none	60	960	$3\frac{1}{4}''$
6	250	560	4″	7	385	none	70	945	$2\frac{1}{2}''$
7	240	560	4″	9	380	none	80	940	5″
8	160†	560	3″	3	380	none	95	940	$1\frac{1}{4}''$
9	260	575	$4\frac{1}{4}''$	12	395	weak	40	970	6″‡

* 1—Georgia Kaolin (soft). 2—Missouri Flint clay. 3—Kentucky Flint clay. 4—Georgia Kaolin (hard). 5—Tennessee Ball Clay. 6—Kaolin (Union Co., Ill.). 7—Missouri Fireclay. 8—Underclay (Grundy Co., Ill.). 9—Dehydrated Halloysite.

† The start of the initial endothermic peak is masked by an exothermic reaction caused by organic material in the clay.

‡ The exothermic peak is actually larger because it went off the record.

The temperature range, temperature, and the size of the exothermic peak can be used to indicate the crystallinity of a kaolinite as is well shown by the values in Table 2. The temperature range is shorter, the temperature at the peak is higher, and the size of the peak is larger for the kaolinites with the higher degrees of crystallinity. The data for dehydrated halloysite again does not agree with the result as determined from x-ray data. The temperature range for the kaolinites with a high degree of crystallinity is short because the structure of the new phase formed may be related to the old structure (8). If the kaolinite structure is well ordered then the transformation should take place faster than if the structure were disordered. The peak temperature of the exothermic reaction is higher for the kaolinites with a high degree of crystallinity

because more energy is needed to transform to a new phase since the old structure is stronger. The size variation of the peak is probably due to a greater energy release by the kaolinites with a high degree of crystallinity. Another possibility is that the new phase which forms is different in the kaolinite with a poor degree of crystallinity than that which forms from one with a high degree of crystallinity.

The measured values and observations which were taken from the original curves are listed in Table 2. The thermal curves in Fig. 3 are shown in the order of their relative degree of crystallinity.

Comparison of *X*-Ray and Thermal Data

A comparison of the relative degree of crystallinity of the kaolinites (Figs. 1 and 3) determined by using *x*-ray powder diffraction data and differential thermal criteria shows that the two methods compare favorably with the major exception of dehydrated halloysite. Dehydrated halloysite has a low degree of crystallinity according to *x*-ray data and a high degree of crystallinity according to differential thermal data.

The detailed structural characteristics of halloysite cannot be considered as established. Bates et al. (9) have proposed a structure that explains the tubular arrangement of hydrated halloysite but the relation of this concept to *x*-ray diffraction data is not clear. When the interlayer water is removed from hydrated halloysite, it is possible that the unit layers, which are structurally similar to the kaolinite layer, come together so that the O—OH relationship between the uppermost hydroxyls on one layer and the oxygens on the base of adjacent layer is satisfied in substantially the same manner as in well crystallized kaolinite. This directional relationship can be satisfied by any of the three hydroxyl strings (Fig. 2). However, the aluminum atoms may not be oriented in the same way as they are in well crystallized kaolinite since the aluminum atoms can have three possible orientations with respect to the hydroxyls, depending on the orientation of the hydroxyl strings. The possibility that the aluminum atoms are not oriented in the same manner in each successive layer could cause the broad diffuse reflections which are characteristic of the *x*-ray pattern of dehydrated halloysite.

On the basis of *x*-ray diffraction data, it seems that there is a gradation between the structure of a kaolin with a good degree of crystallinity to one with poor degree of crystallinity such as dehydrated halloysite. On the basis of the differential thermal analyses, dehydrated halloysite has a high degree of crystallinity. This suggests that *x*-ray reflections reveal both internal structural disorder and random stacking of the unit layers, whereas differential thermal analysis curves indicate only the orderliness of the internal structure of the unit layers. Differential thermal analysis curves do not reflect random stacking of the unit layers but only reflect

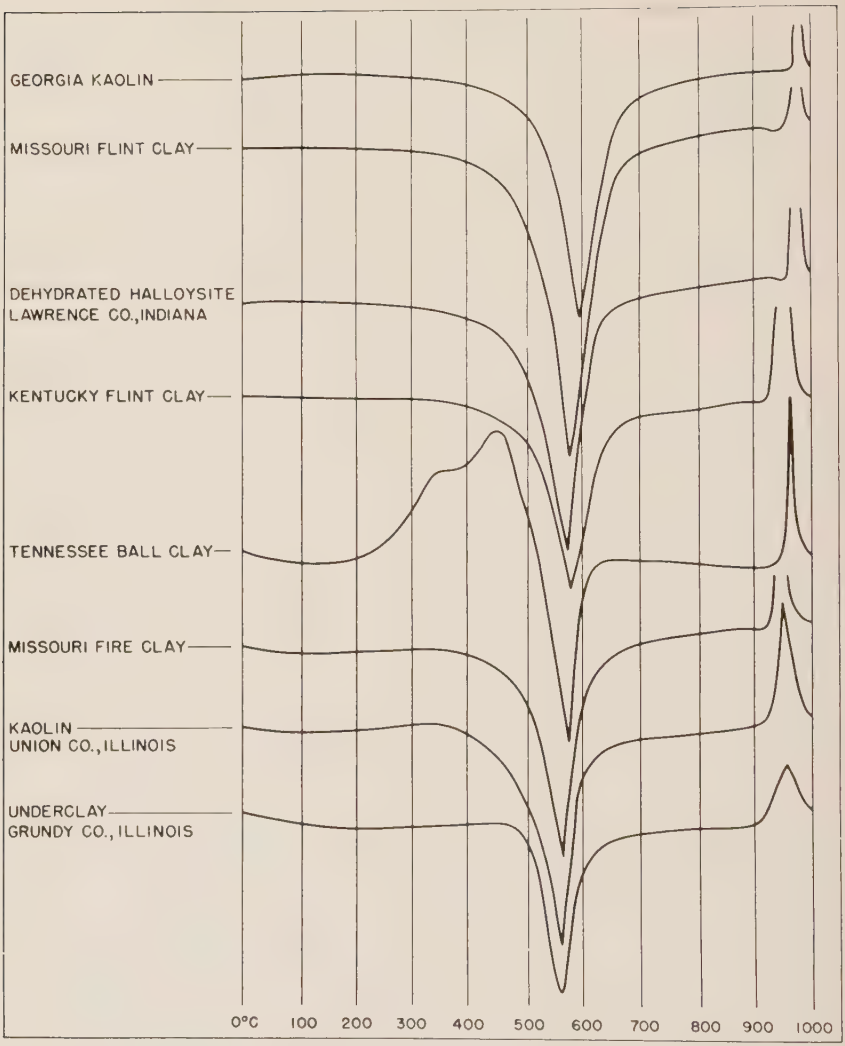

FIG. 3. Differential thermal analysis curves of some kaolin minerals.

the energy changes which occur when a structure breaks down or a new phase forms. This indicates that dehydrated halloysite has a relatively ordered unit layer, as indicated by thermal data, which is stacked upon the next unit layer with complete randomness with respect to the a and b axes, as indicated by x-ray data. The kaolinites, such as the Missouri fireclay, with a poor degree of crystallinity may have random displacements of $nb_0/3$ in different layers but in all probability are not rotated $n\ 2\pi/3$ as are the layers in the dehydrated halloysite. As a consequence,

unit layers are oriented slightly better with respect to the *a* and *b* axes, and therefore, a few more reflections appear on the *x*-ray pattern.

A minor discrepancy is observed in the comparative position of Missouri fireclay and Union County kaolin. The differential thermal analysis curve indicates a higher degree of crystallinity for the Missouri fireclay while the *x*-ray data indicates the opposite. The explanation for this is probably that the kaolin layers of Missouri fireclay have a relatively more random orientation with respect to each other but each individual layer is more ordered than those of the Union County kaolin.

Base Exchange Capacity

Another property which might indicate the degree of crystallinity of kaolinites is their base exchange capacity. Base exchange capacity in kaolinite is due primarily to broken bonds (10), and possibly to negative charges on the lattice due to vacancies of alumina or silica positions in the poorly crystalline kaolinites.

The base exchange capacity was determined by the ammonium acetate procedure widely used in agricultural studies (11). The following are the base exchange capacities as determined on five of the kaolin samples.

	meq/100 gms.
Georgia kaolin	3
Kentucky flint clay	6
Kaolin (Union Co., Illinois)	11
Fireclay	18
Dehydrated halloysite	5

These values suggest that the kaolinites with the lower degrees of crystallinity have a higher base exchange capacity, with the exception of dehydrated halloysite. The kaolinite with the lower degree of crystallinity would have larger surface areas exposed due to random stacking, and relatively more broken bonds would be expected. This data again suggests that dehydrated halloysite is not as poorly crystalline as *x*-ray data would seem to indicate.

Summary

1. *X*-ray analysis indicates that dehydrated halloysite has a poor degree of crystallinity and that some kaolinites have a good degree of crystallinity while others have a poor degree of crystallinity. There appears to be a continuous variation in the crystallinity of kaolinites rather than a step-wise gradation.

2. Differential thermal analysis curves indicate the same results as were obtained using *x*-ray data with the major exception of dehydrated halloysite which was indicated to have a high degree of crystallinity.

3. *X*-ray diffraction data seems to reflect both internal and stacking

variations whereas differential thermal analyses indicate only internal variations.

4. It is possible that the structural layers which make up dehydrated halloysite may be oriented in a manner which is different from that of kaolinite and, for that reason, appear to have a poor degree of crystallinity on the basis of x-ray diffraction data.

5. Base exchange data may be used to indicate degree of crystallinity of kaolinites. Dehydrated halloysite has a low base exchange capacity rather than a relatively high capacity as would be predicted on the basis of x-ray data.

6. Differential thermal analysis curves can be used to determine the degree of crystallinity of kaolinites.

Acknowledgment

The author wishes to acknowledge the helpful guidance of Dr. R. E. Grim of the University of Illinois Geology Department and Dr. W. F. Bradley of the Illinois State Geological Survey. The original work was completed while the author held a fellowship at the University of Illinois sponsored by the Illinois Clay Products Company. The helpful criticisms of Dr. T. F. Bates, who kindly read the manuscript, were greatly appreciated.

References

1. Brindley, G. W., and Robinson, K., Randomness in the structures of kaolinitic clay minerals: *Trans. Faraday Soc.*, **42B,** 198–205 (1946).
2. Brindley, G. W., and others. X-ray identification and structures of clay minerals: *Monograph, Mineralogical Society*, London (1951).
3. Grim, R. E., and Bradley, W. F., Differential thermal curves of prepared mixtures of clay minerals: *Am. Mineral.*, **32,** 493–501 (1947).
4. Grim, R. E., and Rowland, R. A., Differential thermal analyses of clay minerals and other hydrous materials: *Am. Mineral.*, **27,** 746–761 (1942).
5. Grimshaw, R. W., Heaton, E., and Roberts, A. L., Differential thermal analyses of refractory clays: *Trans. Brit. Cer. Soc.*, **44,** 69–92 (1945).
6. Gruver, R. M., Henry, E. C., and Heystek, H., Suppression of thermal reactions in kaolinite: *Am. Mineral.*, **34,** 869–874 (1949).
7. Bramao, L., Cady, J. G., Hendricks, S. B., and Swerdlow, M., Criteria for the characterization of kaolinite, halloysite, and a related mineral in clays and soils: *Soil Sci.*, **73,** 273–287 (1952).
8. Grim, R. E., and Bradley, W. F., High temperature thermal effects of clays and related materials: *Am. Mineral.*, **36,** 182–201 (1951).
9. Bates, T. F., Hildebrand, F. A., and Swineford, A., Morphology and structure of endellite and halloysite: *Am. Mineral.*, **35,** 463–484 (1950).
10. Spiel, S., Affect of adsorbed electrolytes on properties of monodispersed clay-water systems: *Jour. Am. Cer. Soc.*, **23,** 33–38 (1940).
11. Schollenberger, C. J., and Simon, R. H., Determination of exchange capacity and exchangeable bases in soil—ammonium acetate method: *Soil Sci.*, **59,** 13–38 (1945).

Manuscript received Jan. 8, 1953

BRANNERITE FROM CALIFORNIA

A. Pabst, *University of California, Berkeley 4, California.*

Abstract

Brannerite is found in quartz veins about seven miles south of Coleville, Mono County, California. It is very similar in composition to brannerite from the type locality in Idaho and from elsewhere. Initially metamict brannerites from Idaho, California, and Morocco yield similar *x*-ray diffraction patterns after heating. It has proved impossible to index these patterns and so the crystallographic character of heated brannerite remains in doubt.

Occurrence

Several years ago Mr. John Halsey presented to the writer specimens of an unidentified radioactive mineral from Mono County, California. After some delay this was found to be the rare mineral brannerite, hitherto known in the United States only from placer deposits in Kelley Gulch, Custer County, Idaho, the type locality described by Hess and Wells (1920). The following statement concerning the California occurrence was supplied by Mr. Halsey.

"The brannerite was found in 1949 by Mr. D. B. Dean in the canyon of the West Walker River, seven miles south of Coleville, Mono County, California (Bridgeport Quadrangle, T7N, R23E, on the border of sections 4 and 9). Specimens for analysis were collected from several small prospect pits along an abandoned road on the east side of the river, 50 yards from U. S. highway 395.

"The brannerite occurs as a trace constituent of mesothermal quartz veins, $\frac{1}{4}$ inch to 18 inches thick, which traverse late Mesozoic quartz-monzonite along closely spaced subparallel sheeting joints. The veins are considered to be related genetically to nearby pegmatite and aplite veins which are also controlled by sheeting joints and contain the same suite of accessory minerals.

"95% or more of the vein material consists of massive milky quartz. Smoky quartz and clear prismatic quartz are present in minor amount. The most abundant accessory silicate is muscovite. Biotite, orthoclase, epidote, hornblende, garnet, tourmaline and zeolites occur in trace amounts. Non-silicates are chiefly magnetite, pyrite, chalcopyrite and calcite. Molybdenite and bismuthinite occur in minute quantities.

"Of the accessory vein minerals brannerite is by far the least abundant. Fifteen tons or so of carefully sorted vein materials have yielded not more than 10 grams of the mineral. It is randomly distributed through the larger veins and is occasionally associated with slightly radioactive smoky quartz."

Crystal System

In the original description of brannerite, Hess and Wells (1920) left the crystal system in doubt. They considered the mineral to be "an isometric paramorph after either a tetragonal or an orthorhombic form." George (1949) listed it as monoclinic without giving axial elements. This statement was based on inspection of large crystals from Fuenteovejuna, Cordoba, Spain (George, 1952).

The Mono County brannerite occurs in lustrous black crystals firmly embedded in quartz. These crystals are mostly slender prisms not over a few millimeters thick and a centimeter or more in length. This habit is similar to that of brannerite at Chateau Lambert, Vosges, recently described by Branche, Chervet and Guillemen (1951). Though it is very difficult to remove the crystals from the enclosing quartz without damage Mr. Halsey did succeed in isolating some in fairly good condition.

Seven crystals were measured on the reflecting goniometer. Only one showed terminal faces and these were not suitable for measurement. The prism zones included from 6 to 12 measurable faces on the several crystals. Though the measurements leave something to be desired they suffice to establish the character of the prism zone. The angles are close to those of tetragonal zones, e.g. ϕ_{310} 18°26′, but the development is clearly orthogonal. A single orthogonal zone dominating the habit is to be expected only in orthorhombic or monoclinic crystals. The results for the five better crystals are summarized in Table 1.

The axial ratio corresponding to simplest indices for all observed forms, $a/b=0.528$, is near the a/b ratio of yttrotantalite and samarskite. This ratio is associated with the indices {160} for the most persistent form. Simpler indices could be assigned to this form with corresponding change in ratio but only at the cost of introducing higher indices for some of the other observed forms.

Table 1. Summary of Goniometric Measurement of 5 Crystals of Brannerite from Mono County, California

*hk*0	ϕ	Range of ϕ	Number of observations	Calculated for $a:b=0.528$
010	0°00′		5	
160	18 12	16° 4′–19°39′	15	17°31′
130	31 42	30 22 –32 35	5	32 16
120 590 ?	45 35	43 29 –47 25	5	43 26 46 28
110	61 34	60 28 –63 36	8	62 10
210	75 5	74 5 –75 39	4	75 12
310	79 37	79 2 –80 12	2	80 1
610	84 58	84 38 –85 30	4	84 58

Composition

The identification of brannerite from Mono County, California, was accomplished by density determination and comparison of diffraction patterns with those obtained from type material. It was later confirmed by spectrographic examination and chemical analysis.

The density of brannerite from Mono County was found by the Berman balance on four closely checking fragments to be 5.43. This just matches the highest value in the range of specific gravity, 4.5 to 5.43, reported with the description of brannerite from the original locality by Hess and Wells (1920).

Table 2. Brannerite from "Dean's Mine" on the Walker River in Mono County, California
Sample No. AP-1, Lab. No. 66779

Constituent	%	Constituents for R_2O_3	%
SiO_2	0.5	Rare Earth Oxides	6.5[a]
CaO	2.8	ThO_2	5.0
Total R_2O_3	92.2	UO_2	8.2
(Including Rare Earths)		UO_3	32.0
Total H_2O	2.6	TiO_2	32.9
Mn, Mg	.x	FeO	2.4
	98.2+		87.0

[a] Mostly yttrium and erbium.

1. The determined constituents of the R_2O_3 precipitate (when calculated to the proper oxides) amount to 86.7%. The difference of 92.3% (i.e. total R_2O_3) and 86.7% (determined constituents of R_2O_3) is 5.6%. This missing 5.6% is due to Pb, Cb, Ni, Bi, Zr, and Ta. Spectrographic qualitative analysis of a small sample by J. Stich shows that these chemically undetermined elements are present in trace amounts, a "trace" being approximately 0.1–1%.

2. It is impossible on a chemical basis to state definitely what the valence state of iron is in the mineral. Quadrivalent uranium is in excess over iron so that in preparing a solution of the sample any ferric iron would be reduced by the quadrivalent uranium, forming equivalent amounts of ferrous iron and hexavalent uranium.

Following a preliminary spectrographic examination by Dr. T. G. Kennard of Kennard and Drake, Los Angeles, an analysis of the newly identified brannerite was made by analysts of the U. S. Geological Survey through the kind offices of Dr. John C. Rabbitt, chief of the Trace Elements Section. The analysis was carried out on 97 mgs. of carefully purified fragments plus a somewhat greater weight of material slightly contaminated with quartz. The report of the analysis is given in Table 2.

As may be seen from Table 3 the composition of California brannerite is close to that of brannerite from other localities. It seems probable that the silica content reported for the mineral from Chateau Lambert is

Table 3. Analyses of Brannerite

	1	2	3	4
CaO	2.9	2.74	2.7	2.8
BaO	0.3	0.01		
SrO	0.1	0.01		
Mn, Mg	—	—		.x
PbO	0.2	2.34	3.2	
FeO	2.9	3.11	5.4	2.4
Ce_2O_3	none	1.10	0.3	6.5
$(Y, Er)_2O_3$	3.9*		1.8†	
UO_2	10.3	—	—	8.2
UO_3	33.5	—	—	32.0
U_3O_8	—	51.76	43.2	—
ThO_2	4.1	1.20	0.3	5.0
SnO_2	—	—	1.3	—
ZrO_2	0.2	N.D.	—	—
TiO_2	39.0	32.45	35.2	32.9
SiO_2	0.6	0.16	3.3	0.5
CO_2	0.2	—	—	—
H_2O	2.0	2.35	3.7	2.6
Total	100.2	97.21	100.6	—
S.G.	5.42	5.17	4.82	5.43

1. Kelly Gulch, Custer County, Idaho (Hess and Wells, 1920). "No Mg, Sn, W, Ta, Mo, V, Cu or F could be detected." ". . . quartz . . . undoubtedly accounts for the SiO_2. . . ."

* Reported as "Yt_2O_3, etc. Average molecular weight 350." Helium was identified spectrographically (Wells, 1920).

2. Fuenteovejuna, Cordoba, Spain (George, 1949).

3. Chateau Lambert, Vosges, France (Branche, Chervet and Guillemen, 1951).

† Reported as "Y_2O_3."

4. Walker River, Mono County, California (Table 2).

attributable to quartz contamination. Brannerite being metamict as recorded by Palache, Berman and Frondel (1944), the water content is presumably acquired incidental to metamictization.

The formula of brannerite has long been in doubt. Since it has not been possible to obtain cell dimensions (vide infra) the new data do not relieve this situation. There are, however, numerous related minerals whose formulas may be written in the form XY_2O_6, where X includes ions of radius near 1.0 Å mostly in eight-fold coordination and Y embraces ions of radius near 0.75 Å mostly in six-fold coordination, following Machatschki (1941). Among such minerals may be included euxenite, samarskite, tapiolite and others. Table 4 shows that the analysis of brannerite from Idaho may be fitted to such a formula. The close match depends, of course, on suitable distribution of Fe between X and Y posi-

TABLE 4. FITTING OF ANALYSIS OF BRANNERITE FROM KELLEY GULCH, CUSTER COUNTY, IDAHO, TO IDEAL FORMULA, XY_2O_6

	Wt. %	Mol quotient $\times 10^3$	Number of oxygens	Number of cations			
CaO	2.9	52	52	Ca	52		
BaO	0.3	2	2	Ba	2		
SrO	0.1	1	1	Sr	1		
PbO	0.2	1	1	Pb	1		
$(Y, Er)_2O_3$	3.9	11*	33	(Y, Er)	22	262	1.02 X
UO_2	10.3	38	76	U	38		
UO_3	33.5	117	351	U	117		
ThO_2	4.1	16	32	Th	16		
ZrO_2	0.2	2	4	Zr	2		
				Fe	11		
FeO	2.9	40	40				
				Fe	29	523	2.03 Y
TiO_2	39.0	494	982	Ti	494		
			Total 1544			1544	6.00 O

* Taking molecular weight of combined oxides to be 350, as given by Hess and Wells, 1920.

tions. It may be noted that in 1929 Machatschki assigned Fe to the X positions while in 1941 he assigned it to the Y positions.

X-RAY EXAMINATION

Through the courtesy of Dr. George Switzer, brannerite from the original locality in Kelley Gulch, Custer County, Idaho, was made available from the United States National Museum. This consisted of a small portion of the crushed material used for analysis by Hess and Wells, USNM 105793, and some loose crystals, USNM 96873, which included several varieties of euxenite, some closely resembling brannerite, and other heavy minerals. Mr. M. C. Stinson kindly furnished an additional sample of concentrate containing brannerite from his claims in Kelley Gulch and finally a further supply was obtained by purchase from Minerals Unlimited, Berkeley.

Through the kindness of Mr. John B. Jago of San Francisco it was possible to obtain some brannerite from the Bou-Azzer mine, Morocco. This brannerite is in anhedral black grains, up to a few millimeters in dimensions, intergrown with gray quartz and accompanied by a trace of sulfides and clay minerals.

The *x*-ray study was mostly carried out on fragments of single crystals

in the manner previously described (Pabst, 1952, p. 145–146). Brannerite from the three localities is essentially metamict but all of the California brannerite and most of that from Idaho yield a few weak "powder" lines not attributable to associated minerals. Examples of these lines are recorded in Table 5. It is apparent that these correspond closely to lines

Table 5. Diffraction Patterns of Unheated Fragments of Brannerite and of Brannerite Heated at "Moderate" Temperatures Compared with Strong Lines in Microlite and Uraninite Patterns

Brannerite, Custer County, Idaho				Brannerite, Mono County, California				Uraninite, Quebec, a_0=5.468Å (Arnott, 1950)			Microlite, Virginia, "Ignited" a_0=10.424Å (Arnott, 1950)		
Unheated fragment		Same fragment after 2 hours at 600° C.		Unheated fragment		Same fragment after 15 hours at 520° C.		Strong lines only			Strong lines only		
I	*d*	*I*	*d*	*I*	*d*	*I*	*d*	*I*	*d*	*khl*	*I*	*d*	*hkl*
											6	5.98Å	(111)
											4	3.11	(113)
1+	3.11Å	2+	3.08Å	4	3.10Å	4−	3.11Å	10	3.157Å	(111)	10	2.98	(222)
		1	2.68	1	2.69	1−	2.70	5	2.734	(002)	3	2.58	(004)
1	1.92	2	1.91	3	1.91	3−	1.91	8	1.935	(022)	8	1.836	(044)
1	1.626	2	1.630	3−	1.626	2+	1.627	8	1.648	(113)	8	1.563	(226)
				1−	1.238			3	1.252	(133)	3	1.194	(266)
				1−	1.213			3	1.221	(024)	3	1.165	(048)
				1−	1.104			3	1.116	(224)	3	1.064	(448)
				1−	1.037			3	1.052	(333, 115)	3	1.003	(666, 22.10)

ascribable to a cubic face-centered material with a_0 5.39 or 10.78 Å and that the lines are similar in relative intensities to those of the strongest lines in a uraninite or microlite pattern. Prolonged heating at temperatures not in excess of 600° C. produced only a slight weakening of this pattern. No shifts in position or relative intensity and no new lines could be detected. Similar lines suggesting a rudimentary pyrochlore structure but with lattice constant smaller than the usual 10.3–10.4 Å have been obtained from unheated euxenites from several localities.

Physical changes upon the heating of brannerite are not conspicuous. A small weight loss occurs even at 600° C. before the formation of new phases begins. The appearance of clean core fragments is not notably altered by heating. They remain black and sharp edged. Only in a few cases was some dulling of the luster observed in pieces that had been heated to the highest temperatures employed.

Upon heating to 800° C. or more brannerite fragments from all three

localities develop a characteristic and constant diffraction pattern.[1] This pattern consists of perfectly smooth "powder" arcs with no suggestion of orientation. In California brannerite a slight coarsening of grain could be detected after 3 hours or more of heating at 1,300° C. No such effect was observed in the Idaho or Morocco brannerite. Table 6 shows the close correspondence of diffraction patterns for material from the three localities.

Attempts were made at indexing this pattern by the methods of Lipson (1949) and of Ito (1950) and by trials of partial lattices based on the goniometric measurements and of hypothetical lattices based on the linear elements of delorenzite, a rare orthorhombic mineral of related composition. No solution was found. In view of the possible similarity of formula type and partial correspondence of axial ratios to yttrotantalite and samarskite, a comparison was made with the diffraction patterns of these minerals but no marked resemblance was seen. Though the lattice of brannerite remains unknown it seems reasonable to suppose that the diffraction pattern found is that of a single phase since a large number of lines show no variation in spacing or intensity in a number of specimens from different sources treated at various temperatures between 800 and 1,300° C.

Some patterns obtained from heated brannerite showed a few lines in addition to those found to be constant and reported in Table 6. Extra or enhanced lines near 3.1, 2.7, 1.9 and 1.63 Å were registered by two or more heated specimens from each of the localities. These are close to the strongest uraninite lines, (111), (002), (022) and (113) and to the lines found in patterns of unheated brannerite. Presumably they may be ascribed to remnants of the structure existing before heating. Though a trace of rutile was detected in a few patterns of heated brannerite no difference in pattern was found between material close to the crusted surface and from the inner parts of crystals.

Hess and Wells (1920) stated that brannerite is "brownish yellow on the outside but the visible weathering has extended to a depth not exceeding the thickness of paper." Such a crust is lacking on the California and Morocco brannerite but is found covering most of the surface of specimens from Idaho. In many places it is more than "the thickness of paper," commonly being several tenths of a millimeter thick. Fragments of crust from several crystals were examined by *x*-rays. They invariably showed a weak pattern of anatase with broad lines indicating a fine state of division of the crystalline particles constituting the crust. Upon heat-

[1] The earlier report of "two kinds of cryptocrystalline material" (Pabst, 1952, pages 152–153) obtained in brannerite from the type locality was in error.

Table 6. *X*-ray "Powder" Diffraction Patterns from Fragments of Brannerite Heated to About 1,000° C.

Mono County, California		Custer County, Idaho (USNM 105793)		Bou-Azzer mine, Morocco	
I	*d*	*I*	*d*	*I*	*d*
3	6.07 Å	4	6.03 Å	3	5.88 Å
5	4.70	6	4.73	5	4.70
2	4.31	3	4.32	2	4.29
10	3.42	10	3.41	10	3.41
6	3.32	6	3.32	6	3.29
3	3.02	3+	3.02	3	2.98
5	2.91	5	2.92	5	2.90
4	2.76	4	2.75	4	2.74
4	2.511	4	2.508	4	2.491
7	2.455	6	2.462	7	2.449
2	2.426	1	2.432	2−	2.429
7	2.276	6	2.276	6	2.270
2	2.151	2	2.161	2	2.158
1	2.080	1+	2.078	1	2.067
4	2.029	4	2.032	4	2.021
2	2.017	2	2.014	1−	2.000
8	1.903	8	1.903	7	1.903
6	1.861	6	1.864	5	1.857
1	1.776	1−	1.778	1−	1.779
3	1.729	3	1.735	3	1.731
4	1.700	3	1.702	2	1.704
				2	1.684
6	1.623	6	1.625	7	1.618
4	1.609	2	1.609	2	1.598
2	1.585	1−	1.588	?	
5	1.569	5	1.570	6	1.565
3	1.557	2	1.557	2	1.545
1	1.489	2d	1.484	3d	1.477
2	1.481				
2−	1.461	2	1.458	2−	1.457
2+	1.440	3	1.444	2	1.441
1−	1.411	1+	1.413	2−	1.410
4+d	1.371	5d	1.370	4d	1.369
3−	1.308	2	1.311	3	1.308
1+d	1.289	2d	1.287	2	1.286
2−	1.268	1	1.267	1+	1.263
3	1.255	3	1.253	3	1.247
1−	1.242	?	?		
3	1.230	3−	1.229	4	1.227

Plus about 20 more lines, mostly broad and diffuse.

ing, these crustal fragments yield a sharp and complete rutile pattern with a few extra lines whose origin has not been established.

Similar anatase crusts were observed on euxenite found with the Idaho brannerite. These are likewise converted to rutile by heating. This superficial resemblance of associated minerals apparently led to the inclusion of a little euxenite in the analyzed material for some grains in USNM 105793 turned pale brown on heating and yielded a euxenite powder pattern. This seemed strange since Hess and Wells (1920) had stated that no tantalum or niobium "could be detected." Dr. Switzer kindly arranged for a new spectrographic examination of USNM 105793 through Dr. John C. Rabbitt in the Trace Elements Section of the United States Geological Survey. This showed niobium to be present in "minor amount." Another spectrographic examination carried out by Mr. George M. Gordon of the Division of Mineral Technology, University of California, on a crystal from USNM 96873 yielding a euxenite pattern showed niobium and tantalum in a ratio of approximately ten to one. Thus the presence of a trace of euxenitic material in the analyzed type sample of brannerite is indicated but the amount of contamination is not such as to seriously impair the analysis.

Though much of the California brannerite is not crusted a small amount of orange colored material adjacent to it was found to be coarse quartz interspersed with titanium oxide which yielded a rutile pattern upon heating. Other products of alteration remain unidentified.

This study has been supported in part by the Office of Naval Research.

References

Arnott, Ronald J. (1950), *X*-ray diffraction data on some radioactive oxide minerals: *Am. Mineral.*, **35,** 386–400.

Branche, G., Chervet J., and Guillemen, C. (1951), Nouvelles espèces uranifères françaises: *Bull. soc. fran. min. et crist.*, **74,** 457–488.

George, D'Arcy (1949), Mineralogy of uranium and thorium bearing minerals: 198 pages, *RMO-563, USAEC.*

George, D'Arcy (1952), (personal communication dated May 14).

Hess, Frank L., and Wells, Roger C. (1920), Brannerite, a new uranium mineral: *Franklin Institute, J.*, **189,** 225–237.

Ito, T. (1950), A method of indexing the powder photograph of a crystal regardless of its symmetry: pages 187–228 in "*X*-ray Studies of Polymorphism," Maruzen, Tokyo.

Lipson, H. (1949), Indexing powder photographs of orthorhombic crystals: *Acta Cryst.*, **2,** 43–45.

Machatschki, F. (1929), Über die Formel des Risörites und Fergusonites: *Zeits. Krist.*, **72,** 291–300.

Machatschki, F. (1941), Kristallchemische Mineralformeln: *Zentralbl. f Min.*, 55–66.

Pabst, A. (1952), The metamict state: *Am. Mineral.*, **37,** 137–157.

Palache, Charles, Berman, Harry, and Frondel, Clifford (1944), *Dana's System of Mineralogy,* 7th ed., 774.

Wells, Roger C. (1920), Note on brannerite: *Franklin Institute, J.*, **189,** 779–780.

Manuscript received Feb. 7, 1953

MINERALOGY OF KAOLIN CLAYS FROM PUGU, TANGANYIKA

R. H. S. Robertson, *16 Kirklee Road, Glasgow, W.2, Scotland,*
G. W. Brindley,* *Department of Physics, University of Leeds, Leeds, England,* and R. C. Mackenzie, *The Macaulay Institute for Soil Research, Aberdeen, Scotland.*

Abstract

Kaolin clays from Pugu, Tanganyika, have been studied by *x*-ray, thermal, chemical and electron-optical methods. They include deposits of well-crystallized kaolinite and also of the *b*-axis disordered kaolin mineral. The latter give exceptionally clear *x*-ray diagrams which have been studied in greater detail than has previously been possible. Morphologically the disordered kaolin shows small but well-formed hexagonal plates. The cation exchange capacities have been measured and appear to be related to substitutions in both tetrahedral and octahedral lattice positions. The main chemical difference between the ordered and disordered clays appears to lie in the amount of tetrahedral substitution.

Introduction

The work described in this paper is the result of a combination of studies which present an unexpected and, in some respects, unusual picture of the mineralogy of kaolinite. Briefly, from a study of a number of kaolin-bearing sediments from Pugu, Tanganyika, two were selected for detailed study. Electron micrographs showed, in one specimen, slightly elongated hexagonal flakes, some showing a re-entrant angle

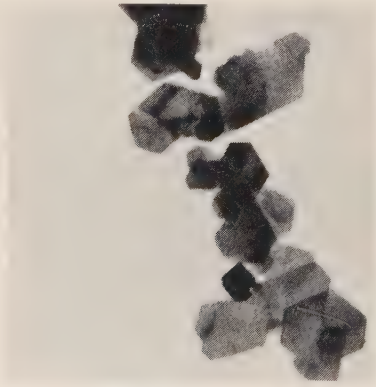

Fig. 1. Electronmicrograph of *Pugu K* Kaolin, ×5000 enlarged to 20,000, showing one crystal of anatase.

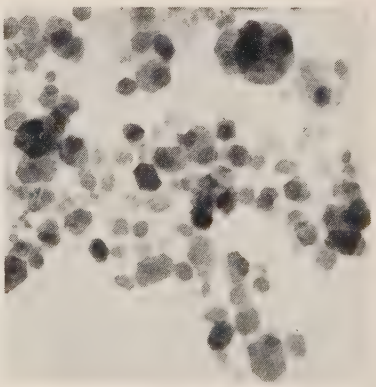

Fig. 2. Electronmicrograph of *Pugu D* Kaolin, ×8000, enlarged to 20,000.

* Now Research Professor of Mineral Sciences, The Pennsylvania State University, State College, Pa.

(Fig. 1), and in the other specimen, smaller but extremely regular and uniform hexagons (Fig. 2). *X*-ray analysis showed the larger flakes to be well crystallized kaolinite, but the smaller flakes gave the type of *x*-ray powder diagram previously obtained with the disordered kaolin structure found in many fireclays (Brindley and Robinson, 1947*a*; Brindley, 1951). Relatively pure specimens of both types of kaolin were readily obtained and their chemical composition, cation-exchange capacity, thermal and mechanical properties studied. The kaolin mineral in fireclays is usually associated with considerable quantities of fine-grained quartz and mica, together with other impurities, which have rendered difficult its detailed examination. It was thought to be worthwhile, therefore, to study in some detail these ordered and disordered forms of kaolin.

Geology of the Deposit

During the recent exploitation of the massive kaolin-sandstone deposits in the Pugu Hills, west of Dar-es-Salaam, Tanganyika, samples of the rock were taken from Adit "*D*" west of the present factory and from Adit "*K*" west of opencast workings previously developed. The samples described came mainly from 40–50 ft. from the portal of Adit "*D*" and from 120 ft. from the portal of Adit "*K*"—and for brevity will be referred to hereafter as "*Pugu D*" and "*Pugu K*" respectively.† Because both samples originated from the same series of strata, a brief account of their geology may be given.

The source rocks of the deposits are the Basement Complex (Archaean) rocks, which extend to within 100 miles of Pugu and which consist of a series of migmatites, biotite-gneisses and gneissose granites (Stockley, 1948). Rapid erosion and transportation in the Upper Cretaceous and variations in land level produced a rhythmic succession of sediments, each cycle beginning with micaceous arkose, slightly kaolinized, passing up into deltaic deposits of mica-free arkose, contemporaneously kaolinized *in situ* to a considerable extent (e.g., *Pugu K*), and ending with a deeper, marine facies consisting of kaolin deposited with finer quartz and feldspar sand (e.g., *Pugu D*).

Pugu K is a white permeable kaolin-sandstone containing, in the specimen tested, 29.4% kaolin, the remainder being sand grains of a narrow particle size range with a median diameter of 0.28 mm. The sand grains, although highly polished, are not so completely rounded as in some desert sands. Judging from photographs of Davies and Rees (1945), their rugosity or angularity (area divided by area of a sphere of the same mass

† By strange coincidence, the *K* material turns out to be good kaolinite and the *D* material the distorted structure.

(Robertson and Emödi, 1943)) appears to be about 1.08. Absence of very small sand grains, the narrow particle size range of the grains, the rarity of mica and the presence of sand-blasted pebbles demonstrate that the sand was subjected to aeolian influence by passing through desert conditions on its way to the sea. Accessory minerals include ilmenite and zircon. Hematite and goethite occur as "iron-staining," especially where the overburden is shallow.

Pugu D is less white, almost impermeable and very uniform in quality throughout; the kaolin content is 52.8% and the sand grains, with a median diameter of 0.18 mm., have a much wider particle size range.

Similar rocks are the kaolinized fine-grained Keuper arkoses at Hirschau and Schnaittenbach in Bavaria and the coarser-grained arkoses found near Steinfels, Weiherhammer and elsewhere (Zwetsch, 1950). In Georgia, U.S.A., kaolin was also formed in the Upper Cretaceous, but here the sand grains are more angular and there is a great variation in clay content and quality over this area (Mitchell and Henry, 1943; Kesler, 1951).

X-Ray Analysis of Pugu *D* and *K* Clays

X-ray analyses of these materials have been carried out with (*a*) a 20 cm. diameter, semi-focusing camera, using flat powder specimens, (*b*) a 19 cm. diameter Unicam instrument, using thin coatings of powder on thin-walled silica tubes of external diameter about 0.025 cm., and (*c*) the same camera using powders packed in thin silica tubes of internal diameter about 0.03 cm. Methods (*a*) and (*c*) require no binding agent; gum-tragacanth was used in (*b*). Filtered CoKα radiation ($\lambda = 1.78659$kX) was employed.

X-ray powder diagrams are reproduced in Fig. 3; diagrams 1 and 2 of *Pugu K* clay and 3 of *Pugu D* clay were taken by method (*b*) and are reproduced without change of scale. Diagrams 4 and 5, of *K* and *D* clays respectively, were taken by method (*c*) and are shown with two-fold enlargements in order to make clear the details of the lower order reflections.

Since the *K* and *D* clays differ in crystal size, it was considered important to determine whether the differences shown in their *x*-ray diagrams could be attributed to the crystal sizes of the materials. Two fractions of the *K* material were therefore prepared, *K1* and *K2*, with crystal sizes respectively 1.4-0.2 μ and less than 0.2 μ equivalent spherical diameter (*e.s.d.*); the corresponding *x*-ray diagrams are numbers 1 and 2 in Fig. 3. The reflections from the two samples are practically identical. Impurity lines from quartz, indicated in the key by dotted lines marked *Q*, are more prominent in 1 than in 2. The reflections in 2 are somewhat less

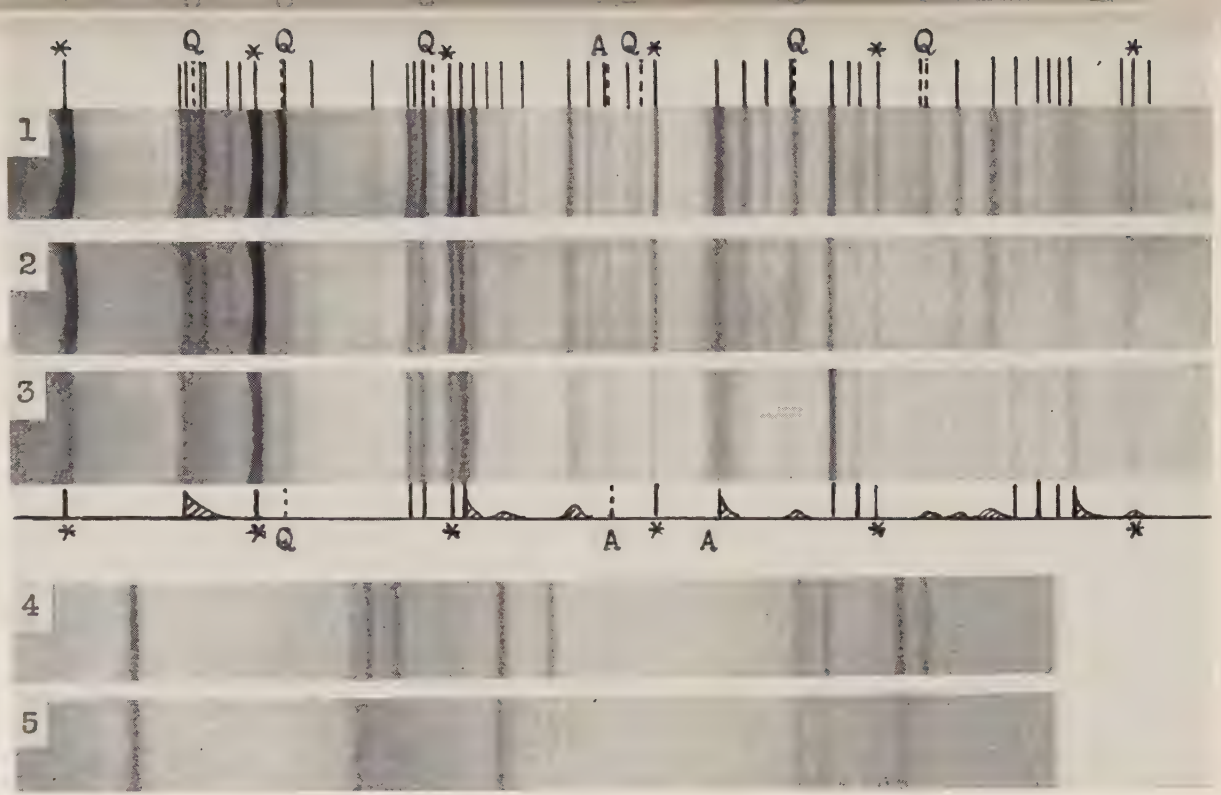

FIG. 3. X-ray powder diagrams of *Pugu* kaolin clays (19 cm. diameter camera; filtered CoKα radiation). (1) *K* clay (1.4–0.2μ particle size. (2) *K* clay (<0.2μ particle size). (3) *D* clay. (4) K clay (×2 enlargement). (5) *D* clay (×2 enlargement). *K* = well crystallized kaolinite; *D* = *b*-axis disordered kaolin mineral; *Q* = quartz reflections; *A* = anatase reflections.

sharp than in 1, in accordance with the smaller crystal size of *K2*, and the weakest reflections from *K2* are less easily seen, *but in all essential respects the coarse and fine fractions are crystallographically identical.*

The full pattern of lines from the *K* clay is indicated in the key in diagram 1, with asterisks marking the basal (00*l*) reflections, and *Q* and *A* indicating impurity lines from quartz and anatase. This diagram agreed in all respects with the data of Brindley and Robinson (1946) for well crystallized kaolinite from which the triclinic structure of the mineral was evaluated. The very close triclinic doublet, $(11\bar{1})$ and $(1\bar{1}\bar{1})$, with spacings 4.170 and 4.120kX, which is resolved by the best crystalline kaolinites, is imperfectly resolved by the *Pugu K* clay, but the doublet character is undoubtedly present and can be seen in the enlarged diagram, number 4.

It is concluded that the *Pugu K* clay, both coarse and fine fractions, consists of a well-crystallized kaolinite together with some fine quartz and anatase. The presence of anatase, shown by one or two lines only in diagrams 1–3, was confirmed by heating the clays to about 600° C. to destroy the kaolin mineral, when the full sequence of anatase lines together with quartz lines is observed.

Crystallographic interest centers mainly in the *Pugu D* clay, the *x*-ray diagram of which shows that it is a very good example of the *b*-axis disordered kaolin mineral first discussed by Brindley and Robinson (1947*a*). The sample prepared for *x*-ray analysis is of a high degree of purity and contains no more than a trace of quartz and anatase. The clarity of the diffraction diagram, Nos. 3 and 5 in Fig. 3, is greatly superior to that obtained from the fireclays previously studied and justifies a full description of the results obtained.

The diagrams in Fig. 3 are arranged so as to facilitate the comparison of the diffraction patterns of the well crystallized kaolinite and the *b*-axis disordered mineral. The outstanding feature of the latter is the broadly spreading band of intensity with a sharp low-angle termination at about 4.47 kX, the nature of which is entirely consistent with two-dimensional diffraction from randomly displaced layers. The well-ordered mineral gives a series of lines in this angular range. This difference is clearly shown in figures 4 and 5.

The lattice spacings, estimated reflection intensities, and characteristics of line profiles, such as sharp, broad or diffused, are tabulated in Table 1 together with the calculated spacings and indices. The following lattice parameters were used:

a	5.14(7) kX	
b	8.91(5)	$\beta = 104.5°$
c	7.38(0)	

TABLE 1. *X*-RAY DATA FOR PUGU D CLAY, A *b*-AXIS DISORDERED KAOLIN MINERAL

hkl	*d*, in kX		*I* (est.)	Characteristics of line profiles
	Calculated	Observed		
001	7.145	7.17	10	sharp
"02"	4.457	4.47	8	band, strongly diffused to higher angles
002	3.572	3.577	10+	sharp
$20\bar{1}$	2.560	2.560	8	sharp
130	2.552			
$13\bar{1}$	2.507	2.497	8	sharp
200	2.491			
003	2.382	2.381	8	sharp
$20\bar{2}$	2.336	2.336	9	diffused to higher angles
131	2.311			
$13\bar{2}$	2.215	2.202	1	very broad
201	2.188			
203	1.988	1.985	4	diffused to higher angles
132	1.961			
$13\bar{3}$	1.865	—	—	not observed
202	1.839			
004	1.786	1.786	4	sharp
$20\bar{4}$	1.662	1.663	5	diffused to higher angles
133	1.639			
$13\bar{4}$	1.560	1.538	1	diffused to lower angles
203	1.540			
060	1.486	1.485	10	sharp
$33\bar{1}$	1.485			
$33\bar{2}$	1.459	1.455	3	broad
061	1.454			
330	1.450			
005	1.429	1.429	2	sharp

TABLE 1—*Continued*

hkl	*d*, in kX		*I* (est.)	Characteristics of line profiles
	Calculated	Observed		
$20\bar{5}$	1.400	—	—	not observed
134	1.382			
$33\bar{3}$	1.379			
062	1.372	1.372	1	broad
331	1.364			
$13\bar{5}$	1.321	1.336	1	
204	1.305	1.307	1	very broad, spreading towards lower angles
$26\bar{1}$	1.2850	1.2847	3	moderately sharp
$40\bar{1}$	1.2827			
$33\bar{4}$	1.2695			
063	1.2605	1.2624	1	
332	1.2515			
$26\bar{2}$	1.2537	1.2476	$\frac{1}{2}$	
400	1.2457			
$40\bar{3}$	1.2385	1.2345	3	diffused to higher angles
261	1.2291			
006	1.1908	1.1918	1	

Additional observed lines, all very weak, of uncertain indices:
d=1.112, 1.042, 1.032, 1.022, 0.972, 0.958 kX.

On the basis of the earlier work the unit cell is assumed monoclinic with $\beta = 104.5°$. A mean value of $c \sin \beta$ is obtained from the $00l$ spacings (l ranging from 1 to 6), viz., 7.145 kX. The b parameter is calculated from $d(060) = 1.485(8)$ kX and the a parameter is taken to be $b/\sqrt{3}$.

The results in Table 1 confirm and amplify the earlier data and the conclusions drawn therefrom. Altogether 23 reflections are now indexed and 6 higher orders of uncertain indices are recorded, as compared, in the earlier work, with 14 indexed reflections and two others which probably did not arise from the kaolin mineral. Of the 23 indexed reflections, 22 are of the type (hkl) with $k = 3n$, where $n = 0$, 3 or 6. The only reflection observed with $k \neq 3n$ is indexed as "02" and is the 'two-dimensional' hk band with its characteristic intensity distribution. The results support the earlier conclusion that the distortion consists of largely random dis-

placements of the structural layers parallel to b and of integral multiples of $b/3$.

One aspect of the data given in Table 1 calls for comment, namely the fact that most of the observed reflections correspond to two or three calculated reflections in close proximity such as doublets of the type $(20l)$, $(13\overline{l+1})$. The question arises whether a more appropriate choice of axes or parameters would bring these calculated groups of lines into coincidence. It should be noted, in the first place, that the β-angle, 104.5°, corresponds very closely with a relative shift of successive structural layers by $-a/3$ along the a-axis. If the displacement is *exactly* $-a/3$, then β is given by $\cos\beta = -a/3c$, which leads to a value for β of 103.5°. With this value of β and with the axial ratio $b/a = \sqrt{3}$, the groups of closely spaced lines are brought into coincidence. Under these conditions a hexagonal cell embracing three structural layers exists which is related to the monoclinic cell by the following transformation matrix

$$\begin{Vmatrix} 1 & 0 & 0 \\ -\frac{1}{2} & \frac{1}{2} & 0 \\ 1 & 0 & 3 \end{Vmatrix}$$

so that if HKL are the hexagonal indices, then $H=h$, $K=-h/2+k/2$, and $L=h+3l$, and the hexagonal parameters are $a_h = 5.14(7)$kX and $c_h = 21.43(5)$kX. The available evidence suggests that $\beta = 104.5°$ is in better agreement with the observations than is the ideal value 103.5° and that the structure is, therefore, more appropriately regarded as being monoclinic, or at least pseudo-monoclinic, than hexagonal. Although it has not been found possible to photograph the calculated doublets and triplets, even at the higher angles where greater resolving power obtains, the diffusion of many of the reflections shown in diagram 3 of figure 3 suggests that the lattice is not based on a clearly defined hexagonal cell. Indeed, this would not be expected since in kaolinite there is a clear evidence that the lattice is triclinic, the translation from layer to layer being only approximately $-a/3$ along the a-axis together with a small translation along the b-axis making the angle $\alpha = 91.8°$.

Thus, the x-ray evidence shows that the *Pugu D* clay is a b-axis disordered mineral of the type described by Brindley and Robinson (1947 *a*); the previous data are confirmed and amplified by the exceptionally clear diffraction diagrams obtained with this clay.

Differential Thermal Analysis of Pugu Clays

The apparatus used for this investigation has already been fully described (Mackenzie, 1952), so it need only be noted that, (*a*) all temperatures quoted refer to the sample, since the temperature thermocouple was positioned in this material; (*b*) differing bulk densities pre-

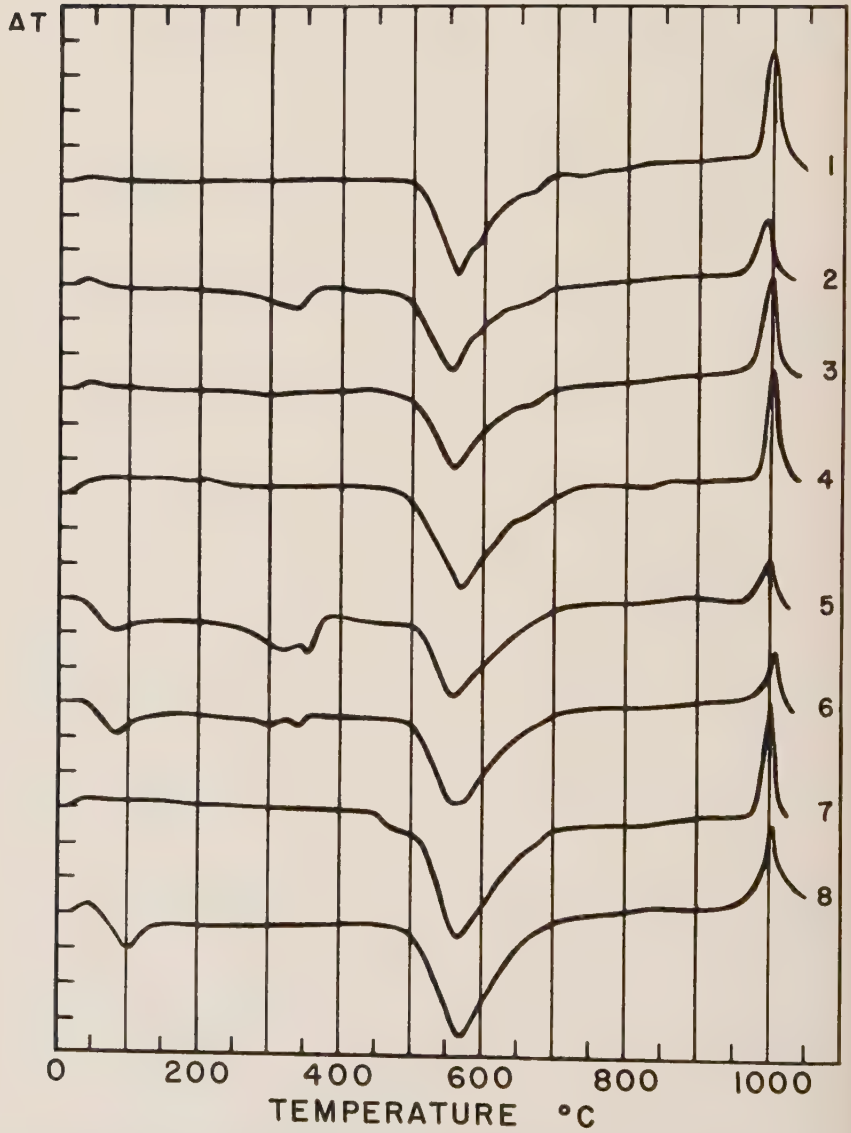

FIG. 4. Thermograms for colored samples of *Pugu* Kaolin. Data are given in Table 2 under the following curve Nos.: 1–253; 2–256; 3–252; 4–251; 5–259; 6–257; 7–314; 8–254.

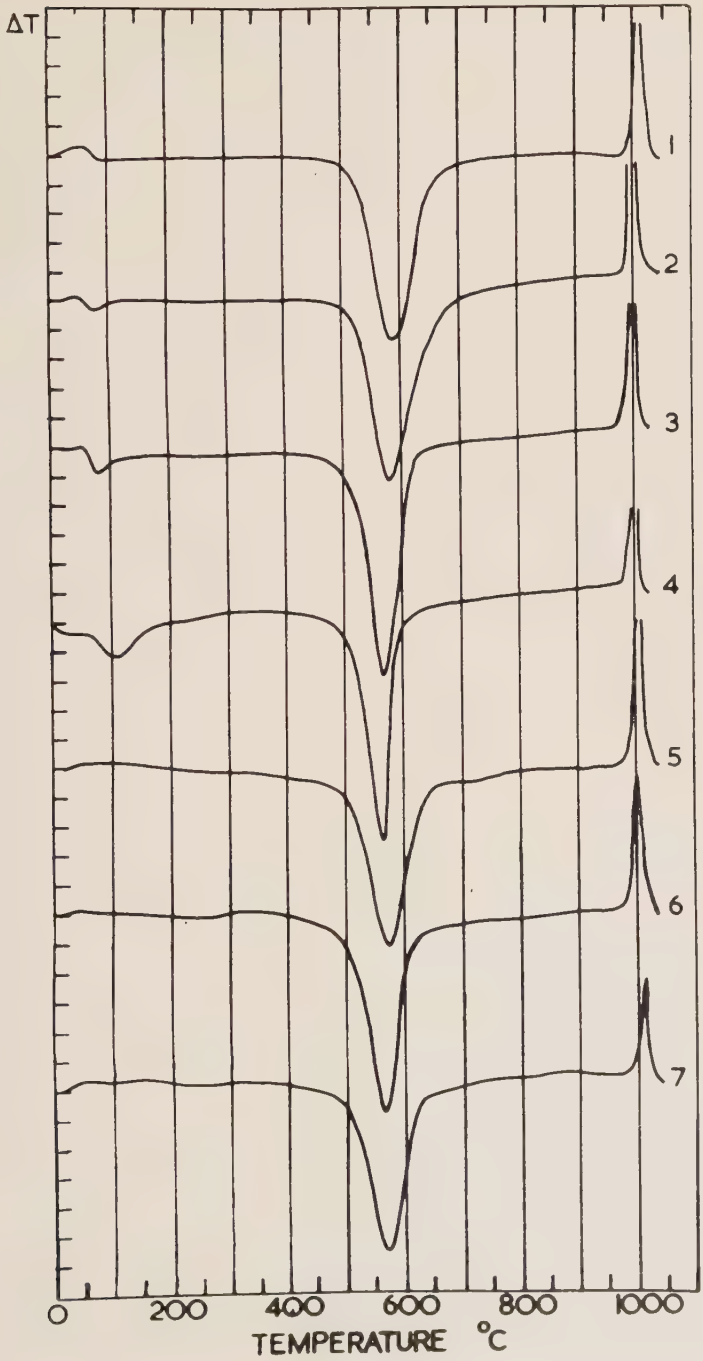

FIG. 5. Thermograms for some kaolin and halloysite samples. Data are given in Table 2 under the following curve Nos.: 1–249; 2–213; 3–379; 4–282; 5–416; 6–414; 7–418.

TABLE 2. THERMAL DATA FOR KAOLIN SAMPLES

Curve No.	Sample No. or Description	Color	Adit	Sample Wt. (g.)	T(endo) ° C.	ΔT(endo) ° C.	Area (endo) mm.²	Wt. of reacting material (g.)	Per cent reacting material*	T(exo) ° C.
249	Cornish Kaolinite	White	—	0.20	588	12.7	1036	0.190	95	1008
309	50% Cornish Kaolinite	White		0.20	570	7.3	550	0.102	51	1005
192	25% Cornish Kaolinite	White	—	0.20	557	3.6	254	0.047	23	992
254	*Lithomarge*	White	—	0.20	571	6.2	537	0.100	50	1002
313	1	White	K	0.20	582	12.4	1014	0.186	(93)	994
314	7	White with pink staining	K	0.25	567	6.6	628	0.117	47	998
259	17	Yellow-stained material	K	0.17	558	4.3	313	0.058	34	1000
257	17	Red with yellow stains	K	0.20	563	4.9	456	0.086	43	1007
253	6	White	C	0.20	563	5.4	395	0.074	37	997
256	6	Yellow stained material	C	0.19	557	4.4	353	0.066	35	993
251	6	Red surface clay	C	0.20	570	5.8	529	0.098	49	1002
252	6	Deep red	C	0.20	560	4.4	374	0.070	35	998
416	Pugu *K1* (1.4–0.2μ)	White	K	0.14	571	11.2	753	0.139	99	1003
414	Pugu *K2* (<0.2μ)	White	K	0.14	566	12.8	743	0.136	97	1001
418	Cornish *K 6* (<0.4μ)	White	—	0.14	571	11.1	745	0.137	98	1010
379	5	White	D	0.18	569	15.5	937	0.175	(97)	997
282	Halloysite (Iowa)	White	—	0.20	560	16.0	720	0.200	(100)	997
383	50% Halloysite (Iowa)	White	—	0.20	543	7.8	356	0.099	50	1005
385	25% Halloysite (Iowa)	White	—	0.20	532	4.0	166	0.046	23	1004

* Values in parentheses are assumed percentages from which other percentages are calculated; values for curves 313 and 379 are those given by other methods (see Table 5).

cluded use of a constant amount for all determinations, although 0.20 g. samples were used wherever possible.

In order to characterize the materials responsible for the red and yellow staining on some of the clay samples, the first specimens examined were a range of colored clays from Adits *C*, *D* and *K*, (Fig. 4). Yellow-stained samples apparently contained goëthite (peak at about 350° C.), with, in the Adit *C* sample (curve 2), possibly some boehmite (peak at 595° C.), and in the Adit *K* samples (curves 5 and 6) a small amount of gibbsite (peak at about 320° C.). The concentrations of these minerals were in all cases low—never more than about 5%. Since red-stained material (curves 3 and 4) did not show the presence of any hydrous oxide, the iron must presumably be present as hematite. At about 665° C., colored clays from Adits *C* and *K* (curves 1–7) showed a small peak, possibly due to a trace of illite. Quartz, if present, would not be observable on any of these thermograms.

It is well recognized that the thermal effects given by members of the kaolin group serve to distinguish them reasonably distinctly—*e.g.* increasing disorder in the lattice (*i.e.* from kaolinite to halloysite) causes a decrease in the temperature of the principal endothermic peak and an increase in its asymmetry (Grimshaw *et al.*, 1945; Brindley and Robinson, 1947*a*). A simple method of numerically evaluating this latter effect has recently been proposed by Bramao *et al.* (1952). In interpreting such thermal data, however, other factors affecting peak temperature and shape, *e.g.* the amount and the particle size of the reactant, must also be considered and, if necessary, allowed for. In the present set of experiments the sample weight was not always constant and consequently correction for the effect of this factor must be made before a rigorous comparison of curves in Figs. 4 and 5 can be attempted.

From the sample-weight data in Table 2, it will be observed that the peak temperatures in column 6 will be slightly too low for curves 256, 259 and 379 and too high for 314. Although the conditions prevailing here are not identical with those normally obtaining when the sample is diluted with foreign material, and the sample weight kept constant, it is considered sufficiently accurate, in view of the relatively small differences in sample weight, to employ the weight of reactant as determined by *the ratio of the area under the peak on each curve to the peak area for the pure material* (the usual relationship for determination of amount of reactant: see MacKenzie, 1952) for correlation with peak temperature (Fig. 6). As, from all available data, the material which gave curve 379 would appear to be practically pure, the amount of reactant here cannot be calculated as an area percentage and it was considered little error would arise by considering the amount of reactant to be 0.175g.—the

weight derived from other measurements (Table 5). The correlation of peak temperature with amount of reactant (Fig. 6) indicates that all the *Pugu C* and *K* samples are reasonably similar to Cornish kaolinite. The slightly lower peak temperature for *Pugu K* than for Cornish kaolinite tends to suggest that it is rather less well-crystallized, while the slightly higher peak temperatures for the sample labelled *Lithomarge*—a compact segregation of kaolinite—and for the red surface clay from sample 6, Adit *C*, seems to indicate, if anything, rather better crystallized material. The differences are slight, however, and broken lines have been inserted to cover what might well be the kaolinite region. The point for *Pugu D* falls well outside this region and, in fact, lies intermediate between the kaolinite and halloysite regions—*i.e.* in the position which should correspond to that for the disordered form of kaolinite found in many fireclays.

In view of the difference in particle size of *Pugu K* and *D* clays it is necessary, however, to examine closely the effects of such variation before drawing any definite conclusions. For this purpose thermograms were obtained for the samples *K1* (1.4–0.2 μ, *e.s.d.*) and *K2* ($<0.2\mu$, *e.s.d.*)—see *x*-ray section—and for *K6*, a $<0.4\mu$, *e.s.d.* fraction of a Cornish kaolinite (curves 5, 6 and 7, Fig. 5). To avoid confusion, the data

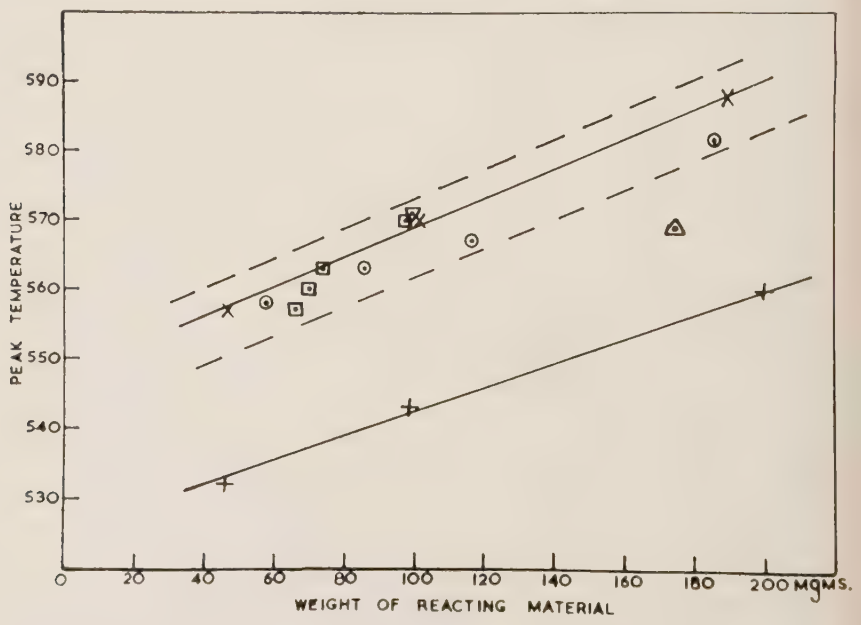

FIG. 6. Relationship between peak temperature and amount of reacting material for various samples: × = Cornish kaolinite; ⊙ = PuguK; ⊡ = Pugu C; ▽ = "Lithomarge"; △ = Pugu D; + = Iowa halloysite.

Table 3. Slope Ratios for Kaolin Samples

Curve Number	Sample Number or Description	Slope Ratio
249	Cornish Kaolinite	0.95
309	Cornish Kaolinite 50%	0.93
192	Cornish Kaolinite 25%	0.91
254	"Lithomarge"	0.96
313	1 Pugu *K*	0.81
314	7 Pugu *K*	0.64
259	17 Pugu *K*	0.60
257	17 Pugu *K*	0.64
253	6 Pugu *C*	0.82
256	6 Pugu *C*	0.86
252	6 Pugu *C*	0.76
251	6 Pugu *C*	0.73
416	Pugu *K1* (1.4–0.2μ)	1.05
414	Pugu *K2* (<0.2μ)	1.26
418	Cornish *K 6* (<0.4μ)	1.26
379	5 Pugu *D*	1.26
282	Halloysite (Iowa)	1.97
383	Halloysite (Iowa) 50%	1.87
385	Halloysite (Iowa) 25%	1.95

for these samples are not plotted on Fig. 6, but from Table 2 it will be appreciated that while both *K1* and *K6*, fall within the kaolinite region, *K2* falls outside. However, although the particle size of *K2* is almost identical with that of *Pugu D* (Meldau and Robertson, 1952), the peak temperature for *K2* is not sufficiently low (by about 5°) to bring it into line with the value for *Pugu D* and, consequently, one seems justified in definitely distinguishing *Pugu K* and *Pugu D* clays.

The "slope ratio" of the thermogram (*i.e.* tan α/tan β, where α is the angle between the perpendicular to the peak and the tangent to the descending side and β the corresponding angle on the ascending side) has recently been proposed (Bramao *et al.*, 1952) as a convenient means of distinguishing members of the kaolin series, provided the particle sizes are reasonably uniform, as kaolinite normally has a smaller slope ratio than halloysite. It has been pointed out, however, that very finely divided kaolinite might give a slope ratio in the halloysite region, although there is little possibility of the reverse happening. The present series of minerals gives values (Table 3) which are of little use in sepa-

rating kaolinite and the disordered form of kaolinite since *K2*, *K6* and *Pugu D* (curve 379), all of a similar particle-size, have slope ratios which are virtually identical. It would appear, therefore, that particle-size is relatively more important in determining the asymmetry of the peak than order or disorder in the lattice—except insofar as order or disorder may encourage or discourage the growth of larger particles. In halloysite, with a very high slope ratio, for example, the sheets are considered to be randomly stacked and here the "crystal" determining the asymmetry of the peak may indeed be the single sheet. From Table 3,

Table 4. Chemical Analyses of Separated Pugu Kaolins

	1	2
SiO_2	44.59	48.14
TiO_2	1.38	0.76
Al_2O_3	38.12	35.74
Fe_2O_3	1.43	1.45
FeO	nil	nil
MgO	0.06	0.11
CaO	0.10	0.19
Na_2O	0.12	0.04
K_2O	0.08	0.14
$H_2O+105°$ C.	13.91	13.14
$H_2O-105°$ C.	0.71	0.48
SO_3	0.09	0.05
P_2O_5	trace	nil
Cl	nil	nil
	100.59	100.14
Fe_2O_3 in residue after extraction	1.15	1.05
Total exchange capacity	7.4 m.e./100 g.	4.6 m.e./100 g.
Exchangeable H^+ ions	2.46 m.e./100 g.	0.0 m.e./100 g.

1. *Pugu D* Kaolin.
2. *Pugu K* Kaolin.
Analyst: A. H. Clarke, M.Sc. (Geochemical Laboratories Ltd.)

however, it would appear that all samples from Adits *C* and *K* are somewhat coarse in particle-size, while *lithomarge* is of the same particle size order as the Cornish kaolinite.

In conclusion, therefore, the thermal analysis results agree with the *x*-ray ones in placing *Pugu K* in the kaolinite group and *Pugu D* in the disordered lattice group and, in addition, demonstrate that, of all the samples from this deposit studied, this seems to be the only one with a disordered lattice. These samples have also provided additional data regarding the effect of particle size upon thermograms of kaolin minerals.

Chemical Data

Samples of *Pugu K* and *Pugu D* of less than 5μ *e.s.d.* were separated from the crude rock by the usual sedimentation procedure using ammonia as the dispersing agent for *Pugu K* and ammonia together with some tetrasodium pyrophosphate for *Pugu D*, and were subjected to chemical analysis (Table 4). The free iron oxides in these samples were determined by the sodium hydrosulphite method (Galabutskaya and Govorova, 1934; Mackenzie and Mitchell), and the cation-exchange capacity was determined by the micro-method of Mackenzie (1951). The exchangeable H^+ was determined from direct titration measurements on the original sandstone.

In calculating the mineralogical analysis, titania was assumed to be anatase, since this mineral was detected by *x*-ray diffraction; the iron oxide made soluble by sodium hydrosulphite was assumed to be goethite, as shown by differential thermal analysis of yellow-stained material; sulfur dioxide may reasonably be ascribed to gypsum. As mica is very rare, and feldspar occurs in the sand, K^+ is probably present in feldspar. The small amount of Na^+ added as pyrophosphate was subtracted from the *Pugu D* analysis, and a correction made for the NH_4^+ (0.04%) replacing H^+. The sum of the analyzed constituents exceeds 100% by 0.55% (after correcting for ammonia) in *Pugu D* kaolin; it was considered probable that an error of this size had arisen in the determination of one rather than of a number of elements. A preliminary calculation threw suspicion on alumina, so the excess was subtracted from the percentage of alumina in the analysis. No correction was made with *Pugu K*.

With these assumptions, the chemical analysis of *Pugu D* kaolin was

Table 5. Mineralogical Analyses of Pugu Kaolins

	Pugu D Kaolin %	*Pugu K* Kaolin %
Kaolin mineral	96.93	92.40
Quartz	—	5.13
Anatase	1.38	0.83
Orthoclase	0.47	0.76
Moisture (70–105° C.)	0.71	0.48
Goethite	0.31	0.44
Gypsum	0.19	0.10
	99.99	100.14
Mineral impurities	2.35	7.26
Mineral impurities without quartz	2.35	2.13

TABLE 6. IONIC CONSTITUTION OF THE CLAY MINERALS, ON BASIS OF O=5.000

	Theoretical for Kaolinite	*Pugu D* Kaolin		*Pugu K* Kaolin	
Mg/2	—	0.002		0.002	
Ca/2	—	0.004	0.021	0.003	0.009
Na	—	0.008		0.004	
H	—	0.007		—	
Al	2.0	1.958		1.957	
Fe^{+3}	—	0.039	2.000	0.037	1.999
Mg	—	0.003		0.005	
Al	—	0.018	2.000	0.009	2.000
Si	2.0	1.982		1.991	
O	5.0	5.000	9.122	5.000	9.092
OH	4.0	4.122		4.092	

employed to calculate the mineralogical composition and the ionic constitution of the clay minerals (Tables 5 and 6). The cation-exchange capacity calculated from the ionic constitution is 7.53 *m.e.*/100 g. of dry clay, which is in excellent agreement with the measured value of 7.4 *m.e.*/100 g., a value which, since it was determined by the micro-method, is probably 1–2% low. With no assumptions as to the excess alumina, however, the calculated cation-exchange capacity is 10.9 *m.e.*/100 g., which is not in accord with the measured value, and which suggests that the above assumptions are valid. If it is assumed that there is the same correspondence between measured and calculated values for *Pugu K*, it is possible to calculate the amount of free silica left by imperfect dispersion. In this connection, it may be remarked that the samples submitted to thermal and *x*-ray analysis, although from the same rock, had been better dispersed before separating.

Also from the ionic constitution of the clay minerals (Table 6), it would appear that there is greater Al^{+3} for Si^{+4} substitution in *Pugu D* than in *Pugu K* kaolin, that *Pugu D* contains more exchangeable Na^{+} (reflecting perhaps its more decidedly marine origin) and also H^{+} ions, and that *Pugu D* appears to have 0.122 more hydroxyls than is required by the formula $Al_2(Si_2O_5)(OH)_4$ and *Pugu K* 0.092 hydroxyls in excess.

ELECTRON-OPTICAL STUDIES

Electron micrographs of *Pugu K* and *D* kaolins, of the paper-coating kaolin *Hydratex No. 2* from Georgia, U.S.A., and of Cornish *Low Viscosity S.P.S.* china clay were obtained, and the *D*-clay crystals were also

TABLE 7. MICROMERITIC MEASUREMENTS OF SOME KAOLIN MINERALS

	Pugu D Kaolin	*Pugu K* Kaolin	Georgia *Hydratex No. 2* Kaolin	Cornwall *Low Viscosity China Clay*
Length, average, mμ	196	512	247	518
Breadth, average, mμ (at 90° to length)	152	348	180	360
Thickness, average, mμ	22.3	ca. 67.2	—	—
Length/breadth	1.29	1.47	1.37	1.44
Elongation	1.12	1.27	1.19	1.24
Rugosity	1.9	ca. 1.8	1.7	ca. 2.1
Specific surface, $m^2/g.$	44.9	15.3	—	—

palladium-shadowed for thickness measurement. The results of micrometric measurements on these electron-micrographs have already been published (Meldau and Robertson, 1952) and, together with the values for more recently determined parameters and with measurements for other kaolins, are collected in Table 7. It should be noted the "elongation" is expressed as the *ratio of the crystal length to the crystal breadth divided by 1.155* (the ratio for a true hexagon). No values for the specific surface of *Hydratex No. 2* or of *Cornish Low Viscosity S.P.S.* china clay are available, but for comparative purposes may be cited the values found by Vassiliou and White (1948) for *Cornish Supreme* china clay using a moisture capillarity/temperature technique, and those of Carman and Malherbe (1950) for an unnamed Cornish china clay using nitrogen adsorption and air permeability—namely, 23 $m.^2/g.$ and 11.4 $m.^2/g.$, respectively.

Electron-optical studies show that about 98% of *Pugu D* crystals are euhedral. In Georgia kaolin the smallest crystals ($<0.5\ \mu$) are euhedral, but large crystals approaching 1 μ in diameter almost all have one re-entrant angle. In *Cornish Low Viscosity S.P.S.* china clay, euhedral crystals are rare, and large crystals often have more than one re-entrant angle or even a jagged, broken edge. These observations amplify those of Clark (1950), who showed that crystals of plastic china clay from Cornwall are thinner and more irregular than in the low viscosity types; and that Zettlitz kaolin is so irregular in outline that crystal angles are rarely seen. Meldau and Robertson (1952) gave some evidence that the viscosity of deflocculated kaolin slips was closely related to rugosity, but not to exchange capacity.

Gold sol adsorption

Electron micrographs showed that unprotected gold sol particles are particularly strongly attracted to the corners and edges of *Pugu D* clay,

whilst relatively fewer are attracted to the *Georgia* kaolin crystals, many remaining near the crystals without being influenced by them. *Low Viscosity S.P.S.* china clay is more weakly attracting still, except at jagged broken crystal edges where the gold particles form a thickly-studded fringe. Gold particles are also attracted preferentially to re-entrant angles.

These observations confirm that *Pugu D* kaolin is very well crystallized, the electrostatic charge being mainly concentrated at the 6 corners. In less perfect crystals the charge is distributed among many points along a longer perimeter and is therefore weaker, while broken crystals have many points of high charge because of unsatisfied valence bonds and consequently attract many gold particles.

Impurities

In view of observations on the occurrence of titania as anatase in fireclays and in sedimentary kaolin (Brindley and Robinson, 1947*b*; Nagelschmidt *et al.*, 1949) the electron-micrographs were scanned for this mineral. Opaque isometric crystals showing hexagonal, and occasionally square and triangular outlines were considered to be anatase (Fig. 1); and this was confirmed by *x*-ray examination in the case of *Pugu D*. It was estimated by counting that anatase crystals are about twice as common in the *Georgia* kaolin as in the *Pugu* kaolins.

Large clouds of 1 μ diameter and extreme thinness, seen in both *D* and *K* clays are believed to be a hydrated iron compound: a coral-like fragment was unidentified, but an opaque sphere may possibly be hematite. Otherwise the *Pugu* and *Georgia* clays appear to be practically monomineralic, whereas the *Cornish* clay shows considerable numbers of wavy mica crystals.

General Discussion and Conclusions

Both *x*-ray diffraction and differential thermal analysis show that *Pugu D* kaolin is the disordered type of kaolin mineral found in many fireclays, and that *Pugu K* kaolin is a well-crystallized kaolinite in which the structural layers are much more regularly superposed, but possibly not so regularly as in the best specimens of kaolinite. Although *Pugu D* shows a high degree of structural irregularity, it is morphologically very perfect; indeed, the crystals are more nearly hexagonal than in any other clay known to us. On the other hand, *Pugu K* is more perfect structurally but less perfect in crystal shape. The two types are regarded as having been formed under different conditions; it seems reasonable to suppose that fine-grained euhedral crystals of *b*-axis disordered

kaolin will not develop into larger grained crystals of well-ordered kaolinite having re-entrant angles. Indeed, if one accepts the dislocation hypothesis of crystal growth as recently discussed by Dekeyser and Amelinckx (1951, 1952) it is quite inconceivable that a disordered system could, with further growth, develop into an ordered one.

The *Pugu D* clay provided an excellent *x*-ray diagram of a *b*-axis disordered mineral of a high degree of purity which confirmed and amplified earlier data and the conclusions drawn therefrom. On the other hand, the differential thermal results amply demonstrated the difficulties which may arise in attempting to distinguish members of a series when particle-size effects are superimposed. Although it has proved possible, even when the samples were relatively impure, to distinguish kaolinite from *b*-axis disordered kaolin, further study of the thermal effects in the kaolin series arising from order and disorder in the lattice and from particle-size differences would appear very desirable.

As the separated clays were remarkably free from impurities, evaluation of their chemical composition was possible. From this, and other evidence, it seems probable that the cation-exchange capacities of these clays arise from substitutions in both the tetrahedral and octahedral positions in the lattice rather than from valences at the edges of the crystals—*e.g.*, observed and calculated exchange capacities for *Pugu D* agree almost exactly if certain reasonable assumptions are made, and although the area of "edge" faces per gram for *Pugu D* is 4.0 times as great as for *Pugu K* the exchange capacity is only 1.61 times as great.

The chemical calculations show that, while the degree of substitution in the silica layer is about twice as great in the *b*-axis disordered as in the ordered mineral, there is relatively little difference in substitution in the octahedral layer, viz., about 1.93% of these positions are occupied by Fe^{+3} and 0.15% by Mg^{+2} in *Pugu D* compared with about 1.85% and 0.28% respectively, in *Pugu K*. The main difference, chemically, between the clays, therefore, appears to lie in the amount of tetrahedral substitution.

Acknowledgments

The authors desire to thank Dr.-Ing. Robert Meldau, Laboratorium für Staubtechnik, Harsewinkel, Westphalia, for conducting that part of of the electron-optical work carried out at the Rheinisch-Westfälisches Institut für Übermikroskopie, Düsseldorf (Director: Prof. B. von Borries), and Dr. Ian M. Dawson for that part carried out at Glasgow University; Kenneth P. Wright for preparing specimens of the clay; N. Tunstall and R. F. Youell who assisted in taking the *x*-ray photo-

graphs; Miss E. S. Murdoch who assisted in the thermal and cation-exchange measurements; and the Pugu China Clay Co. Ltd. for the gift of samples.

References

Borries, B. von, and Kausche, G. A. (1940): *Kolloid Z.*, **90,** 132.

Bramao, L., Cady, J. G., Hendricks, S. B., and Swerdlow, M. (1952): *Soil Sci.*, **73,** 273.

Brindley, G. W., and Robinson, K. (1946): *Min. Mag.*, **27,** 242. (1947*a*), *Trans. Brit. Ceram. Soc.*, **46,** 49. (1947*b*), *Min. Mag.*, **28,** 244.

Brindley, G. W. (Editor) (1951): X-Ray Identification and Crystal Structures of Clay Minerals. London: Mineralogical Society. Chapter II.

Carman, P. C., and Malherbe, P. le R. (1950): *J. Soc. Chem. Ind.*, **69,** 134.

Clark, N. O. (1950): *Trans. Brit. Ceram. Soc.*, **49,** 409.

Davies, W., and Rees. W. J. (1945): *J. Iron Steel Inst.*, p. 71 P.

Dekeyser, W., and Amelinckx, S. (1951): *Compt. rend.* **233,** 1297; (1952), *Compt. rend.*, **234,** 446.

Galabutskaya, E., and Govorova, R. (1934): *Min. Suire*, **9,** 27.

Grimshaw, R. W., Heaton, E., and Roberts, A. L. (1945): *Trans. Brit. Ceram. Soc.*, **44,** 76.

Kesler, T. L. (1951): *Mining Engng.*, **3,** 879.

Mackenzie, R. C. (1951): *J. Colloid Sci.*, **6,** 219. (1952), *An. Edafol. Fisiol. veg.*, **11,** 159.

Mackenzie, R. C., and Mitchell, B. D. *In preparation.*

Meldau, R., and Robertson, R. H. S. (1952): *Ber. deut. keram. Ges.*, **29,** 27.

Mitchell, L., and Henry E. C. (1943): *J. Am. Ceram. Soc.*, **26,** 105 and 113.

Nagelschmidt, G., Donnelly, H. F., and Morcom, A. J. (1949): *Min. Mag.*, **28,** 492.

Robertson, R. H. S., and Emödi, B. S. (1943): *Nature*, **152,** 539.

Stockley, G. M. (1948): *Tanganyika Territory Geol. Surv. Dept. Bull.*, No. **20,** 1–37.

Vassiliou, B., and White, J. (1948): *Clay Min. Bull.*, **1,** 80.

Zwetsch, A. (1950): *Tonindustr. Ztg.*, **74,** 166, 196, 283 and 313.

Manuscript received Jan. 31, 1953.

NOTES AND NEWS

A CORRECTION TO THE "REEXAMINATION OF THE CRYSTAL STRUCTURE OF MELILITE"

J. V. Smith, *Geophysical Laboratory, Washington, D. C.*

It has been brought to my attention that certain sentences in my paper "Reexamination of the crystal structure of melilite" concerning Goldsmith's paper "Some melilite solid solutions" are misleading. The purpose of this note is to correct these errors and to apologize to Goldsmith.

Goldsmith carried out quenching experiments to determine the solubility of $Na_2Si_3O_7$ in the akermanite-gehlenite series and found that the amount of Na_2O varied from 0 per cent in akermanite to 3.85 per cent in gehlenite. This amount explained about half of the Na in the most sodic natural melilites. He then considered various ionic replacements to counter-balance the substitution of Na^+ for Ca^{2+} and came to the conclusion that "with the possible exception of this cation replacement (OH^- for O^{2-}) it is thus improbable that soda can enter the melilites by any means other than as a replacement for Ca with the accompanying Si^{4+} for Al^{3+} substitution." He further states that "The influence of hydroxyl is unknown but probably is not large" and that "the fact that the melilites tend to show high Si contents might be used as an argument against hydroxyl and might favor the argument for $Na_2Si_3O_7$ substitution." In my paper, due to unfortunate wording (especially the accidental omission of the word "other" between the words "only" and "reasonable," line 10, page 657, and in the last sentence of the abstract) the impression is given that Goldsmith postulated that OH replacement is the major balancing mechanism for the replacement of Ca by Na. This was not my intention. In the same section, I came to the conclusion that the presence of H_2O^+ in the melilite analyses was not a result of substitution of Na for Ca, and this confirms Goldsmith's statement that "the influence of hydryoxyl . . . is probably not large."

References

Goldsmith, J. R. (1948), *Jour. Geol.*, **56**, 437.
Smith, J. V. (1953), *Am. Mineral.*, **38**, 643.

HYDROTHERMAL SYNTHESIS OF ANDALUSITE

DELLA M. ROY, *College of Mineral Industries, The Pennsylvania State University, State College, Pennsylvania.*

In a detailed investigation of the system Al_2O_3–SiO_2–H_2O, Roy and Osborn (1952) reported their failure to synthesize consistently and unequivocally the anhydrous aluminosilicates, sillimanite, andalusite and kyanite. Several earlier workers have reported the synthesis of sillimanite (Balconi 1941, Michel-Levy, 1949, Morey, 1942) but positive evidence that the product was sillimanite and not mullite has been lacking. Reports of the synthesis of andalusite (see Doelter, 1917, Baur, 1911, Lacy, 1952) are similarly open to question in view of the absence of evidence for positive identification of andalusite as a product of the reaction.

In the course of an investigation of equilibria in the system MgO–Al_2O_3–SiO_2–H_2O,* a phase with a powder *x*-ray diffraction pattern similar to andalusite was obtained. Although neglected at first as one of several "freak" occurrences, its repeated appearance made worthwhile further investigation. This phase has now been obtained consistently in many runs, using a variety of starting materials such as Langley kaolinite, Florida kaolinite, Macon (Georgia) kaolinite (*API* No. 3), 1:1 and 1:2 Al_2O_3:SiO_2 mixtures and gels, and mixtures in the system MgO-Al_2O_3–SiO_2–H_2O with the molar ratios 12:44:44 and 3:33:64 MgO:Al_2O_3:SiO_2. Representative runs are listed in Table 1. The techniques used for preparation of samples and hydrothermal reaction have been described in earlier papers from this Laboratory, Roy and Osborn (1952) Roy, Roy and Osborn (1950, 1952).

The identification of andalusite as a phase grown under hydrothermal conditions is based on the following criteria: (1) The crystals have the same mean refractive index as andalusite (1.635 ± 0.004) and low birefringence. Accurate determination of the three indices of refraction has not as yet been possible because of the small size of the crystals—maximum diameter about 20 microns. (2) The crystals grow on seeds of natural andalusite. The overgrowths form an interesting pattern, being always oriented at right angles to the seed. Thus seeds which are yellow under crossed-nicols with the gypsum plate are surrounded completely by a fringe of "blue" overgrowths. Thus the synthetic material when it does show any elongation (not pronounced) is length slow as compared to the length fast nature of natural andalusite in its usual habit. The *x*-ray

* This work was conducted as part of a program sponsored by the Office of Naval Research, investigating the stability relations among metamorphic minerals, and appeared as *Tech. Rept. No. 6. Contract N6 onr 26909, Jan. 1952.*

TABLE 1. SUMMARY OF HYDROTHERMAL RUNS

Run No.	Starting Material Composition, Mol. %			Temp. (° C.)	Water Press. (psi)	Duration of run (hrs.)	Comments*	Phases Present*
	MgO	Al_2O_3	SiO_2					
5396		33	67	545	25,000	118		Hydralsite
5400		33	67	540	25,000	190	and. sds.	cor.+mull.+and.
5431		50	50	580	20,000	141	and. sds.	cor.+and.+1. mull.
5255	12	44	44	455	20,000	384		Hydral.+1. AS+1. and.
5213	12	44	44	530	20,000	432		and.+1.AS+1.cord. +1. cor.
5432	12	44	44	580	30,000	141	and. sds.	cord.+mull.+and.
5425	3	33	64	525	25,000	192	and. sds.	and.+Hydral.+cor. +1. qtz.
5433	3	33	64	580	20,000	141	and. sds.	mull.+1.cord.+and. +qtz.
5468	3	33	64	650	20,000	166	and. sds.	mull.+and.+1.cord.
218	Langley kaol.			450	10,000	192		Hydral.+pyroph. +and.
5435	Macon kaol.			505	20,000	141	and. sds.	pyroph.+Hydral. +and.+1. mull.
5436	Florida kaol.			505	20,000	141	and. sds.	pyroph+Hydral. +and.+mull.
5431	Langley kaol.			575	30,000	115		mull.+and.
5459	Langley kaol.			650	20,000	166	and. sds.	and.+mull.

* Abbreviations used: and.=andalusite, cor.=corundum, mull.=mullite, cord.=cordierite, qtz.=quartz, pyroph.=pyrophyllite, sds.=seeds, kaol.=kaoline, l=Little, AS=aluminum serpentine.

diffraction pattern is very similar to that of andalusite, particularly at low 2θ values (see Table 2). Since it has never been obtained as the only phase present, comparison at higher angles is somewhat difficult due to the overlapping of lines and the lack of distinct lines at higher angles. The 001 and 002 reflections are very pronounced and quite distinct from the spacings of any other phase appearing in this part of the system. Mullite, sillimanite, kyanite and all known alumina-silica hydrates are positively eliminated as alternatives by the *x*-ray diffraction pattern.

These recent data suggest that andalusite is a stable phase between 450° and 650° C. at water pressures between 10,000 and 30,000 psi. Roy and Osborn (1952) have decomposed andalusite in the presence of water up to about 425° C., the chief decomposition products being either kaolinite or pyrophyllite. The data also suggest the possible importance of the presence of slightly larger cations such as Mg^{++} or Ca^{++} in aiding

TABLE 2. *X*-RAY DATA ON SYNTHETIC ANDALUSITE; COMPARISON WITH MULLITE AND NATURAL ANDALSUITE

Natural Andalusite (USNM)		Synthetic Andalusite +Mullite			Mullite (Corhart electrically fused)	
d (A°)	I/I_0	*d* (A°)	I/I_0	Identification*	*d*(A°)	I/I_0
5.57	10	5.60	5	A		
		5.45	1.5	M	5.50	7
4.56	6	4.55	3	A		
3.94	3	3.99	2	A		
3.53	6	3.53	3	A		
		3.43	7	M	3.44	10
					2.89	1.5
2.78	10	2.79	10	A		
		2.71	2	M	2.71	5
		2.56	2	M	2.56	3
2.47	9					
					2.44	4
					2.30	1.5
2.28 / 2.26	3					
		2.22	2	M	2.22	7
2.17	5					
		2.13	1	M	2.13	4

* A = andalusite, M = mullite.

the formation of andalusite. Pure gels or alumina-silica mixtures did not yield andalusite except as growth on seeds (or in the presence of seeds) whereas mixtures in the MgO–Al_2O_3–SiO_2 system did so readily. This fact may be connected with the five-fold coordination of one Al^{3+} ion in andalusite; Mg^{2+} entering such a structure would certainly strive for a higher coordination than four. The Macon (Georgia) kaolinite contains .47% MgO and .52% CaO, and the others probably also contain significant amounts of these cations which, although perhaps not essential, may aid greatly in the growing of crystals of andalusite.

REFERENCES

BAUER, E. (1912), Hydrothermal Silicates: *Zeit. Elektrochem.*, **17,** 739; and *Zeit. Anorg. Chem.* **72,** 119 (1911).

BALCONI, M. (1941), Synthesis of sillimanite: *Rend. Soc. Min. Ital.*, **1,** 77.

DOELTER, C. (1927), Handbuch der Mineralchemie. Steinkopf, Leipzig.

LACY, E. D. (1951), Minerals and magmas: Studies at high temperatures and pressures: *Nature*, **168,** 537.

MICHEL-LEVY, M (1950), Reproduction artificielle de la sillimanite: *Compt. Rend.*, **230,** 2213.

Morey, G. W. (1942), Solubility of solids in water vapor: *Proc. A.S.T.M.*, **42,** 986.

Roy, R., Roy, D. M., and Osborn, E. F. (1950), Stability and compositional relationships among the lithium aluminosilicates, eucryptite, spodumene and petalite: *J. Am. Ceram. Soc.*, **33,** 152.

Roy, D. M., Roy, R., and Osborn, E. F. (1953), The system MgO–Al_2O_3–H_2O: *Am. J. Sc.*, **251,** 337.

Roy, R., and Osborn, E. F. (1952), The system Al_2O_3–SiO_2–H_2O: *Am. Mineral.*, **37,** 300 (Abstract).

Roy, R., and Osborn, E. F. (1952), Some simple aids in the hydrothermal investigation of mineral systems: *Econ. Geol.* **47,** 717.

Manuscript received Jan. 29, 1954.

COBALT IN KIMBERLITES

R. S. Young, D. A. Benfield, and K. G. A. Strachan, *Diamond Research Laboratory, Johannesburg, South Africa.*

Nickel has been reported as a constituent of Jagersfontein kimberlite in quantities from 0.08 to 0.14%, and as a component of nodules of eclogite, pyroxenite, phlogopite, and chrome diopside found in kimberlites, in amounts from a trace to 0.26% (4). We have not, however, been able to find a reference to cobalt in kimberlite or its associated minerals.

In the course of complete chemical analyses of the ten different types of kimberlite found in Premier Mine, Transvaal, South Africa, we have found cobalt ranging from 0.003 to 0.008%. Cobalt was determined by the accurate and convenient colorimetric procedure using nitroso-R-salt (5). The results for cobalt, together with those for iron and nickel, are given in Table 1.

Some investigators have seen an analogy between the forces of tem-

Table 1. Content of Cobalt, Iron, and Nickel in Premier Mine Kimberlites

Kimberlite Type	*Percentage*		
	Co	Fe	Ni
1	0.005	5.86	0.10
2	0.003	5.41	0.11
3	0.007	7.32	0.11
4	0.006	6.36	0.12
5	0.007	6.90	0.13
6	0.006	8.73	0.10
7	0.006	7.00	0.09
8	0.008	7.35	0.11
9	0.005	9.35	0.15
10	0.006	7.05	0.11

perature and pressure acting on kimberlite which result in the crystallization of carbon, and the forces operating in the formation of meteorites. Graphite is present in both kimberlites and meteorites, and some of the latter are largely made up of minerals like enstatite and olivine which occur commonly in kimberlite. It is therefore interesting to compare the ratios of iron, nickel, and cobalt in kimberlites with those in meteorites. Since the different types of kimberlite found in Premier Mine are representative of the varieties of this mineral found in other parts of the world, we believe our results are of general application.

The ratio of nickel to cobalt in meteorites has been given by Rankama and Sahama (2) as about 8, and approximately the same ratio has been reported by Beck and La Paz (1) for the stony phase of nortonite, the largest meteorite of any type of witnessed fall. The latter workers reported for the metallic phase of this meteorite a nickel:cobalt ratio of 16, while in the metallic phases of other meteorites this ratio has varied from 5 to 20 (3).

The iron:nickel ratio in both the metallic and the stony phases of other analyzed meteorites gave iron:nickel ratios varying from 2 to 25 (1), while in metallic phases similar ratios have been reported from 17 to 26.

In kimberlites the ratio of nickel to cobalt varies from 14 to 38, with an average of 21, while the iron:nickel ratio ranges from 49 to 87, averaging 64. The nickel:cobalt and iron:nickel ratios in kimberlites are therefore higher than in meteorites. The solubility of carbon in molten metals of the iron group is highest in iron, followed by nickel and then cobalt. On this basis and under the same conditions, it would appear that kimberlite might be a more favorable medium for diamond formation than a meteorite.

References

1. Beck, C. W., and La Paz, L. (1951). The nortonite fall and its mineralogy: *Am. Mineral.*, **36**, 45–59.
2. Rankama, K., and Sahama, Th. G. (1950), Geochemistry. Chicago, University of Chicago Press.
3. Wahl, W. (1950), A check on some previously reported analyses of stony meteorites with exceptionally high content of salic constituents: *Geochimica et Cosmochimica Acta*, **1**, 28–32.
4. Williams, A. F. (1932), The Gensis of the Diamond, Volumes I and II. London, Ernest Benn Ltd.
5. Young, R. S., Pinkney, E. T., and Dick, R. (1946), Colorimetric determination of cobalt in metallurgical products with nitroso-R-salt: *Ind. Eng. Chem., Anal. Ed.* **18**, 474–476.

NOTE ON THE VARIANCE IN X-RAY QUARTZ-POWDER DIFFRACTION PATTERNS

A. F. Gabrysh,* E. F. Preece, M. A. Yager and M. McCutchen**
Engineering Laboratory, Washington District Corps of Engineers, Washington 25, D.C.

Incidental to continuing Debye-Scherrer-method investigations of crystalline structure as part of the study of Electrosmosis[1] which one of us (EFP) is making, there was occasion to note the variance in reflection patterns from the same powdered quartz[2,3] sample using a rotating thread-like target and a stationary wedge-shaped target.

Material for the targets was ground up in a mortar. Powder for the thread, an amount that could be scooped up on the end of a needle, was bound by approximately an equal amount of adhesive[4] of toluene and ethyl-cellulose; then, by rolling between two glass plates, it was drawn into a thin rod .003 -.005 inches in diameter. The wedge-shaped target was formed, without binder, by packing in a small cradle holder and mounted such that the primary beam grazed the edge. Photographs were made with a North American Philips Company x-ray diffraction unit in a cylindrical camera 114.59 mm. in diameter. The weighted average wavelength of K_{α_1} and K_{α_2} copper radiation and nickel filter were employed, the tube voltage and current being 35 KV and 25 ma. respectively; the exposure time was 2.3 hours and the temperature 21.5° C.

By independent methods, several authors[5–9] have obtained expressions for the intensity of x-ray reflection; most of these are in agreement with each other. Compton[9] has derived formulas which are applicable to the following considerations:

* Now at Oak Ridge National Laboratory, Oak Ridge, Tenn.

** Now at Royal Victoria Hospital, Montreal, Canada.

[1] Preece, E. F., *Highway Research Board Proceedings*, **27,** 384–417 (1947).

[2] Many photographs of powdered soil samples displayed the fan-shaped convergence of Fig. 2*C*. By elimination it appeared that the effect was due to the quartz component.

[3] Quartz occurs both as large crystals and as microscopic grains, in both cases apparently with identically the same crystal structure of either primary or secondary radiation.

[4] Dr. Christ and co-workers, U. S. Geological Survey, suggested a mixture in ratio of 5 grams ethyl-cellulose to 100 cc. of toluene; authors used 7 grams and 100 cc.

[5] Debye, P., *Ann. d. Physik*, **43,** 49 (1914).

[6] Bragg, W. L., James and Bosanquet, *Phil. Mag.*, **41,** 309 (1921).

[7] Greenwood, G., *Phil. Mag.*, (7), 3, 936 (1927).

[8] Compton, A. H., *Phys. Rev.*, **9,** 29 (1917).

[9] Compton, A. H., *X-Rays and Electrons.*

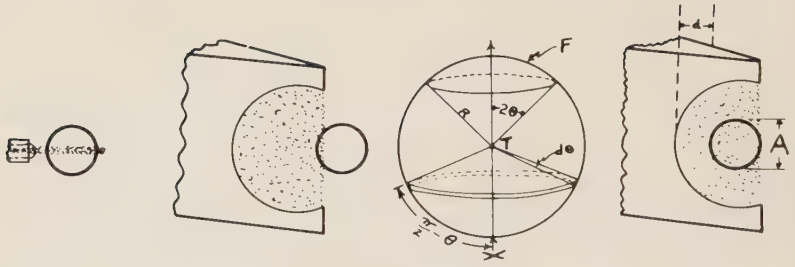

FIG. 1. Relative size and position of target to incident beam of cross-sectional area A: (*a*) rotating "thread," (*b*) stationary wedge barely grazed by incident beam, (*c*) relationship of incident beam X, target T, diffracted rays R, and film F, (*d*) same wedge as in *b* intercepting full x-ray beam.

The thread (Fig. 1*a*) is a small cylindrical mass of rotating crystals whose orientations have a continuous random distribution and whose volume is considered so small that we can neglect absorption of the x rays which bathe it. A small correction may be made for absorption in the binder—cellulose is an organic material consisting of atoms of low atomic numbers and yields very faint, ill-defined x-ray diffraction patterns. This proceeds as for a powder containing ingredients of different absorption coefficients.[10] For a given angle of diffraction the intensity distribution in the resulting halo (Fig. 2*a*) of any cone whose axis is the direction of the incident beam will be uniform. The total energy W reflected by crystals rotated through angle θ with uniform velocity ω is proportional to the volume Δv of the crystal.

$$W = Q\Delta v I_0 = I_0 \int P(\theta)d\theta$$

I_0 is the incident energy in the primary x-ray beam and Q is given by

$$Q = \frac{N^2\tau^3}{2u} F^2 \frac{e^4}{m^2c^4} \frac{1 + \cos^2 2\theta}{\sin 2\theta}$$

where N is the number of atoms per unit volume, u the effective absorption coefficient of the crystal, τ the wavelength of the x rays used, m the mass of the electron, e the charge on the electron, c the velocity of light, $1+\cos^2 2\theta$ the polarization factor, and F is termed the structure factor and is defined by the equation

$$F = Z \int_{-a}^{a} P(z) \cos\left(\frac{4\pi z}{\tau} \sin\theta\right) dz$$

[10] Bradley, A. J., *Proc. Phys. Soc.*, **47**, 879 (1935).

where z is the number of electrons in the atom, a is the maximum possible distance of an electron from its atomic layer and $P(z)$ represents the probability that an electron will be at a distance z and $(z+dz)$ from the mid-plane of the layer of atoms to which it belongs. In the integral, $P(\theta)I_0$ is radiation reflected in direction θ by a particle.

When the incident beam just grazes a stationary wedge (Fig. 1*b*), absorption is again negligible and the normals to the crystal planes which contribute to a halo all lie close to a cone whose semi-vertical angle from X is $(\pi/2)-\theta$ (Fig. 1*c*), or say between two cones whose semi-vertical angles are $(\pi/2)-\theta$ and $(\pi/2)-(\theta+d\theta)$. For random distribution of orientations the possibility of a normal lying between these two cones is equal to the ratio of the area cut off between the two cones from the surface of a sphere with T as center to the whole surface area or $(1/2)\cos\theta\, d\theta$. Considering N particles in all, a number $(1/2)N\cos\theta\, d\theta$ will have their normals lying within the given range, and if $\overline{P(\theta)}$ is the average reflecting power of a particle, the total energy reflected into the halo (Fig. 2*b*) will be

$$\tfrac{1}{2}NI_0\cos\theta d\theta\overline{P(\theta)}$$

or integrating over all values of θ,

$$P = \tfrac{1}{2}NI_0\cos\theta\int\overline{P(\theta)}d\theta$$

where for the small range of effective angles in the vicinity of θ_0, $\cos\theta$ is taken as a constant and equal to $\cos\theta_0$ in the integration. From above

$$P(\theta)d\theta = Q\Delta v$$

then

$$P = \tfrac{1}{2}NI_0\cos\theta_0\overline{dv}$$

where $\overline{dv}$ is the average volume of a particle. Hence, $N\overline{dv}$ is the total volume V of the powder, and

$$\frac{P}{I_0} = \frac{1}{2}\cos\theta_0 QV.$$

Sets of planes with different crystallographic indices, having the same spacing reflect into the same halo. If there are n such sets, then

$$\frac{P}{I_0} = \frac{n}{2}\cos\theta_0 QV.$$

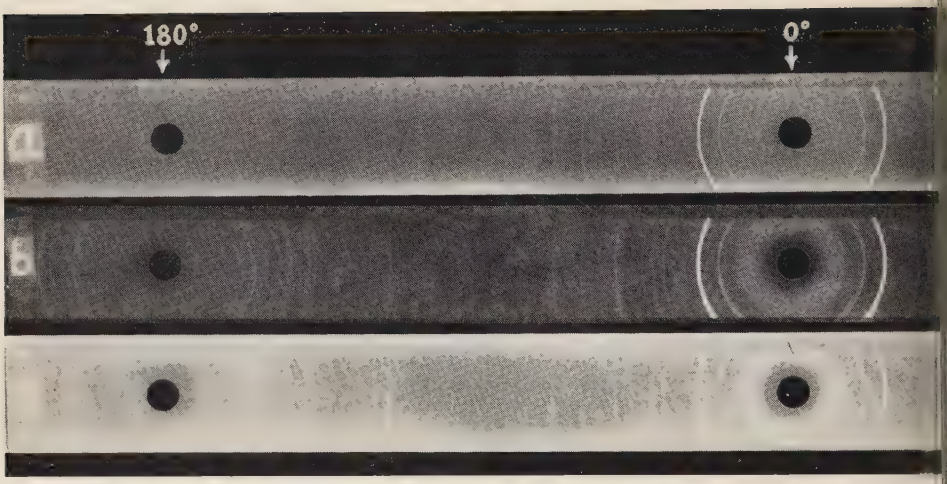

FIG. 2. Quartz-powder photograph: (*a*) rotating thread, (*b*) grazed stationary wedge (*c*) wedge interception of all incident radiation

In the final consideration (Fig. 1*d*) the wedge is mounted such that the rays are perpendicular to a plane bisecting the wedge angle and involve a greater volume of particles with the full incident beam of cross-sectional area A. The total volume irradiated is $(p'/p)(d/2)A$ where p' and p are the densities of the powder and the crystal in bulk respectively; d is thickness through wedge. There is an optimum thickness in the wedge where the energy falling into a halo is a maximum when d equals $1/u$ where u is the linear absorption coefficient of a section for the radiation.

The relative intensities of the lines (Fig. 2*c*), considering that full beam energy is involved, appear influenced by the absorption of the x rays. The fan-shaped convergence with disappearing small illumination spots, absent for the first mounting, appears strongly. This turbulent distribution of interference gives the deception of order effect which does not exist.

The K_α doublet is most conveniently observed in the region where 2θ is nearly 180° (Figs. 2*b* and 2*c*) since dispersion is very high in this region and the components have a wide angular separation. The apparent reversal of the stronger K_{α_1} line with the weaker K_{α_2} line is characteristic of back reflection patterns.[11]

The interest of Dr. J. C. Hubbard, to whom one of us (AFG) is indebted for stimulating discussions, is gratefully acknowledged by the authors.

[11] Clark, G. L., *Applied X-Rays.*

ILLITE IN THE ENFIELD SHALE FROM SOUTHERN NEW YORK

R. Torrence Martin,[1] *Cornell University, Ithaca, New York.*

Data on the mineralogical composition of shales are disappointingly scarce, in view of their abundance and importance. Some results obtained incidental to a mineralogical study of clay fractions from southern New York soils are therefore reported here. The soil clays revealed no measurable differences in mineralogical make-up either with depth in the profile or between the different soils examined, suggesting that perhaps the soil clay was derived by disintegration from flags of Enfield shale which are so prominent in these soils.

A sample of unweathered shale was obtained from the Cornell University Quarry, three miles southeast of Ithaca, New York. Mechanical analysis of the Enfield shale showed 16% clay $<1.0\mu$, 73% silt $50\text{–}1\mu$, and 11% sand. The following results were obtained on the clay fraction:

Test[2]	*Enfield Shale*	*Soil Clay (Average)*
Differential thermal analysis.	Illite only thermally active mineral.	Illite with chlorite in some samples.
X-ray diffraction.	Illite with traces of quartz and boehmite.	Illite with some chlorite and a small amount of quartz.
Total potash (% K_2O)	5.8	4.9
Cation exchange capacity (m.e./100 gm.)	18	22
Glycol retention for internal swelling (mgm. glycol/gm. clay).	15	22

The clay fraction of the Enfield shale is predominantly illite, indicating that the illite was not formed during the current soil cycle but is a reflection of an earlier combination of soil forming factors.

[1] Now at Massachusetts Institute of Technology, Cambridge, Massachusetts.

[2] See Martin, R. T. "Mineralogical Analysis of Some New York State Soil Clays," Cornell University Ph.D. Thesis, 1952, for experimental details.

GRAPHICAL METHOD FOR DETERMINING INTERPLANAR SPACINGS

P. Terpstra, *Rijks-Universiteit, Groningen, Holland.*

Studying Fig. 2 of the article that F. D. Bloss published in *Am. Mineral.*, **37,** 588 one recognizes the following collineations:

0	1	2	3	4	5	6	7	Levels
0	100	200	300	400	500	600	700	are colinear
0	110	220	330	440	550	660	770	are colinear
0	125	250	375	500	625	750		are colinear
0	150	300	450	600	750			are colinear
0	200	400	600	800				are colinear

This means that the whole "grid" is determined by the 1-level grid scale. Indeed this scale—being a graph of the function $\sqrt{1+x^2}$—suffices for the rapid determination of the interplanar spacings. The method that uses only this scale requires the construction of the common crystallographic gnomogram showing the gnomon-circle and the poles (hkl). The center O_1 of the gnomon-circle corresponds to the point O_1 in Fig. 3 of the article of Bloss; and the length of the radius of the gnomon-circle is one fifth of the distance on the 1-level scale between the points 100 and 510 (because $\sqrt{1+5^2}=5$, 1). G_{hkl} values for all the face-poles having $l\neq 0$ (we suppose the plane of projection to be perpendicular to the crystallographic c-axis) are read on this scale by transfixing its point 100 to the center of the gnomon-circle and rotating it around this point in order to bring it in contact with the face pole under consideration. The real G_{hkl} value is found if the number pointed out by the scale is multiplied by l.

The G_{hkl} value for a pole $(hk0)$ is found by taking with a simple measuring-staff (0-level scale of Bloss), having the gnomon-length for unit of length, the distance between the face poles (001) and $(hk1)$.*

* Compare Fig. 147 in P. Terpstra: Kristallometrie (Groningen, 1946).

International Union of Crystallography

The Third General Assembly and International Congress of the Union will be held in Paris from 21 to 28 July 1954. Full details of the meeting are now available in the First Circular, copies of which may be obtained from the General Secretary of the Union (R. C. Evans, Crystallographic Laboratory, Cavendish Laboratory, Cambridge, England), from the Secretary of the Programme Committee (A. J. Rose, Laboratoire de Minéralogie, 1 rue Victor Cousin, Paris 5, France), or from any of the following regional representatives of the Programme Committee: G. Menzer (Universitätsinstitut für Kristallographie and Minéralogie, Luisenstrasse 37/II, München 2, Germany), W. H. Taylor (Crystallographic Laboratory, Cavendish Laboratory, Cambridge, England), J. D. H. Donnay (The Johns Hopkins University, Baltimore, Maryland, U.S.A.).

At the congress papers will be presented on all aspects of crystallographic research; there will also be an exhibition of crystallographic apparatus and books. After the Congress two specialized Symposia will be held on 'The Location and Function of Hydrogen' and 'The Mechanism of Phase Transitions in Crystals,' and there will be visits to localities of mineralogical interest. Offers of papers for the Congress and Symposia and notice of enrolment must reach the Secretary of the Programme Committee (preferably on the form accompanying the First Circular) by 15 February 1954. All general correspondence should also be addressed to the Secretary of the Programme Committee.

(See September issue of *Acta Crystallographica* for full details).

The Arizona Geological Society announces that it has sponsored reprinting the following report:

"Report on studies of stratification in modern sediments and in laboratory experiments" by Edwin D. McKee, Office of Naval Research, Project Nonr 164 (00), NR-081-123.

This report constitutes a record of characteristic types of stratification as found today in certain environments of deposition such as beaches, dunes, alluvial fans, lagoons, and tidal flats. The report also includes the results of laboratory experiments on the development of various kinds of stratification. It includes 61 pages of description, illustrated by 12 tables, 12 plates of photographs, and 28 text figures, mostly 3-dimensional drawings.

Copies can be obtained at $1 each, postpaid, by sending your remittance and order to: Arizona Geological Society, P.O. Box 2270, Tucson, Arizona.

Dr. G. W. Brindley, of the physics department, University of Leeds, England, has joined the staff of the Pennsylvania State University as research professor of mineral sciences. In recent years Dr. Brindley has carried on a detailed crystallographic study, first of the kaolinite-halloysite minerals, then the chlorite minerals, and finally of the whole range of layer lattice minerals.

Word has been received of the death of Dmitri Stepanovich Belyankin (1876–1953), Russian mineralogist and petrologist.

The Austin Flint Rogers Research Fellowship in Mineralogy has been established at Stanford University. This fellowship is open to graduate students in the field of mineralogy and preference may be given to those who have had a year of graduate work. The emolument will be $2000 and teaching duties will not be required of the Fellow.

Further inquiries should be made to Professor C. Osborne Hutton, School of Mineral Sciences, Stanford University, Stanford, California.

Correction

In the paper entitled "A spectrographic method for determining trace amounts of lead and zircon and other minerals," by C. L. Waring and Helen Worthing, *Am. Mineral.*, September–October 1953 issue, there are two errors on page 832. In both cases the ratio $\frac{\text{Bi } 2898.0}{\text{Pb } 2833.1}$ should have been stated $\frac{\text{Pb } 2833.1}{\text{Bi } 2898.0}$.

Beyrichite—Charles Milton, U. S. Geological Survey, Washington 25, D. C. is interested in studying this mineral, and would like information as to the whereabouts of any specimens so labelled.

BOOK REVIEWS

CLAY MINERALOGY by Ralph E. Grim, New York, McGraw-Hill Book Company, Inc., 1953, 384 pages, 121 figures, 46 tables, Price $9.00.

This book is the most complete, authentic summary of Clay Mineralogy that has appeared. The well-known clay specialist of the Illinois Geological Survey and now Research Professor of the University of Illinois has compiled in fourteen chapters the available knowledge on many topics of interest to all who have investigated or utilized clays.

These topics include: old and new concepts of the composition of clay materials, classification and nomenclature of clay minerals, structure of clay minerals, x-ray diffraction data, shape and size of clay minerals in electron micrographs, ion exchange, clay-water system, dehydration, rehydration, and changes during heating, clay-mineral and organic reactions, optical properties, solubility, infrared spectra, density, origin, synthesis and occurrence of clay minerals.

Included among the questionable and discredited clay minerals are beidellite and celadonite. Ross and Hendrick's definition of beidellite (1945) as a member of the montmorillonite group, in which no substantial amounts of magnesium and iron are present and in which replacement of Si^{4+} by Al^{3+} accounts for the cation-exchange capacity, is given and is followed by the statement that because of past usage of the term it is believed desirable to drop it entirely in order to avoid confusion. The inclusion of celadonite among the questionable minerals is contrary to the recommendations of Ross and Hendricks (1941) and Kerr and Hamilton (1948). Time will tell whether geologists are ready to discard these terms.

The reader will find the scores of references useful in tracing the progress and the growth of the available knowledge on each subject. The footnote references make it possible to consult the original papers and to credit the contribution of each investigator. However, this reviewer found no reference to the original paper (1928) on the discovery of the only anauxite in the United States listed in this book or to the description of the Ione formation of California (1929) from which specimens of this anauxite were furnished for several of the investigations mentioned.

Some students of igneous petrology may disagree with the final sentence of the book, "There seems to be no reason why the clay minerals could not be formed directly in some igneous rocks," and with his previous suggestion " . . . that some clay minerals can occur as primary igneous components." The occurrence of clay minerals in the spherulites of a rhyolite from Sardinia and "late magmatic" clay minerals in a lamproite from West Kimberly, Australia, raises the question of their formation by deuteric, hydrothermal, or even weathering processes acting on unstable compounds formed in these situations rather than being true "igneous clay minerals" as the section heading indicates. That Professor Grim appreciates these possibilities is suggested by his statement: "It is manifestly difficult to distinguish with certainty between clay minerals of hydrothermal origin and those of possible igneous origin."

Students of sedimentation will learn that "glauconite is a rather unique illite type of clay mineral that is formed during marine diagenesis." Geologists will find of special interest the sections on soils and weathering, clay minerals of hydrothermal origin, recent and ancient sediments and the selected chemical analyses in the appendix.

Professor Grim and the publisher are to be congratulated on this significant book, in which the reproduction of electron micrographs of Kerr and Bates is excellent and in which typographical errors are almost absent. The reviewer recommends this book to mineralo-

gists, geologists, soil scientists, ceramicists, and engineers, as a valuable and useful contribution to the literature on clay.

VICTOR T. ALLEN, *Institute of Technology, Saint Louis University, Saint Louis, Missouri*

SELECTED PETROGENIC RELATIONSHIPS OF PLAGIOCLASE, by EMMONS, R. C., *Editor* (1953), *Geol. Soc. Amer., Mem.*, no. **52,** pp. x+142, 16 plates, 38 figures, and 11 tables. $2.00.

This memoir contains the following chapters:

(1) Selection and preparation of samples, by R. M. Gates and S. E. Clabaugh, pp. 5–10.
(2) Chemical analyses, by R. C. Emmons, pp. 11–22.
(3) Feldspar optics, by R. M. Crump and K. B. Ketner, pp. 23–40.
(4) A twin zone relationship in plagioclase feldspar, by R. C. Emmons and Virgil Mann, pp. 41–54.
(5) Petrogenic significance of perthite, by R. M. Gates, pp. 55–70.
(6) Petrogeny of the syenites and nepheline syenites of central Wisconsin, by R. C. Emmons, pp. 71–88.
(7) Genetic and radioactivity features of selected lamprophyres, by R. C. Emmons, C. D. Reynolds, and D. F. Saunders, pp. 89–100.
(8) A mode of evolution of a granitic texture, by Charles Bradley and E. J. Lyons, pp. 101–110.
(9) The argument, by R. C. Emmons, pp. 111–117.

Certain criticisms apply to the nine papers as a whole. The bibliography lists few of the many important papers on this subject, which is all the more unfortunate in view of the fact that many of the conclusions offered contradict and reject careful studies by other workers. Throughout much of the memoir, the organization of subject matter is confusing and makes for difficult reading. In many places it is not clear which statements are observation and which are interpretation. Supporting field evidence is not adequately detailed.

Chapters 1 through 3 comprise a single unit, and they form the most interesting and valuable part of the memoir. As the authors state, "The aim of the initial phases of this feldspar study was to extract pure plagioclase fractions of uniform composition, representing the complete plagioclase series, from each of a large number of normal plutonic and volcanic rocks." The study is concerned with a further investigation of the relations between optical measurements and the anorthite content of analyzed plagioclases. Plagioclase feldspars from pegmatites were purposely mostly excluded from this study. Chapter 1 presents a description of the criteria for choice of samples and of the means used in separating the plagioclases from the rocks. Separates of plagioclase as free from alterations and inclusions and as homogeneous as possible were sought.

Chapter 2 opens with remarks on the known scatter of points about the Federov migration curves, the subject of several earlier papers (e.g., Barber, C. T. (1936) *Geol. Surv. India, Mem.*, vol. **68,** pt. 2) which are not cited in this memoir. In view of the common reporting of plagioclase compositions to the nearest 0.5% on the basis of optical data alone, Emmons' emphasis of the lack of precision in optical determinations is most timely. In addition, he argues that optical evidence of high- and low-temperature plagioclase optics is not acceptable in view of the data given in the third chapter. Inasmuch as these data consist of optical measurements of analyzed but inhomogeneous samples, Emmons' conclusion does not carry conviction, and in addition it is contradicted by recently published work of the Carnegie Institution laboratories. The remaining part of this chapter is concerned with a discussion of the 32 chemical analyses made for this study.

Chapter 3 concerns the optical measurements made on the analyzed samples, in part on the grains of the separated samples and in part on equivalent grains in thin-section. The values of indices of refraction, optical angle, and extinction angles in the (010) zone show how much variation occurs within each sample; these variations are aptly summarized in figure 6 and are much greater than any hitherto claimed. The discussion of these data, of the cautions to be heeded in interpreting them, and of the meaning of the differences within single samples is well-conceived, but incomplete. One critical point should have been stressed. It is apparent from the content of these three chapters that the analyzed samples were not homogeneous, either on the basis of optics or on the basis of specific gravity measurements. This admitted heterogeneity is emphasized by the variable optical data listed for each sample in this chapter. No firm correlations can be made between the differing optical constants of isolated grains and chemical analyses of bulk samples containing similar grains and presumably also grains of yet different optical character. Variable optical constants of plagioclase crystals of a given anorthite content to the extent claimed in this memoir cannot be convincingly argued from measurements of chemically analyzed but optically inhomogeneous samples. For the determination of optical variations between crystals of a single anorthite content, analyses and optical measurements must be made on optically homogeneous material, and preferably on single crystals. However, such data can be used judiciously for the determination of curves of optical constants useful for the identification of plagioclases, and this the authors have done.

These first three chapters deserve the reader's careful and cautious study. The authors are to be commended for this much-needed research; it is to be hoped that their studies in this realm will be continued, and that they will compare and correlate their data with the wealth of good data recorded in the literature.

Much speculation on the meaning and nature of twinning and of zoning in plagioclase crystals is contained in chapter 4. For brevity, I shall mention only three items. Polysynthetic twinning of plagioclase is assumptively stated as a late feature of mechanical origin. This thesis has frequently appeared in the literature. The possibility is not to be denied, but it is to be regretted that the authors did not see fit to repeat their reasons for accepting a mechanical origin of polysynthetic twinning.

The infrequently mentioned possibility of adjacent twin lamellae in a single crystal having different anorthite contents is argued solely on optical grounds, a basis which many claim to be insufficient. The problem is not one to be lightly dismissed; it appears in routine work all too often. A number of explanations for the asymmetrical extinction of twin lamellae have been offered, such as that it is due to distortion of the indicatrix resulting from the strain incident to mechanical twinning or that it is because the twin composition planes are vicinal forms. Perhaps more than one explanation will prove to be valid. The problem can be solved only by chemical means, and probably only by indirect chemical techniques not dependent on the nearly impossible physical separation of twin lamellae.

An argument for the thesis that mechanical twinning removes zoning and that "zoning is a prerequisite for twinning and that the untwinned plagioclase . . . is in reality unzoned plagioclase, for whatever reason, and is incapable of twinning" is difficult to evaluate solely on the limited empirical grounds offered by the authors. This thesis is the basis for many genetic arguments. A few of the photographs cited in this respect indicate that the idea may merit further investigation, but the likelihood of this point has not been convincingly established in this paper.

Gates' chapter (5) on perthites contains many observations that lead him to two principal conclusions. The sodic plagioclase of a rock is argued as having originated by exsolution from potassic feldspar. The second conclusion is that unmixed sodic plagioclase migrates to and collects in regions of low pressure. The first conclusion is well documented to the extent that reasonable evidence is offered for the argument that perthite does collect into

discrete grains in the fabric of a rock. The second conclusion, while reasonable, is not sufficiently documented or well explained, especially with respect to the causes and nature of this mechanism. These events in the history of a rock are said to be deuteric.

Chapter 6 concerns some syenite and nepheline syenite dikes along shear zones in the cupola of a granite batholith. These dikes are interpreted as resulting from the deuteric recrystallization of cataclastic material along shear zones with the addition of sodium by means of the mechanism proposed by Gates. Sofar as the syenites are concerned, the chemical analyses offered in support of this interpretation are not conclusive. An adequate evaluation of this thesis requires more knowledge of the occurrence than can be gleaned from Emmons' description.

The thesis is offered in chapter 7 that lamprophyres represent a deuteric accumulation of mafic materials from a granite in much the same fashion that perthite is argued to provide a deuteric accumulation of sodium for the formation of the syenites described in chapter 6—thus the inclusion of this paper in a memoir devoted to plagioclase. A similar behavior of uranium to that argued for the mafic materials is developed. The idea is intriguing, and has partial support in a few analyses; unfortunately the rocks called lamprophyre are not described. Too few data are presented to permit an appraisal of the hypothesis.

Chapter 8 on the evolution of a granitic texture fails to provide a single description of a complete rock texture. On the basis of a few samples (from an area in California and one in Wisconsin) of isolated "phenocrysts" of plagioclase showing possible textural and mineralogical changes from the wall rocks of granitic bodies into the central parts of the same bodies, it is claimed that the granites originated by granitization of greenstone. The argument is incomplete; much critical information is lacking; contradictory statements are abundant; and some surprising remarks are made, such as "plagioclases have developed an apparent textural breakdown, with rotation of their component parts . . . optically but without concomitant rotation physically" and "the crystal passed through a stage of viscous fluidity"! There is no adequate reason given to beg the likelihood that the phenocrysts are simply xenocrysts.

The final chapter summarizes and synthesizes the assumptions and arguments offered in the preceding chapters. Although adding no evidence, it presents an organized discussion and philosophy. A variety of interpretations will undoubtedly arise from a reading of this chapter. My interpretation is that Professor Emmons and his associates assume that all granites, except some of those in the form of dikes, are the products of granitization and that this opinion is not only a conclusion but also the assumption fundamental to all of the petrogenic writings in this memoir.

George J. Neuerburg,
U. S. Geological Survey, Pasadena, California

MANUAL FOR GEOMETRICAL CRYSTALLOGRAPHY by Caleb Wroe Wolfe, xii–263 pp., numerous figures, paper bound, Edwards Bros., Inc., Ann Arbor, Michigan, 1953, distributed by Geopublishing Co., 171 School Street, Watertown 72, Massachusetts, Price $4.00.

In his *Manual for Geometrical Crystallography*, Professor Wolfe stresses those aspects of crystallography that are of especial interest to the student of two-circle goniometry and crystal drawing. A very commendable feature of the work is the definition of crystal systems in terms of symmetry rather than in terms of geometry. The author has wisely chosen the Groth-Rogers crystal class names. Consistent with this he has followed, with a few modifications of dubious value, the Federov-Rogers method of naming forms. Some definitions lack rigor. For example, it would be difficult for the student to name the (*h*0*l*)

form on a crystal of the rhombic pyramidal class from the definitions of dome and sphenoid given on page 30.

The discussion of Bravais lattices is marred by certain alternative ways of outlining non-primitive cells in order to make these cells primitive; *i.e.*, it is stated that the cubic F lattice can be outlined as octahedral, and an alternative "cubic bipyramidal" cell is given for the cubic I lattice. Such cells will not " . . . completely and homogeneously partition space without omission or overlapping." From the hexagonal P lattice a trigonal cell is chosen.

Symmetry elements used in the International Symbols are discussed. Mention is made of the use of the physical properties in determining symmetry. The necessity of developing general forms during etching to determine class symmetry and the use of optical activity are not mentioned.

In the chapter on geometrical concepts in crystallography, Miller indices are treated as coordinates of points in the reciprocal lattice. The discussion of the hexagonal system is unnecessarily complicated. If a three axis reference system is used for calculations in the hexagonal system, no ambiguity exists because of the redundant axis. Thus the question of selecting a unique symbol for a zone (coordinates in the direct lattice) or for a plane (coordinates of a point in the reciprocal lattice) does not arise. If it is desirable, the proper third symbol may be added after calculations have been completed. The cross multiplication zonal calculations are given without proof. A simple geometrical proof may be given from the linear projection, if an analytical treatment seems undesirable. Likewise, the Weiss zone law is not proved.

Many practical suggestions in the use of the two-circle goniometer are given. Unfortunately, the adjustment of the instrument is not described. The one adjustment given (page 145) is geometrically unsound. The gnomonic and stereographic projections are treated in the chapter on crystal projections. Selection of the unit cell from the gnomonic projection is discussed. Crystal drawing is largely restricted to the use of the Stöber method, in which an orthographic projection on an inclined plane (axonometric projection) is derived from the stereographic projection. The reviewer would like to see a treatment of the use of the intercepts on an axial cross. The use of orthographic plans and elevations in the graphical solution of elementary problems would also be a desirable addition. The final chapter discusses twinning from Friedel's point of view.

Probably the most useful part of the book is the chapter on crystallographic calculations. It is well written and clearly discusses the procedure in the various systems. The scheme of presentation of data used in the 7th edition of Dana's *System of Mineralogy*, to which Wolfe made a major contribution, is followed.

Since Professor Wolfe states in the preface that this edition should be considered a preliminary one, the reviewer anticipates a revised edition which will eliminate the inaccuracies as well as the typographical errors. The addition of an index would greatly enhance the usefulness of the book. The figures are for the most part adequate. The fact that considerable material which is scattered through the literature is conveniently consolidated in one book increases its value. Basically, the work should be well worth while for the student of structural as well as morphological crystallography.

Reynolds M. Denning,
University of Michigan, Ann Arbor, Michigan

PRAKTISCHE EDELSTEINKUNDE, by Dr. Ing. Walther Fischer. Verlag Gustav Feller-Nottuln, Kettwig/Ruhr, Germany. 187 pp., 48 figures, 3 plates, 5 tables. 1953. Paper-bound, 16.8 R.M., or $4.00.

This work is No. 3 of the series Opuscula Mineralogica et Geologia, short works in the fields of mineralogy and geology. The book is intended for both professional and amateur

lapidaries, but should have interest to the gemologist and the mineralogist as well. The experience of the author has fitted him particularly to produce such a work. He was director of the State Museum of Mineralogy and Geology, Dresden, for 20 years, and is now director of the trade schools of Idar-Oberstein, including the School of Diamond-, Gem-, and Gold-Working of that famous gem-cutting center. In addition to his own broad experience in mineralogy and gemology, the author had available to him the accumulated knowledge of the Idar gem-cutting industry and some of the master cutters of that center.

About one-half of the book is devoted to the general principles of crystallography, crystal-physics and crystal-optics and the relation of these to the lapidary art. Hardness, for instance, is given detailed treatment, particularly as it relates to grinding and polishing. Density, heat conductivity and heating effects, electrical properties, even wet-ability, are all succinctly but adequately considered.

Stress is given to optical properties as they affect the appropriate proportions and orientation of the cut gem, emphasis being given to pleochroism as it affects the color of the finished gem, a characteristic often ignored by the lapidary. The exposition of these subjects is terse and succinct, but could hardly have been better presented for the reader it is intended to reach.

The second part of the book relates to 62 gem mineral species and their varieties, synthetic stones, glass and plastics. The list of gems is up to date, including the new minerals taaffeite and sinhalite. Included in the subject on each gem are brief sections on properties, occurrence, distinguishing features and cutting. Appropriate angles and proportions are given for facetted gems, as well as the kind of laps and abrasive suitable for each mineral. Figures of crystal form together with a figure of a facetted gem in proper orientation are shown.

Five tables of the properties of gem minerals, a short bibliography, a comprehensive index and three plates complete the work.

Much has already been written for the lapidary on equipment and mechanical techniques. This is the first authoritative work on the fundamental scientific principles of the lapidary art. The book, although succinctly written, is comprehensive and authoritative. It should be of particular value and interest to the lapidary and gemologist.

W. F. Foshag,
U. S. National Museum, Washington, D. C.

DIAMOND TECHNOLOGY—PRODUCTION METHODS FOR DIAMOND AND GEM STONES, Second Revised and Enlarged Edition, by Paul Grodzinski. XXXIV +784 pp., 486 illustrations and 93 tables. N. A. G. Press, Ltd., London, 1953. Price 54 shillings 6 pence, postpaid.

This very impressive and comprehensive book is a greatly enlarged revision of Grodzinski's Diamond and Gem Stone Industrial Production which was published in 1942. The pages have been increased from 256 to XXXIV+784, the illustrations from 183 to 486, and the tables from 32 to 93. Every endeavor has been made to bring the various subjects up-to-date. The treatment is encyclopedic in character. There are extensive references to recent scientific publications.

As technical editor of *Industrial Diamond Review* and *The Bibliography of Industrial Diamond Applications*, Grodzinski is in an unusually favorable position to produce a unique and standard work on subjects in this technical field in which many significant advances have been made during the past decade.

The book consists of 16 chapters (712 pages), a selected bibliography (3 pages), an appendix (42 pages), a name index (11 pages), and a subject index (15 pages). The general portion of the book is divided into two parts:—(I) General Manufacturing Methods, and (II) Special Manufacturing Methods. In Part I the following subjects are treated:—Tech-

nology of Machining Methods, Dividing Diamonds and Gem Stones, Bruting, General Survey of Grinding and Polishing, Grinding and Polishing Gem Stones, Grinding and Polishing Diamond, Drilling and Boring of Holes, Carving and Engraving, Diamond Powder—Its Production and Use; in Part II: Polishing Gem Stones for Jewellery, Manufacture of Watch and Instrument Jewels, Manufacture of Diamond and Sinter Carbide Dies, Industrial Diamonds—Selection and Orientation, Setting Diamond in Tools, Grinding and Lapping of Sintered Carbides, and Production of Piezo-Electric and Optical Crystals.

The volume is profusely illustrated with line drawings and half-tone cuts. Unfortunately several cuts illustrating crystallographic features are not properly oriented. The numerous tables are very helpful.

This important volume should be made available to all persons and laboratories interested in diamond technology and related fields.

EDWARD H. KRAUS,
University of Michigan, Ann Arbor, Michigan

FOUR CENTURIES OF EUROPEAN JEWELRY by ERNLE BRADFORD. 226 pp., including 48 pages with 102 half-tone cuts, 7×10 inches. Philosophical Library, New York, 1953. Price $12.00.

This book is designed for lovers and collectors of jewelry. It gives a survey of jewelry in ancient times followed by detailed discussions of the developments from the 16th through the 20th centuries. There are chapters on the use of diamonds and various gemstones in jewelry; also on Cameos and Intaglios, Rings, Enamels, and Precious Metals. The History and Properties of the Precious Stones, Birthstones, and the Craft of Gem-cutting are described in separate chapters. There is a glossary, a selected bibliography, and an index.

The illustrations are excellent and the book is well printed. It is a valuable reference book.

EDWARD H. KRAUS,
University of Michigan, Ann Arbor, Michigan

NEW MINERAL NAMES

Alvarolite

WILLER FLORENCIO, Alvarolita (Um novo mineral da familia dos tantalatos). *Anais Acad. Brasileira Cienc.*, **24**, 261–266 (1952).

The mineral occurs in twinned crystals up to 2×1.7 cm. in a pegmatite vein, municipio Salinas, northern Minas Gerais. Analysis (average of 3) gave: Ta_2O_5 85.15, Nb_2O_5 0.23, MnO 14.85, FeO 0.01, Al_2O_3 trace, TiO_2 none. This gives MnO:Ta_2O_5 = 1.07:1. The color is reddish gray, streak pale yellow, luster vitreous to adamantine, G. = 7.27, hardness 6½, fracture conchoidal, cleavage prismatic. Optically biaxial, positive, extinction 45°, *n*s α 2.250, β 2.255, γ 2.3, 2V = 38–40°, pleochroism X and Y pale yellow, Z strong pale yellow.

The name is for Admiral Alvaro Alberto da Motta e Silva, President of the Conselho Nacional de Pesquisas.

DISCUSSION: There is no discussion whatever in the paper as to what the differences are between alvarolite and mangantantalite. Possibly the distinction is based on the optics and the figure given for extinction. A possibly monoclinic manganese tantalate from Southern Rhodesia has been described by Macgregor, *Mineralog. Mag.*, **27**, 162–164 (1946). Alvarolite can not be accepted as a mineral species until proof is given that it is not mangantantalite.

MICHAEL FLEISCHER

Ribeirite

WILLER FLORENCIO, Uma nova variedade da zirconita. *Anais Acad. Brasileira Cienc.* **24**, 249–259 (1952).

The mineral occurs in a pegmatite at Macarani, Bahia, Brazil. Analyses by Willer Florencio and Fernando Peixoto gave, respectively, SiO_2 27.43, 27.074; Fe_2O_3 4.35, 4.300; Al_2O_3 0.71, 0.666; CaO 0.219, 0.254; MgO 0.007, 0.008; MnO 0.151, 0.154; TiO_2 0.079, 0.086; BeO 0.196, 0.192; ThO_2 none; Y_2O_3 earths 7.45, 7.300; (Ta, Nb)$_2O_5$ 0.10, 0.099; Bi_2O_3 trace; U_3O_8 0.51, 0.535; ZrO_2+HfO_2 51.08, 51.074; P_2O_5 none; H_2O 8.43, 8.306; sum 100.722, 100.048%. G. = 3.50 to 3.54, hardness 4½, partly birefringent and partly isotropic, *n* 1.683. The analyses are compared to those of other varieties of zircon. The name is for Professor Joaquim Costa Ribeiro.

DISCUSSION: An unnecessary name. Detailed study of this peculiar variety of zircon—if it is that—is highly desirable, especially *x*-ray study. Similar material containing rare earths has been described as cyrtolite (1867), anderbergite (1886), alvite (1855), yamagutilite (1936) (contains P_2O_5), oyamalite (1925), and hagatalite (1925), among others.

M. F.

Manganese-hoernesite

O. GABRIELSON, Manganiferous hoernesite and manganese-hoernesite from Långban, Sweden. *Arkiv Mineral. och Geol.*, **1**, 333–337 (1951).

Crusts in fissures were analyzed by R. Blix who found As_2O_5 40.78, MnO 22.87, MgO 9.47, CO_2 1.35, H_2O 25.64; sum 100.11%. This gives $(Mn,Mg)_3(AsO_4)_2 \cdot 8H_2O$ with Mn:Mg = 292:235, after deduction of rhodochrosite. *X*-ray powder and oscillation photographs gave: $a = 10.38$, $b = 28.09$, $c = 4.774$ Å, $\beta = 105°40'$; the unit cell contains four molecules. G. (calcd.) = 2.76. Monoclinic, space group probably $C^5_{2h}-P2_1/c$. Optically positive with $\alpha = 1.579$, $\beta = 1.589$, $\gamma = 1.609$; X = *b*, Z∧*c* 31°, 2V = 65–70°. Another sample contained MnO 14.8, MgO 15.0 (Mn:Mg = 21.37) and had $\alpha = 1.576$, $\beta = 1.587$, $\gamma = 1.606$. This is referred to as manganiferous hoernesite (manganoan would be better M.F.).

M. F.

Farallonite

N. N. KOHANOWSKI, Secondary enrichment in Bolivian tungsten deposits. *Mines Mag.* (Colo.) **43,** No. 2, 17–24, 51, 59 (1953).

The name farallonite is given to an alteration product of wolframite. Found as sky-blue to whitish material formed on outcrops during the rainy season, this is stated to be an intimate mixture of anthoinite and farallonite. Cryptocrystalline with weak birefringence. Outlines of monoclinic crystals were observed. A partial biaxial figure and positive sign were obtained on one such crystal. Luster waxy to pearly. Cleavage good on (100), fracture flat conchoidal. Indices of refraction on sky blue material were 1.81 to 1.82. An *x*-ray study by R. L. Wild gave a pattern similar to that of diopside. The formula $2MgO \cdot W_2O_5 \cdot SiO_2.nH_2O$? is given, with no indication as to how it was obtained. Found at the Farallon mine, Tasna, Bolivia, also from the Zongo district, Bolivia.

Siliceous Scheelite

N. N. KOHANOWSKI, *op. cit.*

The name siliceous scheelite is given to a "mineral," formula given as $2CaO \cdot SiO_2 \cdot 12WO_3 \cdot 24H_2O$? All the data given are as follows: "Siliceous scheelite is of a protogenetic significance. Occurring in suspension in mine waters, it has been found in all tungsten deposits examined by the writer. During the re-opening of the Rocher de Boule mine in British Columbia, coatings of siliceous scheelite in various stages of transition to scheelite were found even on old track rails. It may easily be confused with lardite, which is a colloidal hydrated silica, but fluoresces a somewhat different hue."

DISCUSSION: There is no excuse for cluttering the literature with names for material so poorly described.

M. F.

NEW MINERAL NAMES

Bystromite

BRIAN MASON AND C. J. VITALIANO, *Am. Mineral.*, **37,** 53–57 (1952).

Robinsonite

L. G. BERRY, J. J. FAHEY AND E. H. BAILEY, *Am. Mineral.*, **37,** 438–446 (1952).

Aurostibite

A. R. GRAHAM AND S. KAIMAN, *Am. Mineral.*, **37,** 461–469 (1952)

Unnamed (Cobalt-nickel-copper selenide)

S. C. ROBINSON AND E. J. BROOKER, *Am. Mineral.*, **37,** 542–544 (1952).

Hurlbutite

M. E. MROSE, *Am. Mineral.*, **37,** 931–940 (1952).

M. F.